



<https://theses.gla.ac.uk/>

Theses Digitisation:

<https://www.gla.ac.uk/myglasgow/research/enlighten/theses/digitisation/>

This is a digitised version of the original print thesis.

Copyright and moral rights for this work are retained by the author

A copy can be downloaded for personal non-commercial research or study, without prior permission or charge

This work cannot be reproduced or quoted extensively from without first obtaining permission in writing from the author

The content must not be changed in any way or sold commercially in any format or medium without the formal permission of the author

When referring to this work, full bibliographic details including the author, title, awarding institution and date of the thesis must be given

Enlighten: Theses

<https://theses.gla.ac.uk/>  
[research-enlighten@glasgow.ac.uk](mailto:research-enlighten@glasgow.ac.uk)

**DEVELOPMENT OF AN AUTOMATED SCREENING TOOL FOR DIABETIC  
RETINOPATHY USING ARTIFICIAL INTELLIGENCE**

**JOANNE MCDONAGH**

Thesis submitted to the University of Glasgow for  
the degree of Doctor of Philosophy

This research was conducted in the Department of Clinical  
Physics and Bio-Engineering at the Tennent Institute of  
Ophthalmology, University of Glasgow

March 2005

ProQuest Number: 10753981

All rights reserved

INFORMATION TO ALL USERS

The quality of this reproduction is dependent upon the quality of the copy submitted.

In the unlikely event that the author did not send a complete manuscript and there are missing pages, these will be noted. Also, if material had to be removed, a note will indicate the deletion.



ProQuest 10753981

Published by ProQuest LLC (2018). Copyright of the Dissertation is held by the Author.

All rights reserved.

This work is protected against unauthorized copying under Title 17, United States Code  
Microform Edition © ProQuest LLC.

ProQuest LLC.  
789 East Eisenhower Parkway  
P.O. Box 1346  
Ann Arbor, MI 48106 – 1346

GLASGOW  
UNIVERSITY  
LIBRARY:

## ACKNOWLEDGEMENTS

*'No man is an island, entire of itself'* (John Donne), and as such no thesis is compiled without the help of many others. I would now like to express my gratitude to some of these people.

I would like to thank Diabetes UK (formerly the British Diabetic Association) for their funding support throughout the project, especially all the local groups throughout the UK who adopted our project. Grant No. BDA RD97/001569 & BDA RD97/0001585.

I would like to thank my two supervisors Dr David Keating and Dr Stuart Parks (ElectroDiagnostic Imaging Unit, Tennent Institute of Ophthalmology, Glasgow) for all the help, guidance and support throughout.

The foundations of this project are built on the classification of digital images and therefore I would like to thank John McCormick and Ian Smith the two ophthalmic photographers (Tennent Institute of Ophthalmology, Glasgow) for their help and advice in the commissioning of the fundus camera and their expertise in collecting the images. I am also grateful to the ophthalmologists at the Tennent Institute of Ophthalmology, Glasgow, who took the time to fill out the referral questionnaires and Dr Tom Barrie for performing the tiring task of classifying each image.

I would like to thank my nieces Megan and Clare who provided me with many welcome periods of distraction. And finally to my parents... I am eternally indebted for all the support, love, patience and encouragement that you have given me over the years – thank you.

## **AUTHOR'S DECLARATION**

The material presented in this thesis is the author's own work with the following exception.

Chapter 4 – Performance testing on the normal retina. The results presented for the detection of the optic disc and macula using Aphelion™ software was performed in collaboration with the Department of Electronics, Clinical Physics and Bio-Engineering, Southern General Hospital, Glasgow.

## LIST OF CONTENTS

<b>TITLE</b>	<i>Page</i>
	1
<b>ACKNOWLEDGEMENTS</b>	2
<b>AUTHOR'S DECLARATION</b>	3
<b>LIST OF CONTENTS</b>	4
<b>LIST OF ILLUSTRATIONS</b>	9
<b>LIST OF TABLES</b>	14
<b>LIST OF PUBLICATIONS AND PRESENTATIONS</b>	15
<b>LIST OF ABBREVIATIONS</b>	16
<b>ABSTRACT</b>	17
<b>CHAPTER 1 – INTRODUCTION</b>	
1.1. The Human Eye	18
1.1.1. Anatomy	18
1.1.2. The retina	19
1.1.3. The optic disc	20
1.1.4. The macula	20
1.2. Blindness and visual disability	20
1.2.1. Leading causes of world blindness	21
1.3. The case for screening	21
1.4. Diabetes and diabetic eye disease	22
1.4.1. Epidemiology	22
1.4.2. Complications	23
1.4.3. Prevalence of diabetic retinopathy	24
1.5. Features of diabetic retinopathy	25
1.5.1. Micro-aneurysms	25
1.5.2. Dot and blot haemorrhages	26

1.5.3. Hard exudates	26
1.5.4. Cotton wool spots	26
1.5.5. Intraretinal microvascular and venous abnormalities	27
1.5.6. Neovascularisation	27
1.6. Classifying the progression of diabetic retinopathy	27
1.6.1. Background retinopathy	28
1.6.2. Pre-proliferative retinopathy	29
1.6.3. Maculopathy	29
1.6.4. Proliferative retinopathy	29
1.6.5. Advanced diabetic eye disease	30
1.7. Treating Diabetic Retinopathy	32
1.8. Screening guidelines	32
1.8.1. Current screening modalities	34
1.8.2. Potential screeners	34
1.8.3. Choosing an optimal screening mode	37
1.9. Summary	38
<b>CHAPTER 2 – LITERATURE REVIEW</b>	
2.1. Normal background retina	40
2.2. Locating the optic disc and macula	41
2.3. Retinal vasculature recognition	42
2.4. Features associated with diabetic retinopathy	44
2.4.1. Micro-aneurysms and haemorrhages	44
2.4.2. Exudates	45
2.5. Summary	46
<b>CHAPTER 3 – AUTOMATED SCREENING APPROACHES</b>	
3.1. Image standardisation	48
3.2. Digital image processing	48
3.2.1. Edge detection	49
3.2.2. Median filtering	51
3.2.3. Clustering algorithms	52
3.3. Neural networks	53
3.3.1. Structure of the human brain	53

3.3.2. Neural network structure	54
3.3.3. Applications of neural networks	57
3.3.4. Network design	58
3.3.5. Selecting a network architecture	58
3.3.6. The backpropagation algorithm	60
3.3.7. Training the network	63
3.3.7.1. Transfer function	64
3.3.7.2. Learning rule	65
3.3.7.3. Hidden layer	66
3.3.7.4. Training iterations	68
3.4. Assessing performance of a diagnostic test	69
3.4.1. Receiver operating characteristic curve	69
3.5. Summary	72

#### **CHAPTER 4 - IMAGE DATA SET FORMULATION**

4.1. Image acquisition	73
4.1.1. Digital fundus photography	73
4.1.2. Photographic protocols	73
4.1.3. Digital fundus camera specifications	74
4.2. Image handling	77
4.2.1. Borland Delphi	77
4.2.2. Diabetic Retinopathy Image Classification Programme	77
4.2.2.1. Main / parent form	82
4.2.2.2. Preference form	83
4.2.2.3. Receiver operating characteristic curves	84
4.2.2.4. Child window / contact form – displaying and processing images	85
4.2.2.5. Tool form	86
4.3. Digital fundus images	89
4.4. Formulation of datasets	91
4.5. Summary	93

#### **CHAPTER 5 - PERFORMANCE TESTING ON MAIN RETINAL COMPONENTS**

5.1. Normal background retina	94
-------------------------------	----

5.2. Locating the optic disc	95
5.2.1 Method 1 – custom written software	95
5.2.2. Method 2 – commercial software	96
5.2.3. Automated optic disc findings	97
5.3. Locating the macula	105
5.4. Retinal vasculature recognition	113
5.5. Summary	117
<b>CHAPTER 6 – PERFORMANCE TESTING – THE DIABETIC RETINA</b>	
6.1. Haemorrhages	119
6.2. Exudates	123
6.3. Sight threatening diabetic retinopathy	128
6.3.1. Neovascularisation elsewhere on the retina	129
6.3.2. Neovascularisation at the optic disc	132
6.3.2.1. Circular Intensity Profiling	132
6.4. Summary	140
<b>CHAPTER 7 - PERFORMANCE TESTING OF THE DIABETIC RETINA</b>	
7.1. Validation of neural network performances	141
7.1.1. Recognition of vessels	142
7.1.2. Recognition of haemorrhages	143
7.1.3. Recognition of exudates	144
7.2. Macular Analysis	145
7.3. Full image classification	147
7.4. Summary	149
<b>CHAPTER 8 – CONCLUSIONS AND FURTHER WORK</b>	
8.1. Review	151
8.2. Recognition of normal retinal features	151
8.3. Recognition of features associated with background diabetic retinopathy	153
8.4. Detecting diabetic maculopathy	154
8.4.1. OCT and diagnosing diabetic macula oedema	156
8.5. Detecting new vessels at the optic disc	157
8.6. Discussion	158

<b>APPENDIX I</b>	161
<b>APPENDIX II</b>	168
<b>APPENDIX III</b>	169
<b>APPENDIX VI</b>	173
<b>LIST OF REFERENCES</b>	177

## LIST OF ILLUSTRATIONS

Fig 1.1. External eye	18
Fig 1.2. Cross section of eye	18
Fig 1.3. Digital fundus image of a normal retina.	19
Fig 1.4a. Example of micro aneurysms on colour fundus image	26
Fig 1.4b. Example of micro aneurysms on fluorescein angiography fundus image	26
Fig 1.5. Dot and Blot Haemorrhages	26
Fig 1.6. Hard Exudates	26
Fig 1.7. Cotton wool Spots	26
Fig 1.8. Intraretinal Microvascular & Venous Abnormalities	27
Fig 1.9a. New vessels in the peripheral retina	27
Fig 1.9b. New vessels at the optic disc	27
Fig 1.10. Progression of diabetic retinopathy flowchart	28
Fig 1.11a. Background retinopathy	31
Fig 1.11b. Pre-proliferative retinopathy	31
Fig 1.11c. Diabetic maculopathy	31
Fig 1.11e. Advanced diabetic eye disease	31
Fig 1.12. The seven standard photographic fields	36
Fig 3.1a. Ideal edge step between lower and higher intensity level.	49
Fig 3.1b. Realistic step between edges, where contours are contaminated by noise	49
Fig 3.2. Typical Sobel operator kernels	50
Fig 3.3. Aphelion™ developer Sobel operator on normal fundus image	51
Fig 3.4a. Original image	51
Fig 3.4b. Median filter applied using Adobe Photoshop®.	51
Fig 3.5a. Anatomical image of human brain.	53

Fig 3.5b. Basic schematic structure of a human neuron.	53
Fig 3.6.a The brain consists of tens of billions of neurons densely interconnected	55
Fig 3.6b. A neural network also has a large number of interconnected processing elements.	55
Fig 3.6c. Basic structure of biological neuron.	55
Fig 3.6d. Basic structure of a neural network processing element	55
Fig 3.7. Developmental cycle for a neural network.	63
Fig 3.8. Sigmoid and hyperbolic tangent transfer functions	65
Fig 3.9. ROC cut-off criterion distribution curves	70
Fig 4.1. OCULab digital fundus camera system at GGH.	76
Fig 4.2a. Diabetic Retinopathy Image Classification Programme flow chart	78
Fig 4.2b. Diabetic Retinopathy Image Classification Programme preferences function chart	79
Fig 4.2c. Diabetic Retinopathy Image Classification toolform function chart	80
Fig 4.3. Screenshot of main form	83
Fig 4.4. Screenshot of the two main option tabs in the preferences form	83
Fig 4.5. Screenshot of active ROC curve	84
Fig 4.6. Screenshot of contact strip and overlying image	85
Fig 4.7. Individual screenshots of each of the four tab features of the ToolForm	86
Fig 4.8. The BatchFunction menu	88
Fig 4.9. The diabetic retinopathy screening process.	88
Fig 4.10. Diabetic retinopathy referral questionnaire	90
Fig 4.11. Laser treated retina	89
Fig 4.12. Each image is dissected into 20 x 20 pixel cells	91
Fig 4.13. Magnified view of four classified cells	92

Fig 5.1a. RGB digital fundus image before processing	94
Fig 5.1b. Post processed image with Sobel filter on green plane	94
Fig 5.2. Calculating average dimension of optic disc...	95
Fig 5.3. Screenshot taken from DRICP, location of the optic disc...	96
Fig 5.4. Screenshot taken from Aphelion™ disc detection of macula...	97
Fig 5.5a Histogram of results from 100 normal retinal images displayed within pixel accuracy to the actual disc location.	102
Fig 5.5b. Histogram of results from 100 retinal images displaying background retinopathy features.	102
Fig 5.6. Statistical correlation plots for comparison of both techniques in the identification of the optic disc...	104
Fig 5.7a Histogram of results from 100 normal retinal images, results displayed within pixel accuracy to the actual macula location...	110
Fig 5.7b. Histogram of results from 100 retinal images displaying background retinopathy features...	110
Fig 5.8. Statistical correlation plots for comparison of both techniques in the identification of the macula...	112
Fig 5.9a. Original image	113
Fig 5.9b. Green plane information.	113
Fig 5.9c. Sobel enhanced image, clearer visual definition of vessels.	113
Fig 5.10. ROC analysis of NNW performance to find optimal...	115
Fig 6.1a. Original image.	120
Fig 6.1b. Green plane information.	120
Fig 6.1c Sobel enhanced image, clearer visual definition of haemorrhages	120
Fig 6.2. ROC analysis of NNW performance to find optimal...	121

Fig 6.3a. Original image.	125
Fig 6.3b. Green plane information.	125
Fig 6.3c Sobel enhanced image, clearer visual definition of exudates.	125
Fig 6.4. ROC analysis of NNW performance to find optimal...	126
Fig 6.5a. Original image.	131
Fig 6.5b. Green plane information.	131
Fig 6.5c Sobel enhanced image, clearer visual definition of new vessels	131
Fig 6.6a. Normal optic disc, unprocessed.	133
Fig 6.6b. Image after the application of a high pass filter...	133
Fig 6.6c. Image contrast is increased to further enhance vessels	133
Fig 6.7. DRIC program, records the co-ordinates and pixel intensity values of the optic disc...	133
Fig 6.8a. Typical normal optic disc.	134
Fig 6.8b. Normal image after the application of a high pass filter...	134
Fig 6.8c. Contrast enhancement is applied to make vessels more prominent...	134
Fig 6.8d. Normal disc intensity profile plots for radius values...	134
Fig 6.9a. Optic disc with new vessel growth	135
Fig 6.9b. NVD image after the application of a high pass filter...	135
Fig 6.9c. Contrast enhancement is applied to make vessels more prominent...	135
Fig 6.9d. NVD intensity profile plots for radius values of 20,30, 40 & 50 pixels	135
Fig 6.10. Circular intensity profiles taken from normal disc...	136
Fig 6.11a. Normal optic disc arc segmentation.	137
Fig 6.11b. Disc with new vessel growth arc profile	137
Fig 6.11c,d,e,f. CIP are segmented into 4 arcs, the plots of the normal discs...	137

Fig 6.12. Distribution of turning points NVD vs normal radius 40	139
Fig 7.1. Screenshot of neural network results file analysis through DRICP	142
Fig 8.1. Humphrey OCT system	156
Fig 8.2a. Macular Oedema	156
Fig 8.2b. Macular hole	156

## LIST OF TABLES

Table 1.1. Sensitivity and specificity for the detection of sight threatening diabetic eye disease used by various health professionals.	37
Table 3.1. Calculation equations for sensitivity and specificity	71
Table 4.1. Diabetic Retinopathy Image Classification Program unit summary	81
Table 4.2. No of images collected for each classification	92
Table 5.1. Automatic optic disc findings on normal retinal images	98
Table 5.2. Automatic optic disc findings on diabetic retinopathy images	100
Table 5.3. Automatic macula detection on normal retinal images	106
Table 5.4. Automatic macula detection on diabetic retinopathy images	108
Table 5.5. Optimal NNW performance for vessels	114
Table 5.6. NNW performance for hidden units – for comparison	116
Table 6.1. Optimal NNW performance for haemorrhages	122
Table 6.2. NNW performance for hidden units – for comparison	122
Table 6.3. Optimal NNW performance for exudates	127
Table 6.4. NNW performance for hidden units – for comparison	127
Table 6.5. Optimal NNW performance for new vessels	130
Table 6.6. Number of turning points identified for each radii.	138
Table 7.1. Performance testing of vessel recognition	143
Table 7.2. Performance testing of haemorrhage recognition	144
Table 7.3. Performance testing of exudate recognition	145
Table 7.4. Detection of maculopathy	146
Table 7.5. Full image classification	148

## LIST OF PUBLICATIONS / PRESENTATIONS

- [1] **McDonagh J**, Keating D, Parks S, Evans AL. Development of a computer based screening tool for Diabetic Retinopathy. Clinical Physics Lectures, Beatson Oncology Centre, Western Infirmary Glasgow, November 2002.
- [2] Keating D, Parks S, **McDonagh J**, Evans AL. Artificial intelligence for screening in diabetic retinopathy. Asia Pacific BioTech News 6, 75-76,2002.
- [3] **McDonagh J**, Evans AL, Keating D, Parks S, Barrie T. Automated Retinal Feature Detection from Digital Fundus Images, Brit.J.Op.Phot, 4, 33-38, 2001
- [4] Keating D, Parks S, **McDonagh J**, Evans AL. Automated screening for Diabetic Retinopathy, Singapore Eye Research Institute, Singapore, September 2001
- [5] Keating D, **McDonagh J**, Parks S. Imaging Diabetic Retinopathy, British Diabetic Association, Penrith, November 2000
- [6] Keating D, **McDonagh J**, Parks S, Evans AL. The Role of Computer Analysis of Digital Photography in Diabetic Screening, The Irish College of Ophthalmologists Annual Meeting, Dublin, Ireland, May 2000
- [7] Keating D, Parks S, **McDonagh J**, Evans AL. Screening for Diabetic Retinopathy, Singapore Eye Research Institute, Singapore, February 2000
- [8] Keating D, **McDonagh J**, Parks S. Image Processing of Diabetic Images, British Diabetic Association, Glasgow, November 1999
- [9] Keating D, **McDonagh J**, Parks S. Anatomical and Functional Imaging in Diabetic Retinopathy, British Diabetic Association, Glasgow, March 1999
- [10] **McDonagh J**, Parks S, Keating D, et al.. Application of Artificial Intelligence to the Detection of Diabetic Retinopathy. Research Workers Annual Symposium, Tennent Inst of Ophthalmology, Glasgow, April 1997

## LIST OF ABBREVIATIONS

- BP*** Back propagation
- BDR*** Background diabetic retinopathy
- CIP*** Circular intensity profile
- CWS*** Cotton wool spots
- DR*** Diabetic retinopathy
- DRIC(P)*** Diabetic retinopathy image classification program
- GGH*** Gartnavel General Hospital
- HSI*** Hue saturation intensity
- IDDM*** Insulin dependent diabetes mellitus
- NIDDM*** Non- insulin dependent diabetes mellitus
- NNW*** Neural network
- NVD*** New vessels at disc
- NVE*** New vessels elsewhere
- OCT*** Optical coherence tomography
- OD*** Optic disc
- PE*** Processing element
- RGB*** Red green blue
- ROC*** Receiver operator characteristic curves
- ROI*** Region of interest
- RPE*** retinal pigment epithelium
- VA*** Visual acuity

## ABSTRACT

Diabetic retinopathy is the commonest cause of blindness in the working age population in the Western world. It is widely recognised that screening for this treatable condition is highly cost effective. However, there is a shortage in the number of trained personnel required to screen for sight threatening forms of the disease. It has been shown that many of the features of diabetic retinopathy such as microaneurysms, cotton wool spots, exudates and haemorrhages can be identified automatically with high levels of sensitivity and specificity.

This work describes the development of an automated computerised system for the screening of diabetic retinopathy through the integration of an artificial intelligent system and the development of custom written software (Diabetic Retinopathy Image Classification Programme) to enable image acquisition, image processing, neural network training and testing to be performed in a structured manner. A combination of conventional image processing and neural network methods are utilised for the identification of the basic features associated with the normal and diabetic fundus image. Preliminary investigations into the identification of sight-threatening features are also described. Identification of normal retinal vasculature and diabetic associated features was performed using three separately trained back-propagation neural networks. Localisation of the optic disc and macula was achieved by region of interest pixel intensity scanning. Assessment of the optic disc for sight-threatening new vessel growth was performed by comparing the variance in circular intensity profiles of normal optic discs to the variance of those with neovascularisation. Patients were classified as having maculopathy if hard exudates were identified within one disc diameter of the fovea.

The overall aim of this project is to develop an automated screening programme for diabetic retinopathy. The initial phase details the development and comparison of a range of algorithms for the detection of features associated with diabetic retinopathy. The final phase details the clinical evaluation of the current screening system.

## CHAPTER 1 – THE EYE & SCREENING FOR DIABETIC RETINOPATHY

### 1.1 THE HUMAN EYE

In its simplest form the operation of the human eye is similar to that of a camera. To understand the fundamental features of the eye it is easier to think of it in terms of a single captured picture in one moment of time i.e. a photograph rather than a continually updated image like that of a movie.

#### 1.1.1. ANATOMY OF THE EYE

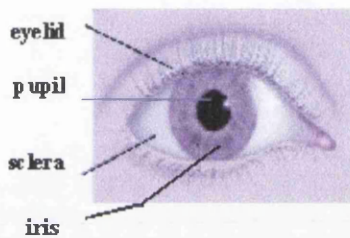


Fig 1.1. External eye adapted from *Eye Anatomy 1996*.

Externally the eye has a protective white coating known as the sclera, (*Fig1.1.*). The clear protrusion at the front end is known as the cornea, which provides 90% of the focusing power of the eye. Behind the cornea lies the iris, the coloured area of the eye. The tissue at the back of the iris comprises brown pigment cells, these cells absorb incoming light as well as prevent light from scattering within the eye. What we perceive to be the colour of a person's iris is in fact dependent upon the thickness of the front layer of the tissue; as the thickness increases the bluer the eye appears to be. The black hole at the centre of the iris is the pupil; this contracts to protect the delicate tissues housed within when the surrounding light is too bright and dilates when the light is dim. Internally the eye is filled with a clear jelly like substance known as the vitreous.

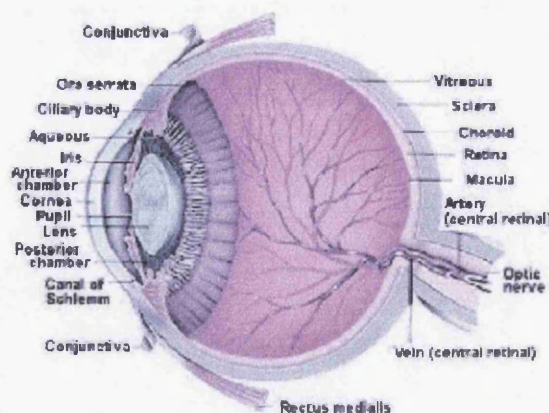
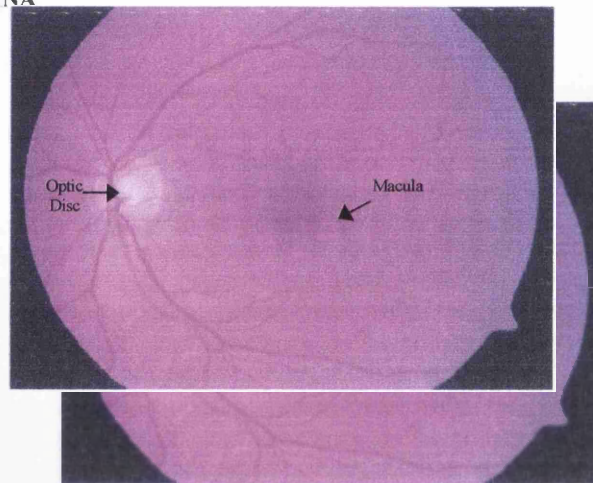


Fig 1.2. Cross section of eye, adapted from *Anatomy of the eye 1999*.

Taking a slice through the eye (*Fig 1.2.*), we find that the next object that a photon of light would come in contact with is the lens. The lens is held under tension by the ciliary muscles, which have the ability to change its shape. As an object gets closer, the eye must alter its light bending power: this is accomplished by the contraction of these muscles.

The parts of the eye described thus far act for the fundamental good of the photographic paper of the eye – the retina. The iris and pupil protects the retina from overexposure to light, while the cornea and lens focus the image.

### 1.1.2. THE RETINA



*Fig 1.3. Digital fundus image of a normal retina.*

The retina is a thin sheet of neural tissue that lines the back of the eye, (*Fig 1.3.*). It is less than  $\frac{1}{4}$  mm thick & 42mm in diameter and consists of three layers of nerve cell bodies and two layers of synapses. The retina is nourished by its own supply of blood vessels and capillaries that radiate from the optic disc. Metabolic needs are provided by the retinal pigment epithelium (RPE).

The cells responsible for the absorption of light entering the eye are called photoreceptors (rods and cones). Rod cells are most useful in aiding vision in dim conditions. Due to their abundance out with the central retinal area they have the largest contribution to peripheral sight. Cone cells on the other hand provide colour

(red, green, blue) vision and fine resolution. These cells provide us with our central visual acuity: they allow us to read and differentiate between the features that we use to recognise people, *Carr & Siegel 1990*.

### **1.1.3. THE OPTIC DISC**

The optic disc is approx. 1.5mm in diameter and is distinguished by its paler yellow colouring. Electrical signals generated from the photoreceptors are carried via the ganglion cell axons and converge at the optic disc. The signals are then conducted along the visual pathway to the visual cortex within the brain for interpretation.

### **1.1.4. THE MACULA**

Two and half disc diameters from the optic disc is the area of the retina which provides central vision (acuity) known as the macula 1.5mm in diameter. At the centre of the macula is the fovea 0.35mm in diameter this only contains cones. Consequently, a reduction in function of the cones in the macula region can lead to severe visual impairment or even blindness. Outwith the fovea, the number of cones rapidly decreases, while the number of rods increases reaching a peak concentration at about 20 degrees of visual angle from the fovea.

## **1.2. BLINDNESS AND VISUAL DISABILITY**

The International Statistical Classification of Diseases, and Related Health Problems, tenth revision (ICD-10), defines blindness as a visual acuity (VA) of less than 3/60. This corresponds to the loss of navigational vision or the inability of the patient to count fingers held up by the examiner at a distance of three meters. Severe visual impairment, on the other hand, is defined as a VA in the better eye equal to or less than 6/60 to 3/60, and low vision corresponding to a VA of less than 6/18 but equal

to or better than 3/60 in the better eye with best possible correction (visual impairment categories 1 and 2 in ICD-10), *WHO 2004*.

### **1.2.1. LEADING CAUSES OF WORLD BLINDNESS**

Blindness can occur as a result of a number of infections, non-communicable diseases or injuries. Glaucoma, Cataracts and Trachoma account for over 70% of the world's blind or visually impaired population. With the exception of Trachoma these diseases mainly effect the older population (>50), *WHO 1997*.

One of the major leading causes of blindness in the working age group (25-65) in Britain and the rest of the economically developed countries is Diabetic Retinopathy; a consequence of long term Diabetes, *Fact Sheet 3 2000*. It is estimated that there are almost 150,000 adults with diabetes in Scotland, *Scottish Diabetes Framework 2000*.

### **1.3. THE CASE FOR SCREENING**

In a bid to alleviate world health problems WHO defined four cardinal principles for the screening of human disease in a public health paper, these were, *WHO 1968*:

1. The condition should be an important health problem with a recognisable pre-symptomatic state.
2. An appropriate screening procedure that is acceptable both to the public and health care professionals.
3. Treatment for patients with a recognisable disease should be safe, effective and universally agreed.
4. The economic cost of early diagnosis and treatment should be considered in relation to total expenditure on health care, including the consequences for leaving the disease untreated.

The St Vincent Declaration was established with a view to reducing the number of cases of new blindness due to diabetic retinopathy by a third over the five year duration of the target plan, *WHO 1990*.

#### **1.4. DIABETES AND DIABETIC EYE DISEASE**

To the average layperson, diabetes is best known through its association with a lack of insulin, the primary regulator of carbohydrate metabolism in the body and first identified by Banting and Best in the 1920's. Diabetes mellitus is the name given to the medical condition where there is a lack of insufficient production of insulin, or indeed an inability of the body to effectively use insulin. This in turn gives rise to an increase in blood glucose levels, clinically referred to as hyperglycaemia. It is a serious life long disease, which has a large economic burden upon our National Health Service (NHS), accounting for 9% of hospital expenditure or in literal terms over £2 billion per annum, *Fact Sheet 3 2000*.

##### **1.4.1. EPIDEMIOLOGY**

The World Health Organisation estimates there to be 177 million people suffering from diabetes worldwide and speculate this number could increase to 300 million by the year 2025, *WHO 2002*. Unhealthy diets, obesity and a rise in longevity have all contributed to this upsurge in the global incidence of the disease. In Britain alone the charity Diabetes UK estimates that there are over 1.4 million known diabetics with a further million affected by the disease but as yet undiagnosed, *Fact Sheet 2 2000*.

The condition is commonly classified into two categories, *Fact Sheet 1 2000*.

##### **Type I Diabetes**

Type I Diabetes or insulin dependent diabetes (IDDM) develops when there is a severe lack of insulin in the body due to the destruction of most or all of the cells in the pancreas that produce it. This is the least common type of diabetes accounting for

about 5% of the diabetic population. It usually appears in people under the age of 40, with symptoms often presenting in childhood.

Generally, it develops due to an autoimmune disorder, where the body's immune system mistakenly sees one of its own tissues as a foreign body and creates antibodies to fight the foreign tissue and hence destroys cells responsible for the production of insulin. Other instances have been known to occur following a viral infection such as mumps, rubella, measles, influenza or polio. Some rarer cases have evolved from injuries to the pancreas arising from toxins, trauma, or after the surgical removal of the majority (or all) of the pancreas.

Type 1 diabetics are usually totally dependent on insulin injections and must follow a strict balanced diet control.

### **Type II Diabetes**

Non-insulin dependent (NIDDM) or adult onset diabetes, is much more common and accounts for 90-95% of all diabetes cases worldwide. Its incidence increases with age and there are also strong genetic influences.

NIDDM results from the body's inability to respond properly to the action of insulin or the pancreas produces an insufficient amount. Depending upon the severity of the disease treatment can either be by diet alone or hypoglycaemic agents (sugar lowering), in more severe cases insulin injections are required.

### **1.4.2. COMPLICATIONS**

Diabetes is associated with many complications; the areas most affected are the heart, the nervous system, the kidneys and the eyes. These complications do not usually develop for 10-15 years after diagnosis in Type I diabetes. However symptoms are more than likely already present in Type II diabetics due to the delay in diagnosis.

Diabetic retinopathy (DR) is probably the commonest complication of diabetes. Sight threatening DR affects 2% of the diabetic population. Early detection of sight threatening retinopathy and treatment by laser therapy has been shown to be effective in preventing the onset of visual impairment. With appropriate medical and ophthalmological care blindness may be prevented in at least one eye, by treating both eyes, in 60-70% of cases with macular oedema and in over 90% with proliferative retinopathy. Protection lasts for over 10 years in two thirds of treated patients, *ETDRS 1991, Hamilton 1996*.

### **1.4.3. PREVALENCE OF DIABETIC RETINOPATHY**

The prevalence of diabetic retinopathy in Type I diabetics is twice that of Type II, and is strongly linked to the duration of diabetes. However, once established, the clinical features, progression and treatment of the disease is the same for both groups. In 1983 the economic burden of DR in terms of costs to the NHS and the tax paying population was calculated, *Foulds et al. 1983*. The cost of treating a patient at risk of blindness was estimated to be £387. It transpired that this sum was 17 times less than the annual amount of money which would be accredited to these people in social benefits if they were to lose their vision and therefore render them unfit to work.

At any one time, up to 10% of people with diabetes will have retinopathy requiring ophthalmological follow up or treatment. The annual incidence of retinopathy requiring ophthalmological follow up or treatment has been reported to average 1.5% after one year. Untreated, between 6-9% of the people with sight threatening retinopathy (proliferative) or severe non-proliferative disease would become blind each year. A diabetic is 10-20 times more likely to go blind than a person in the general population.

After 15 years of diabetes nearly all (97.5%) patients with Type I diabetes and over 60% of patients with Type II diabetes have some degree of retinopathy. Moreover, up to a fifth of newly diagnosed diabetics will already exhibit some features of

retinopathy. The rising prevalence of diabetes will ensure that diabetic retinopathy remains a major health and economic problem.

## 1.5. FEATURES OF DIABETIC RETINOPATHY

Diabetic retinopathy is a progressive disease categorised by certain key features. Most of the retina's blood vessels have tiny openings that allow fluid to pass through the vessel walls. The increased blood glucose levels of diabetes induce strain on these delicate retinal vessels; they become more porous and as a result allow larger molecules to pass through the vessel walls into the surrounding retinal tissue. Water molecules can be quickly reabsorbed into the vessels or into the tissue under the retina; however, fatty molecules are absorbed very slowly and remain visually as yellow deposits upon the retina. The capillaries are usually the first vessels to be damaged: it is these vessels that are essential for the delivery of oxygen and nutrients to the retina and the export of carbon dioxide and other waste products.

### 1.5.1. MICRO-ANEURYSMS

The earliest clinically detectable manifestation of DR are micro-aneurysms, (*Fig 1.4.*). These are micro vascular abnormalities 10 to 100 microns in diameter, and develop in association with areas of capillary closure. They appear as small sacs or tiny red dots budding off from the vessels. They are usually concentrated at the posterior pole and especially temporal to the fovea, *Kanski 1984, Ryan 1994, Hamilton 1996.*

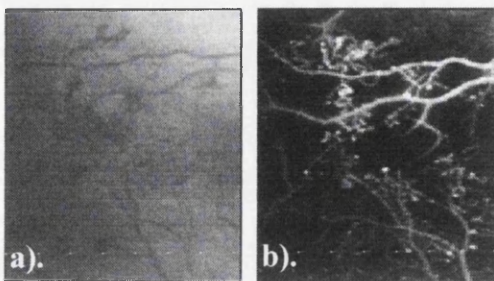


*Fig 1.4. a). Example of micro aneurysms seen on the retina when viewed through an ophthalmoscope or fundus camera. b). Same portion of retina - this time the aneurysms are highlighted by fluorescein leakage as the small white dots.*

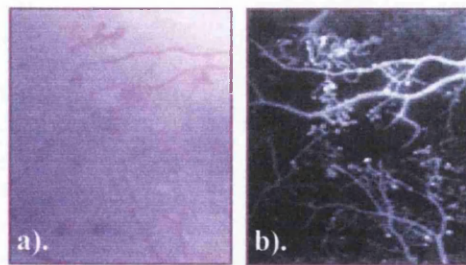


Fig 1.4. a). Example of micro aneurysms seen on the retina when viewed through an ophthalmoscope or fundus camera. b). Same portion of retina - this time the aneurysms are highlighted by fluorescein leakage as the small white dots.

### 1.5.2. DOT AND BLOT HAEMORRHAGES



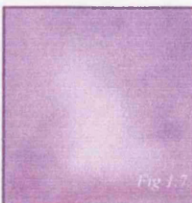
When the wall of a capillary or microaneurysm is sufficiently weakened, it can rupture, giving rise to an intra-retinal haemorrhage, (Fig 1.5.). If the haemorrhage is deep (i.e., in the inner nuclear layer or outer plexiform layer), it usually is round or oval (dot or blot). Dot haemorrhages appear as bright red dots and are the same size as large microaneurysms. Blot haemorrhages are larger lesions, which are located within the mid retina and are often surrounding areas of ischaemia (areas starved of blood).

### 1.5.3. HARD EXUDATES



Hard exudates are features caused by proteins and lipids from the blood leaking into the retina through damaged blood vessels. They appear on the retina as hard white or yellow areas, sometimes in a ring like structure around leaking capillaries, (Fig 1.6.).

### 1.5.4. COTTON WOOL SPOTS (CWS)



Cotton Wool Spots or soft exudates form as a result of a blockage within the retinal pre-capillary arterioles supplying the nerve fibre. Their appearance is as pale white, almost smudge like lesions in the nerve fibre layer (Fig 1.7.).

### 1.5.5. INTRARETINAL MICROVASCULAR & VENOUS ABNORMALITIES



These irregularly shaped blood vessels appear in localized areas of the retina and look like squiggly lines when viewed through an ophthalmoscope. They are also known as omega loops or tortuous vessels, (Fig 1.8.) and signify irregular dilation of retinal blood vessels in response to poor blood circulation.

### 1.5.6. NEOVASCULARISATION

New vessels initially proliferate in the space between the inner limiting membrane of the retina and the posterior face of the vitreous. They appear like rosettes of tightly packed capillaries (Fig 1.9.). Eventually they extend into the vitreous cavity, and become entwined with fibrous tissue. This increases the risk of traction on the underlying retina, culminating in tears or detachment of the fine retinal tissue.

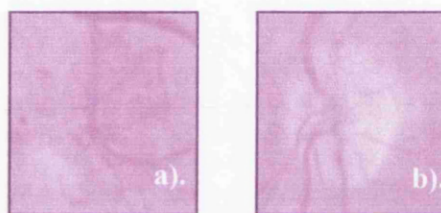


Fig 1.9. (a). Example of new vessel growth in peripheral retina. (b) New vessels at the optic disc

### 1.6. CLASSIFYING THE PROGRESSION OF DIABETIC RETINOPATHY

The classification of the severity of DR is dependent upon the location and accumulation of the above-described features. The typical advancement of the disease is depicted in the flow chart below. Each significant sub-classification is described in terms of advancement and the features associated with it, (Fig 1.10.), Kanski 1984, Ryan 1994, Hamilton 1996.

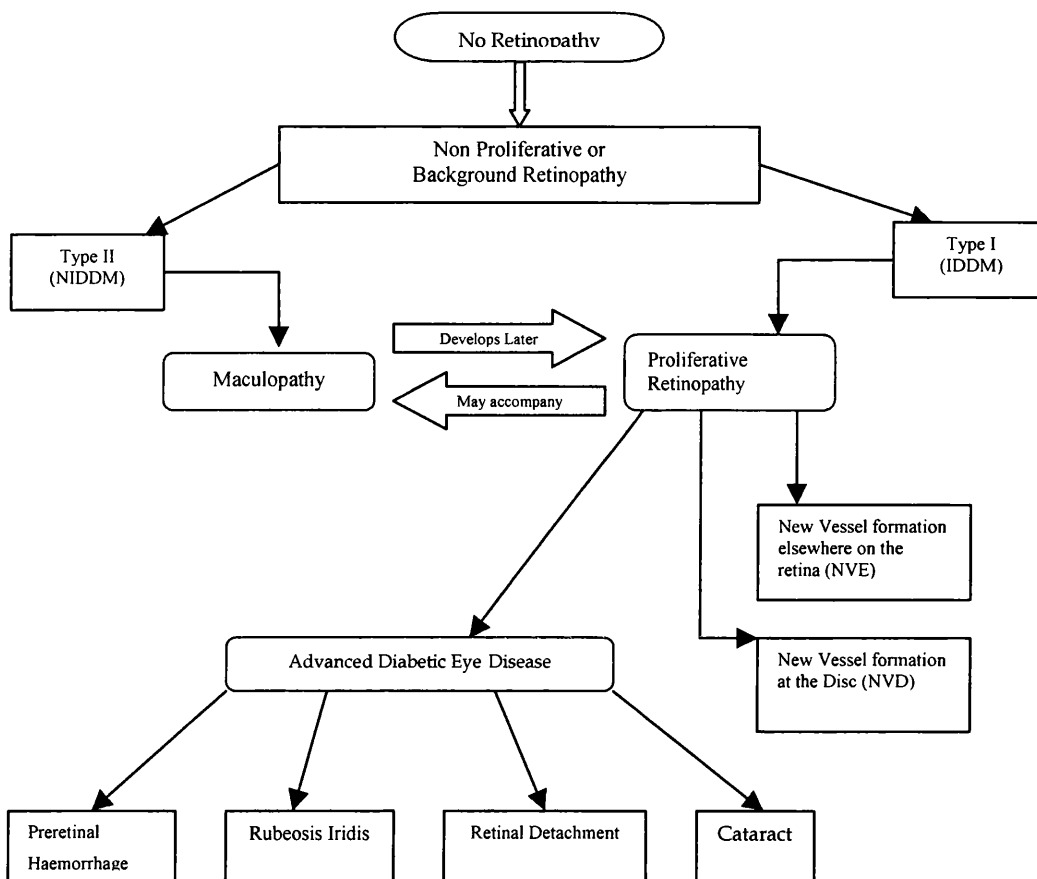


Fig 1.10. Progression of diabetic retinopathy flowchart

### 1.6.1 BACKGROUND RETINOPATHY

Background diabetic retinopathy (BDR) is typically asymptomatic and evolves from gradual progressive damage to retinal blood vessels. It is rare before 8-10 years duration of diabetes. The initial signs include: irregularities within blood vessel walls, microscopic size haemorrhages or microaneurysms and exudates. The presence, locations and quantities of these features differ greatly between individuals, (Fig 1.11a).

### **1.6.2. PRE-PROLIFERATIVE RETINOPATHY**

Pre-proliferative retinopathy is a more advanced stage of damage to the eye than the early signs found in BDR. Once this stage is present, vision can worsen rapidly if the progression is not monitored regularly. Additional features associated with pre-proliferative retinopathy are cotton wool spots and or intraretinal microvascular abnormalities, (*Fig 1.11b.*).

### **1.6.3. MACULOPATHY**

Maculopathy is a leading cause of severe visual impairment in diabetics and occurs if swelling, leakage, or hard exudates arise within the macula or foveal region of the retina. Visual blurring occurs in the middle or just to the side of the central visual field and subsequent visual loss may progress over a period of months, or can be noticed by an inability to focus clearly.

The Modified Airlie House Criteria defines maculopathy as the presence of retinal oedema within 500 $\mu$  of the fovea, or hard exudates within 500 $\mu$  of the fovea if associated with adjacent retinal thickening, or retinal oedema that is one disc diameter or larger in size; where any part of it is residing within one disc diameter of the centre of the fovea, *ETDRS 1991*. Macular oedema is the leading cause of legal blindness in diabetics. The predominant feature is a widespread leakage of intercellular fluid arising from the leaking microaneurysms or from a diffuse capillary leakage, which causes a reduction in visual acuity, (*Fig 1.11c.*).

### **1.6.4. PROLIFERATIVE RETINOPATHY**

Proliferative retinopathy refers to a severe stage of diabetic retinopathy in which new blood vessels proliferate on the surface of the retina. Most patients with this form of retinopathy have had background diabetic retinopathy for at least a few years prior to developing this more advanced form of the disease. It is diagnosed through the

presence of new proliferating blood vessels (neovascularisation) arising from the retina or optic disc and growing on the retinal surface or into the vitreous cavity. Over time, the tiny fine new vessels gradually become larger and more mature, (*Fig 1.11d*).

#### **1.6.5. ADVANCED DIABETIC EYE DISEASE**

The new vessels generated to supply blood and nutrients to starved areas of the retina tend to be very fragile and are prone to bleeding. When these haemorrhages occur in the vitreous, blood begins to disperse through the vitreous cavity causing a reduction in vision. The eye has the ability to clean the blood from the vitreous cavity as long as there is not too much: this process is slow and the speed at which the blood is removed can be quite variable for each individual.

With the eye full of blood, it is difficult or impossible for an ophthalmologist to tell if the proliferating vessels are continuing to grow and if they are damaging the retina with traction or scarring. One of the most severe complications of diabetic eye disease is retinal detachment. This is caused by a contraction in scar tissue. These detachments can be limited and have little effect on the vision, or they may be extensive and cause complete blindness. Once the central part of the retina has detached, visual prognosis is poor, even if the retina is successfully re-attached, (*Fig 1.11e*). For this reason, the emphasis in diabetic eye care is upon prevention and early treatment whenever possible. Standard guidelines have been compiled to predefine the stages of diabetic retinopathy, the features associated with each stage, which features require treatment and to identify the frequency of follow up examinations.

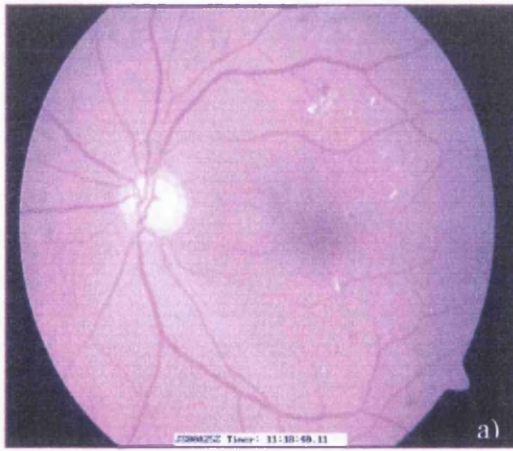


Fig 1.11a. Background retinopathy, showing multiple small lesions of hard exudates and microaneurysms.

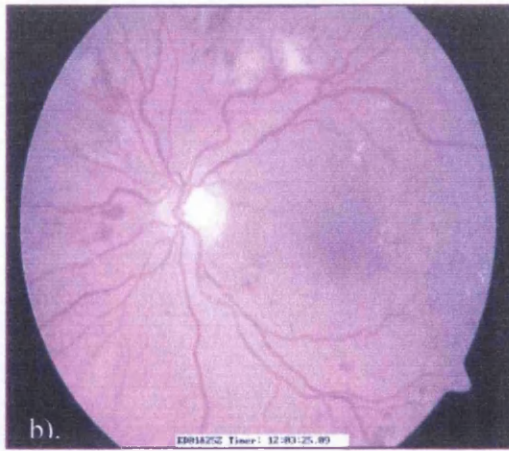


Fig 1.11b. Pre-proliferative retinopathy. The region of interest is the formation of cotton wools spots.

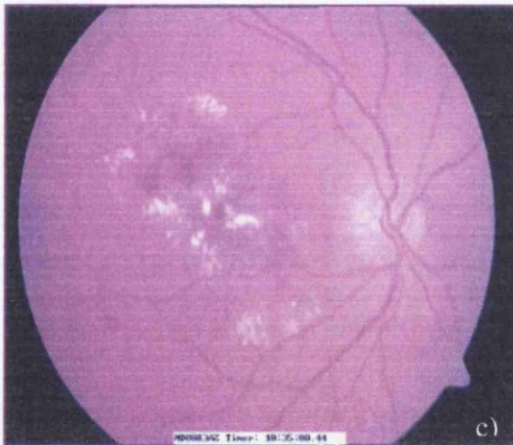


Fig 1.11c. Diabetic maculopathy - hard exudates and haemorrhages reside and encroach upon the central macula region.

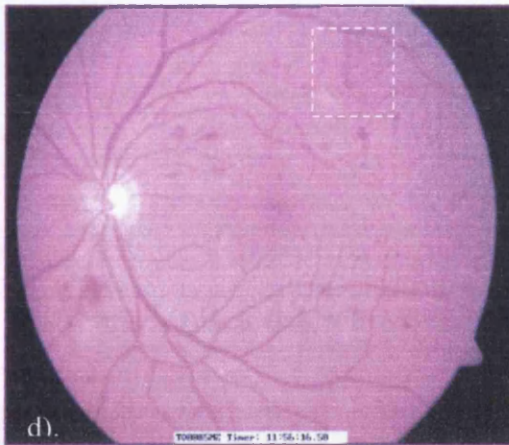


Fig 1.11d. Proliferative retinopathy – a region of neovascularisation is shown within the white dashed box.



Fig 1.11e. Advanced diabetic eye disease. A large vitreous haemorrhage is obscuring the macula region making central vision difficult.

All images obtained from diabetic review clinic at GGH.

## **1.7. TREATING DIABETIC RETINOPATHY**

Laser photocoagulation treatment of DR can either be employed to dry up leaking vessels or alternatively to destroy diseased areas of retinal tissue. This process of eliminating unhealthy, oxygen starved tissue from the retina is achieved through inflicting thermal injury upon it. It works by causing the abnormal blood vessels to dry up, thus stopping their growth and potential for inflicting sight threatening damage. There are two different laser treatment formats applied depending upon the area of the retina that is affected *Ryan 1994, Hamilton 1996*.

- ❧ **Focal laser photocoagulation** - A very narrow beam of laser light is accurately focused in the vicinity of the macular. The beam coagulates the leaking blood vessels and is used to treat macula oedema.
  
- ❧ **Pan-retinal photocoagulation** - Hundreds of spots are targeted across the starved peripheral retina thus stemming the growth of new vessels as seen in proliferative diabetic retinopathy and this in turn reduces the chance of a more serious haemorrhage.

Laser treatment is designed to maintain vision not improve it. It is highly effective in most patients and blindness can be prevented in 80-90% of cases.

## **1.8. SCREENING GUIDELINES**

Recently, the UK National Screening Committee published guidelines on screening for diabetic retinopathy, *National Screening Committee 2004*. The preferred modality is digital fundus photography with image interpretation by trained screeners. The committee acknowledge that this method cannot detect macular oedema, yet treatment of macular oedema prevents blindness in 60 – 70 % of cases. At each review the retina is categorised into one form of retinopathy by a screener based on classification guidelines, the most common method used is the Modified Airlie House Classification, *ETDRS 1991*.

## NON-PROLIFERATIVE DIABETIC RETINOPATHY

<b>Phase 1 – Background Retinopathy</b> Microaneurysms Dot and blot haemorrhages Hard ( intra-retinal ) exudates	<b>Phase 2 – Pre-Proliferative Retinopathy</b> Phase 1 lesions plus: Cotton-wool spots Venous beading and loops Intraretinal microvascular abnormalities
---	--

## PROLIFERATIVE DIABETIC RETINOPATHY

Neovascularisation of the retina, optic disc or iris Fibrous tissue adherent to vitreous face of retina Retinal detachment Vitreous haemorrhage Pre retinal haemorrhage
---

## MACULOPATHY

Clinically significant macular oedema (CSME ) Ischaemic Maculopathy
--

These classifications are then used to determine the follow up procedure. If there is any evidence of sight threatening features such as new vessels on the optic disc or elsewhere in the retina, pre-retinal hemorrhage or fibrous tissue then it is advised that the person requires immediate referral to a consultant ophthalmologist for assessment and possible treatment. This also extends to vitreous haemorrhage, fibrous tissue, retinal detachment and rubeosis iridis.

Lesions which are only slightly less threatening but still requiring fairly urgent assessment by an ophthalmologist are features which are associated with pre-

proliferative retinopathy i.e. venous irregularities (beading, reduplication, loops), multiple haemorrhages, multiple cotton wool spots and intra-retinal microvascular abnormalities (IRMA).

And finally if the lesions remain static from the previous visit and are still shows evidence of background retinopathy i.e. microaneurysms, dot haemorrhages and hard exudates then no immediate action is necessary and the patient can continue with annual screening if the facilities are available.

### **1.8.1. CURRENT SCREENING MODALITIES**

Many different modalities of screening are in use depending on local availability of facilities. These variables include the number of available ophthalmologists, other trained healthcare professionals, equipment and resources available for screening. However, the method used should have sufficient sensitivity (>80%) and specificity (>95%) for a single modality screening process, *British Diabetic Association 1997*.

Recording and archiving of images have traditionally been done using 35-mm slides or Polaroid prints. The role of new technology in the form of digital computerised imaging offers the prospect of immediate high quality images that can be easily and quickly transferred from screening camera to a central reference centre. Storage and reproduction are inexpensive and quick using this medium.

### **1.8.2. POTENTIAL SCREENERS**

The task of screening would seem straight forward, but the present environment of care has led to diversity of views generating much debate. Potential screeners for diabetic retinopathy are: -

- |                           |                                |
|---------------------------|--------------------------------|
| ❧ Ophthalmologists        | ❧ General practitioners        |
| ❧ Diabetologists          | ❧ Optometrists                 |
| ❧ Junior hospital doctors | ❧ Retinal photography services |

☞ Or a combination of all these

The implicit Gold Standard for identifying and grading retinopathy is a retinal examination using indirect biomicroscopy by a senior ophthalmologist or seven field stereoscopic photographs of each eye interpreted by experienced readers.

In the UK there are an insufficient number of ophthalmologists to undertake annual retinal examination for all diabetics, in 1994 there were an estimated 433 full time consultant ophthalmologists, equating to one ophthalmologist for every 1100 diabetics. Diabetologists can provide eye screening as a part of the total package of diabetic care; they are experienced in this field and review the patient at regular intervals for their diabetic care. However a large proportion (40-60%) of diabetics are not seen by a diabetologist but are cared for by their general practitioners. Diabetologists may also have limited facilities, in that a dark room may not be available and retinal examination is mostly carried out using a direct ophthalmoscope.

Screening provided by ophthalmologists, diabetologists or junior hospital doctors would have to be hospital based. This involves long travelling distances, waiting times and extra visits to the hospital. Typically a medical student's experience is limited to, at best, 10 hours of retinal observation and thus they tend to perform poorly as screeners for diabetic retinopathy.

General practitioners are easily accessible to the patients and thus well placed to undertake screening in the community. However they may not get sufficient experience in diagnosing and grading retinopathy. They generally use direct ophthalmoscopy and may lack dark room facilities. As a consequence eye screening provided by general practitioners often appears to be inadequate.

Another option for screening people who reside in rural areas is through the use of a mobile retinal photography service. This method utilises the Gold Standard for photographic screening. It consists of seven 30-degree fields using stereoscopic

pairs, (Fig 1.12.). This needs two frames from each field to simulate a stereoscopic view; thus fourteen frames from each eye are needed.

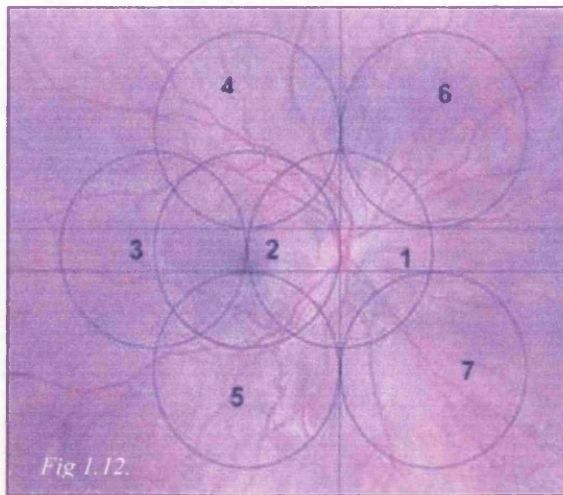


*Fig 1.12. The seven standard fields. Each covers 30 degrees. Field 1 is centred on the optic disc; field 2 is centred on the macula; and field 3 is just temporal to the macula. Fields 4-7 are tangential to horizontal lines passing through the upper and lower poles of the disc and to a vertical line passing through its centre.*

The recommended a photographic protocol which requires two 45° or 50° images and which covers a 15% field of view of the retina. The photographs can be taken by a technician and assessed later by a trained reader or an ophthalmologist, *National Screening Committee 2004.*

Optometrists are generally accessible from the patient's home or workplace and in any case a large proportion of patients visit their optometrist on an annual or biannual basis. Most have the facilities to measure visual acuity in a standardised way, assessing the retina through indirect ophthalmoscopy / slit lamp biomicroscopy all housed within a dark examination room, in addition to being familiar in the use of mydriatics. Optometrists are therefore well suited to carry out screening for diabetic retinopathy in the community and through appropriate training they are able to detect diabetic retinopathy and make the correct decision regarding the need to refer the patient for secondary care.

### 1.8.3. CHOOSING AN OPTIMAL SCREENING MODE

It is not possible to make an accurate and direct comparison of the effectiveness of the types of screening personnel. This is because published studies differ in the definition of retinopathy used for grading, along with a inconsistency in the numbers of the population screened for the disease. An attempt was made to assess the relative sensitivities and specificities achieved by the available screening personnel, the results of which are in Table 1.1., *Hutchinson et al. 2000.*

	Sensitivity	Specificity
General Practitioner reader	77% - 100%	48% - 96%
Optometrist reader	88% - 91%	67% - 82%
Diabetologist reader	72% - 89%	91% - 93%
Trained graders	81% - 100%	97% - 100%
Ophthalmic clinical assistant	89%	86%

*Table 1.1.: Sensitivity and specificity for the detection of sight threatening diabetic eye disease using Mydriatic 45 degree retinal photographs by various health professionals.*

The choice of screening modality to use in a given setting is dependent on local factors. The number of trained ophthalmologists available is the limiting factor thus favouring general practitioners, optometrists and retinal photography as the preferred mode of easily accessible screening in the community.

Availability of resources and infrastructure together with local remunerative practices will dictate the choice amongst these. Some societies may find the cost of photography too high, but in other settings this may be the cheaper method of screening. The advent of digital computerised imaging has the potential to reduce the cost per patient and to improve archiving and retrieval. Improvements in information technology have made instantaneous transfer of these images from screening centre to a referral centre possible. These may tilt the balance in favour of photographic techniques once these technologies are proven. It is therefore the ability to combine

digital photography with conventional computer processing and artificial intelligence applications which has the potential to be the best answer for screening.

## **1.9. SUMMARY**

The retina is a very delicate and complex array of neural tissue incorporating its own unique supply of blood vessels to bring nourishment to the cells responsible for the absorption and conversion of photons of light to electrical signals. These signals are then transported to the brain via the optic nerves. Damage to the retinal structure may severely impair the vision of a person or indeed them blind.

The disease diabetes arises when the pancreas is unable to produce sufficient levels of insulin. It affects an estimated 120 million people globally; there are suggestions that significantly larger numbers are affected but are as yet un-diagnosed. There are two forms of diabetes: Type I where there is a lack of insulin in the body and Type II, where there is an inability of the body to respond properly to the action of insulin. During the long duration of the disease with its poor glucose control many of the smaller blood vessels and capillaries are affected throughout the body. The delicate vessels of the retina are extremely susceptible to damage; after a significant duration of diabetes (15 years) approximately 97% of people with Type I and 60% of people with Type II diabetes will exhibit some degree of retinopathy.

Diabetic retinopathy is the commonest cause of blindness in the working age group of socially developed countries. Its incidence is ever increasing due to obesity and poor diet, and the rise in the average longevity of the human life span. In 1990, the detection of diabetic retinopathy was targeted by the World Health Organisation to force local governments to provide adequate screening procedures for the detection and treatment of the disease before it develops into potentially sight threatening stages. The goal is to significantly reduce the amount of new blindness from diabetic retinopathy with the incentive being that governments would make substantial savings from social benefits compared to the cost of screening and treatment. There has been little advancement towards the set target due to ever increasing numbers of

diabetics and the relatively few trained personnel capable of providing the service. Thus, the challenge for this century is to devise a relatively cost effective automated screening tool, which will divert some of the burden from the medical personnel, enabling them to spend less time screening and more time on treatment.

## CHAPTER 2 - LITERATURE REVIEW

Before this project started in 1998, little had been done to produce a fully automated system capable of detecting sight threatening diabetic retinopathy. Up until 1996 the majority of work concentrated on identifying specific features in isolation using a variety of image processing techniques. In 1996 the first automated system using neural networks was described, *Gardner 1996*.

The initial investigations were limited by the computer systems available. Computer processors were not capable of calculating complex algorithms within short time periods. Therefore it was not possible to obtain an instantaneous classification result. Another constraint was that digital fundus cameras were not commercially available and restrictions were and still are imposed on image resolution, *National Screening Committee, 2004*. Therefore polaroid slides or films of retinal images had to go through the arduous task of being manually digitised. However, recent advances in computer technology have opened the gateway to a new digital era. With this new technology there has been renewed enthusiasm in the development of an automated screening tool for diabetic retinopathy.

This Chapter review's some of the techniques that have been applied to the identification of specific retinal features associated with diabetic retinopathy. Much of the work described has been performed in parallel to the work presented by the author. The relative advantages and disadvantages of each technique will be discussed in this chapter with a comparison of the results described in Chapter 8.

### 2.1. NORMAL BACKGROUND RETINA

The retina is a thin layer of tissue on the surface of a sphere and as such its uniformity is affected by discrepancies in illumination. Consequently, this may affect the performance of feature recognition algorithms. To minimise the adverse effects of this, pre-processing algorithms can be applied to the images to restore uniformity of the background retina.

Images can be altered by manipulating their red, green and blue or hue, intensity and saturation (HIS) components. To pre-process images prior to feature detection analysis, *Zahlmann et al. 2000*, *Lee & Wang et al. 1999* and *Goldbaum et al. 1989* discarded the information provided by the red and blue band. The benefit of this technique is that it does not require much in computational time. Moreover, by removing these two bands you are effectively reducing the number of discrepancies that would otherwise be introduced by these bands. Alternatively, contrast variations can be minimised independently of the colour plane by performing analysis on the intensity plane, *Sinthanayothin et al. 1999*. This involves converting the image into its HIS format and altering the intensity plane before converting it back into its colour format. This is a multi stage approach and therefore slightly more time consuming. Another option is to apply a median filter which can reduce the variation across an image, *Ege et al. 2000*. The amount of computational time is dependent upon the size of the matrix. Moreover, care has to be taken when employing this technique, as a large matrix will result in poorer definition of the feature edges. *Frame et al. 1998*, successfully employed a large-scale median filter and subtracted the resultant image from the original, thus effectively removing the background and leaving the vessels and microaneurysms. This technique then requires further algorithms to be applied for classifying the remaining features.

The work described within this thesis shows the benefits of discarding the red and blue information by increasing the performance of neural networks trained to identify specific features, Chapter 5 & 6. This is due to a greater contrast between feature edges and background retina.

## **2.2. LOCATING THE OPTIC DISC AND MACULA**

The successful automatic detection of the optic disc (OD) and macula is a requirement of any screening tool. The identification of these features may also assist in the analysis of images for other diseases such as glaucoma or age related macular degeneration.

The optic disc is approximately 1.5mm in diameter and is distinguished by its paler yellow colouring. To detect the optic disc *Sinthanayothin et al. 1999* based their disc detection algorithm on a dimensional space of 80 x 80 pixels. This was swept across the whole image to calculate a local measure of pixel intensity variance. Similarly, *Lee et al. 1999* used the average brightness value alone to identify the OD. The dimension of the matrix for the OD region of interest (ROI) depends on the image resolution; the actual size of the optic disc does not vary greatly between individuals. The benefit of this technique is that it can be fully automated and relatively quick to compute. The scanning of a ROI across the image allows the positional co-ordinates of the OD to be recorded for use at a later stage.

Conversely, more complex algorithms have been applied to the task with similar successful results. These algorithms detect shape rather than colour intensity values alone. *Kochner et al. 1998* and *Yulong et al. 1990* utilised the structure of radiating vessels and combined this with Hough transforms to detect the OD. These algorithms are able to identify basic shapes such as circles and lines, but require multiple kernels of processing. At each stage pixels are eliminated until the final region converges upon the centre of the OD. To efficiently perform these complex algorithms more computer storage space and faster processors are required. The results obtained have shown no benefit over the results achieved by the identification of the OD in colour alone.

The macula is located two and half disc diameters from the optic disc and can be recognised as an area of lowest pixel intensity. The techniques applied to the detection of the OD can easily be adapted for the identification of the macula. With similar success *Sinthanayothin et al. 1999* adapted their technique by halving their scanning ROI (40 pixels) from that of their optic disc template.

The identification of the optic disc and macula described within this thesis employed a similar technique to that applied by *Sinthanayothin et al. 1999*. This work is detailed in Chapter 5.

### 2.3. RETINAL VASCULATURE RECOGNITION

Vessels can be distinguished from background retina through their darker hue. The ability to isolate vessels from the rest of the retina enables more specific analysis to be performed on vessel contour. Alterations in the shape and hue of the retinal vasculature from what is deemed as being normal can provide valuable information. For example by analysing the tortuosity of a vessel's contour it is possible to obtain an early insight into the formation of omega loops which are representative of the pre-proliferative progression of diabetic retinopathy.

Image processing techniques can be applied to differentiate vessel contours through a number of different approaches. One such method is the application of fuzzy set theory, *Yannis & Panas 1998, Hoover & Goldbaum 2003*. Fuzzy set theory was originally introduced in the 1960's, *Zadeh 1965*. Like human reasoning, it uses the approximation of information and uncertainty to generate decisions. This is achieved by grouping variables measured into different classification bins, allowing them to overlap so that a variable may be classified in both the large and medium categories, with varying degrees of membership to each. Thus it is a technique that can be applied to any methodology such as classical arithmetic and programming. This technique is combined with binary functions so that multiple rules can be applied to make classification decisions which more closely mimic the human decision making process. The advantage of this approach is that classification programmes can be created based on small training sets, unlike statistical and neural network based approaches, which require a greater number of examples. The negative side is that it often requires user input to identify new starting points when the end of a vessel segment has been identified.

The application of image processing techniques to vessel identification can be divided into those that use edge detection i.e. Sobel and gradient operators and those that use matched filtering or thresholding techniques, Chapter 3.2. The Sobel operator is an edge detection filter that has been successfully applied to the identification of vessel edges as described by *Wang et al. 1997*. With similar effect *Goldbaum et al. 1989* and *Yang et al. 2000* opted for Gaussian filters. *Gregson et al.*

1995 applied thresholding techniques to images. This technique works by comparing the differences in adjacent pixel intensity values and accepting those that lie within a predefined upper and lower limit.

All of these techniques share some similar traits. They can be computationally time consuming depending upon the number of iterations that have to be applied. They are susceptible to problems arising from vascular branching. Therefore starting points have to be introduced by the user and can not be performed automatically. On the positive side they are highly effective in identifying vessel edges. However they do require additional processing for subsequent classification.

A technique that can be fully automated to recognise and classify vessels has been described by *Gardner et al. 1996, Sinthanayothin et al 1999*. They successfully trained a back propagation neural network to identify a variety of key retinal features including vessels with results comparable to that of an ophthalmologist.

A concurrent problem throughout the literature is the inability of these techniques in identifying the sight threatening growth of new vessels. This thesis attempts to address the identification of new vessels using neural networks and circular intensity profiles, Chapter 3.3. & 6.3. The work described within this thesis is an expansion of *Gardner's* work.

#### **2.4. FEATURES ASSOCIATED WITH DIABETIC RETINOPATHY**

The successful identification of the most common features associated with diabetic retinopathy is a fundamental requirement of any automated screening system. This section discusses the techniques that have been applied to the identification and classification of these features.

### 2.4.1. MICRO-ANEURYSMS AND HAEMORRHAGES

Micro-aneurysms (MA) are the earliest clinically detectable manifestation of diabetic retinopathy. The identification of these lesions is not an easy task as they vary in size from 12-125  $\mu\text{m}$ . It has been shown that there is a correlation between disease progression and increasing numbers of micro aneurysms, *Hipwell et al. 2000, Cree et al. 1997, 1996, Spencer et al. 1992, Klein et al. 1989 and Kohner et al. 1986*. While this technique is helpful in research, it does not distinguish between sight threatening and non-sight threatening DR. Nevertheless as a preliminary analysis it does provide valuable information if incorporated alongside other feature detection methods.

Image-processing techniques have been applied to images in a bid to automatically detect and count the number of micro-aneurysms present. For example, *Frame et al. 1998* applied a combination of matched-filtering and region growing algorithms to localise MA's within digital angiography images, a technique they adapted from *Spencer et al. 1992* and *Cree et al. 1997, 1996*. However the intravenous injection of fluorescein is too invasive to be used as part of a screening process. Although the algorithms can be applied to digital colour fundus images the results will not be as good as MA's are difficult to detect on non-angiographic images.

Thresholding algorithms have successfully been applied to the task of identifying possible candidate haemorrhage lesions, *Ege et al 2000 & Lee et al 1999*. Under normal colour fundus photography conditions it is difficult to separate micro-aneurysms from small dot haemorrhages. Thresholding techniques locate possible candidate lesions if pixel colour information falls within predefined upper and lower limits. These candidates then have to go through a subsequent process of classification. This can be automated by using trained NNWs or performed manually.

NNW analysis alone has been shown by *Gardner et al. 1996* to provide results that are comparable to a consultant ophthalmologist. Their data sets were compiled from both micro-aneurysms and small dot haemorrhages. The investigation of image pre-processing techniques and NNW performance for haemorrhage detection is discussed in Chapter 6.1.

### 2.4.2. EXUDATES

A variety of techniques can be applied to the detection of exudates based upon their hue, unique edges and pattern (they typically form in clusters). *Osareh et al. 2003*, segmented retinal images using fuzzy c-means clustering. The principle of this technique was to detect exudates based on their colour by grouping pixels that were spatially connected and then using a back-propagation network to classify them, no mention was made of location information.

Thresholding algorithms can be applied to images after the removal of background features such as the optic disc and vessels, *Zahlmann et al. 2000*, *Kochner et al. 1998*. This technique is therefore dependent upon the successful detection and subsequent removal of the aforementioned features. As with the detection of haemorrhages *Gardner et al. 1996* successfully employed artificial neural networks to the task of classifying exudates. The investigation of image pre-processing techniques and NNW performance for exudate detection is discussed in Chapter 6.2.

At the end of this section it is worthwhile to note that many of the features are identified in isolation. The authors do not say if these techniques are capable of providing the location of each individual feature and how this information can be utilised. For example, the identification of exudates within the macula region is a crucial indication of the development of sight threatening maculopathy.

### 2.5. SUMMARY

This chapter reviews the techniques that have been applied to the detection of normal retinal features and features associated with diabetic retinopathy. It has been shown that neural network analysis as a feature classification tool has proved to be a potential substitute to the current mode of screeners, *Williamson et al. 1997*, *Gardner et al. 1997, 1996*. Studies have shown this method of analysis for detecting haemorrhages and exudates is comparable to that of a consultant ophthalmologist

when differentiating a normal retinal fundus image from one that displays diabetic features, *Usher et al. 2003 & Sinthanayothin et al. 2002*.

Image processing techniques can be effective in improving image quality. They can also be used to detect candidate lesions associated with diabetic retinopathy. It would seem that the grading of DR images is such a widely varied task that a combination of image processing techniques and neural networks should offer an efficient automated grading tool.

It is the author's aim to develop an automatic screening tool capable of identifying sight threatening diabetic retinopathy on digital fundus images. Such a system requires the accurate identification of normal retinal components in addition to features associated with background and sight threatening DR. The forthcoming chapter will explain in detail the application of some of the image processing techniques applied by the author. This is followed by a description of the software which was custom written by the author. This software was specifically designed to enable image acquisition, image processing, neural network training and testing to be performed in a structured and integrated manner which has not previously been performed. The training, testing and validation of the current system is reported in Chapters 5 to 7. Finally Chapter 8 concludes with a comparison between the results obtained by the author and the results described within the literature.

## **CHAPTER 3 – AUTOMATED SCREENING APPROACHES**

### **3.1. IMAGE STANDARDISATION**

In ophthalmology, the recording of retinal images provides a method for monitoring the progression of disease over time. The way in which these images are acquired, processed, and presented has to be standardised to ensure reliability of interpretation. Since digital images are nothing more than a set of numbers, corrections can be made based on pixel statistics and enhancements can be standardised so that all images are enhanced in exactly the same way. In addition, digital imaging also provides a much more extensive collection of image manipulation possibilities.

### **3.2. DIGITAL IMAGE PROCESSING**

Digital image processing enables images to be altered through the application of mathematical algorithms. There are a wide range of image processing and pre-processing algorithms available. They can be individually incorporated into custom written programmes if the user wants to apply them to a specific problem, or for more general use they can be applied through a variety of commercial software packages. Image analysis algorithms can be used to detect specific features within an image, while pre-processing algorithms are used more simply to improve image quality by removing background noise or distortion, or for the standardisation of a group of images. Some of the common techniques applied to the detection and grading of retinal images for the identification of features associated with diabetic retinopathy have been discussed in Chapter 2. This section describes some of basic principles of these algorithms.

### 3.2.1. EDGE DETECTION

Edge detection is based upon the detection of local discontinuities, which mainly correspond to the boundaries of objects in the image. An edge is usually defined as a transition in the intensity or amplitude of the image; edge detection filters therefore search out the borders between areas of different colour, thereby tracing the contours of objects in the image. They are often used to make selection easier. *Gonzalez and Woods 1992.*

Typically an ideal 1-D edge can be defined as a step from a low to high intensity, (*Fig 3.1.*). Normally this transition is contaminated by noise, whereby the real edge is defined as the transition from an average low to an average high intensity.

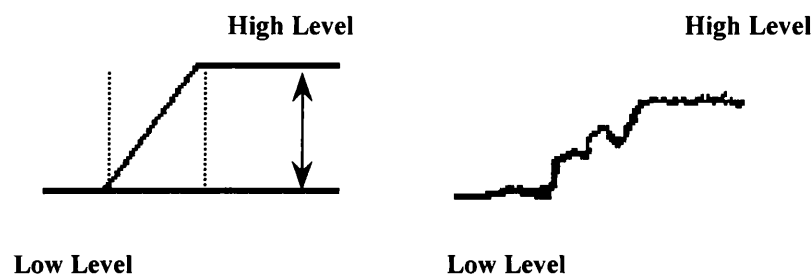


*Fig 3.1. a) Ideal edge step between lower and higher intensity level. b) Realistic step between edges, where contours are contaminated by noise.*

There are several well-known gradient filters, Sobel operators, Roberts operators, Prewitt operators and Isotropic operators, *Sobel edge detector 2003.*

One way to detect edges in a digital image is by using a 2-D gradient operator, e.g. the Sobel operator. The Sobel operator performs a 2-D spatial gradient measurement on an image, the result of which emphasises regions of high spatial gradients that correspond to edges.

The Sobel operator is generated by a pair of 3 x 3 convolution matrices, (*Fig 3.2.*); constructed in such a way that the second matrix is simply the former rotated by 90°.

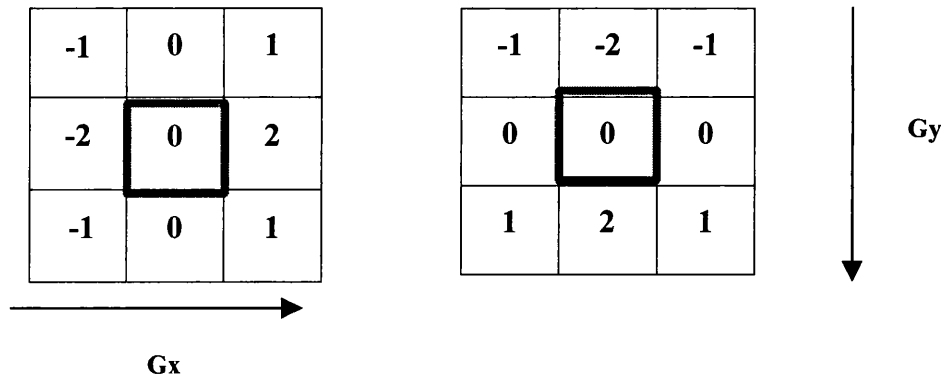


Fig 3.2. Typical Sobel operator. The kernel origin is located at the centre and the arrows indicate the direction that each kernel measures.  $G_x$  convolves from left to right and  $G_y$  from top to bottom.

In general, each matrix computes the gradient in a specific direction and then these partial results are combined together to produce the final result using the equation above. It is the output of this absolute magnitude that the user sees. Each partial result computes an approximation to the true gradient by either using Euclidean distances or absolute differences. Absolute value computations are faster operations when compared to square and square-root operations. Thus, a way to speed up the process of calculating the gradient magnitude ( $G_m$ ) is by summing the absolute values of the gradients in the  $G_x$  and  $G_y$  directions.

The Sobel operator is relatively slow to compute, but it has the advantage of being a large convolution mask and thereby smoothes the input image to a greater extent, thus making it less sensitive to noise. Typically it is used to find the approximate absolute gradient magnitude at each point in an input greyscale image. In the example below using Aphelion™ developer software, the colour information of the

original image is discarded and converted to greyscale prior to the application of a Sobel filter, (Fig 3.3.).

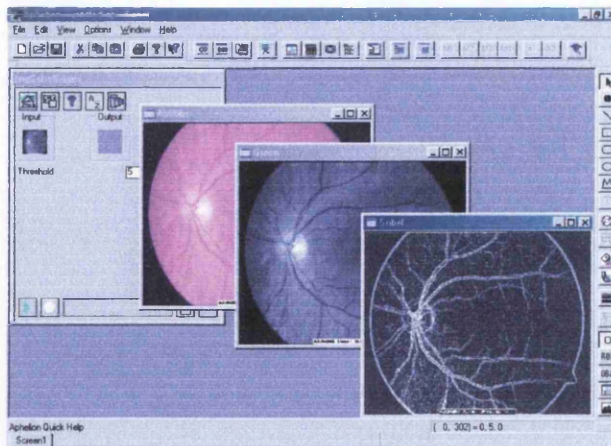


Fig 3.3. Aphelion™ developer Sobel operator on a normal fundus image, edge detection is only performed on one colour plane.

### 3.2.2. MEDIAN FILTERING

Random noise arises from statistical and other variations in pixel intensity values. Median filtering serves to remove this noise from an image by replacing each pixel in an image with the median value of all the pixels in a selected neighbourhood mask. The median value  $m$  of the pixels residing within the selected area is the value in which half of the population have a smaller value than  $m$  and the other half a larger value. Very rarely would the median neighbourhood value compute to be the same as that of the random noise value, *Gonzalez and Woods 1992*.

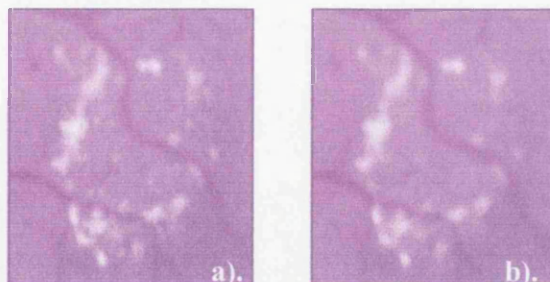
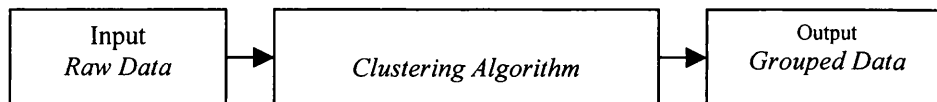


Fig 3.4. a) Original image. b). Median filter applied using Adobe Photoshop®.

### 3.2.3. CLUSTERING ALGORITHMS

A clustering algorithm attempts to find natural groups of data based on some similarity and group them into smaller sets. This is achieved by finding the centroid: the point whose parameter values are the mean of the parameter values of all the points in the clusters. The output from a clustering algorithm is basically a statistical description of the cluster centroids with the number of components in each cluster, *Everitt 1977*.



Generally, the distance between two points is taken as a common metric to assess the similarity among the components of a population. The most commonly used distance measure is the Euclidean distance which defines the distance between two points  $p = (p_1, p_2, \dots)$  and  $q = (q_1, q_2, \dots)$  as :

$$d = \sqrt{\sum_{i=1}^k (p_i - q_i)^2}$$

Clustering algorithms operate on the raw data set where the various clustering concepts available can be grouped into two broad categories:

#### ⌘ *Hierarchical methods*

These methods include those techniques where the input data are not partitioned into the desired number of classes in a single step. Instead, a series of successive fusions of data are performed until the final number of clusters is obtained.

#### ⌘ *Nonhierarchical methods*

These methods include those techniques in which a desired number of clusters are assumed at the start. Points are allocated among clusters so that a particular clustering criterion is optimised. A possible criterion is the

minimization of the variability within clusters, as measured by the sum of the variance of each parameter that characterizes a point.

### 3.3. NEURAL NETWORKS

Conventional computers use an algorithmic approach i.e. the computer follows a set of instructions in order to solve a problem. These instructions are compiled in a high-level programming language. This is translated into machine code so that the computer can perform the task set. The fundamental problem with this type of approach is that unless the specific steps are known the computer cannot solve the problem. Neural networks, however, take a different approach to problem solving than that of conventional computers. They process information in a method which is crudely analogous to the human brain.

#### 3.3.1. STRUCTURE OF THE HUMAN BRAIN

The human brain is composed of cells embedded in a mass of fine felt-like processes, named neuropil. Each individual nerve cell, or neuron, consists of a cell body from which a mass of fine branching processes radiate, called dendrites. The signalling units in which messages arrive via the dendrites are known as axons, (*Fig 3.5.*).

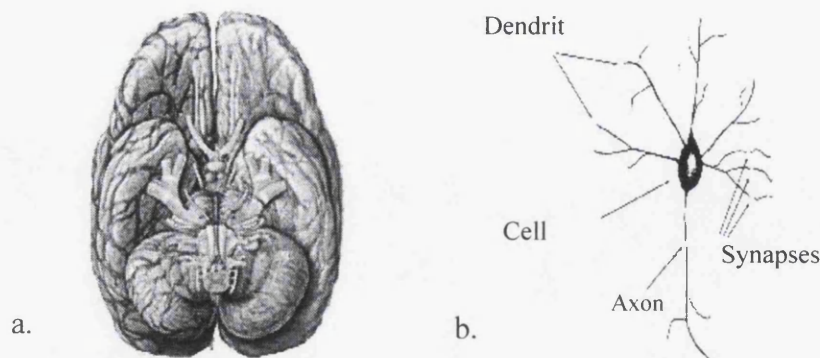


*Fig 3.5. a) Anatomical image of human brain. Adapted from Images of the human brain 1999.*

*b) Basic schematic structure of a human neuron. Adapted from NeuralWare 1996.*

The function of these cells can be perceived by imagining each neuron as a simple micro-processing unit, which receives and combines signals from many other neurons through its input processing elements (PE's), the dendrites. An action, be it from a thought or to create a movement of a body part can be interpreted as the output which requires a neuron to be fired along the axon or the output path. A chemical process within the brain path initiates an action and the output depends upon the strength of this signal, *Martini 2001*.

It is this functional process which NNW's try to mimic.

### **3.3.2. NEURAL NETWORK STRUCTURE**

A neural network is composed of a large number of highly interconnected processing elements (PE's), which are analogous to the neurons of the brain and work in parallel to solve a specific problem, (*Fig 3.6.*). Its processing elements are modelled on the biological neurons of the brain with input paths analogous to the dendrites and output paths to the axons. A mathematical summation and transfer unit replaces the cell body. They learn by example and therefore cannot be programmed to perform a specific task. Examples must be chosen carefully otherwise the network might arrive at an incorrect answer. Because the network finds out how to solve the problem by itself, its operation can be unpredictable.

Neural networks are usually characterized in terms of the number and types of connections between individual PE's and the learning rules applied when data is presented to them. The particular organization of neurons and connections is often referred to as the neural network architecture.

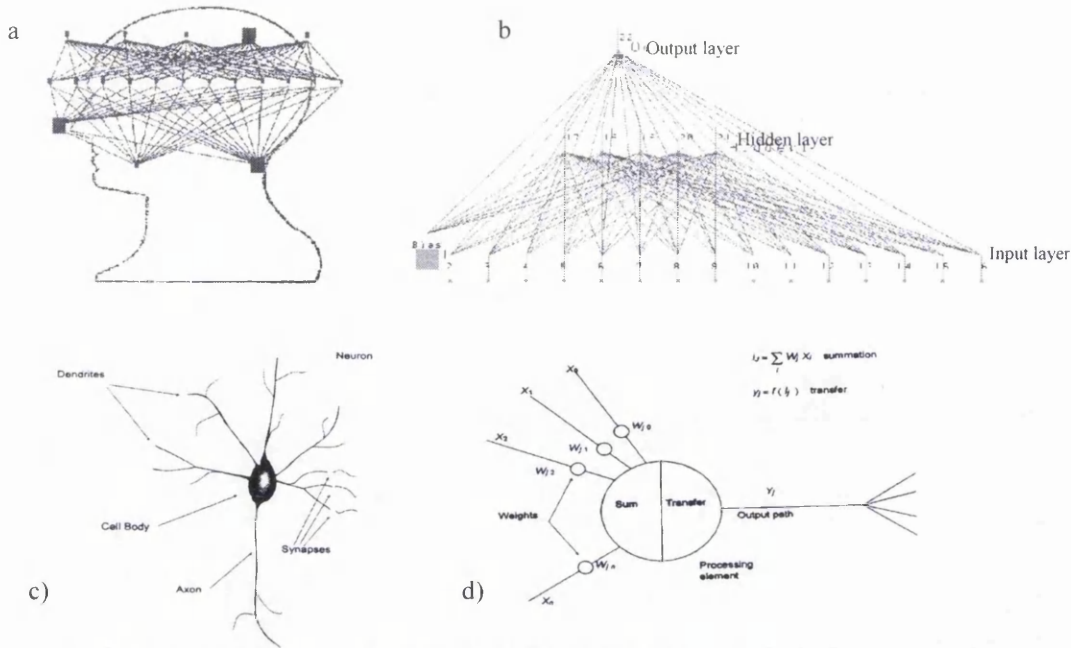


Fig 3.6. A Neural Network is analogous to the human learning system. a) The brain consists of tens of billions of neurons densely interconnected; the processing of information in the neuron forms the basic memory mechanism of the brain. b) A neural network also has a large number of interconnected processing elements. c) Basic structure of biological neuron. d) Basic structure of a neural network processing element. (a,c,d Adapted from NeuralWare 1996)

Each individual neuron has a transfer function, typically non-linear, that generates a single output value from all of the input values that are applied to it. Every connection has a weight that is applied to the input value associated with the connection. The power of neural networks comes from their ability to learn from experience in that they learn to identify patterns by adjusting their weights in response to data input. This process of learning can be supervised or unsupervised.

In supervised training each output unit is told what its desired response ought to be in association to the input signals. The difference between the known output value and the neural network output value is used during training to adjust the connection weights in the network. The aim is to determine a set of weights which will minimise the error between the desired and computed unit values. Whereas unsupervised training or self-organised learning is where the NNW identifies clusters in the input data and detects their emergent collective properties based on some mathematical definition of distance. In either case, after a NNW has been trained, it can be

deployed within an application and used to make decisions or perform actions when new data is presented.

There are a multitude of different types of NNW's, some of the more popular include:

- **Hopfield:** a fully connected symmetrical two-layer recurrent network. The output of each processing element is coupled back to the inputs of every other PE except itself. The classic Hopfield network in fact is made up of three layers: an input buffer layer connected to a 'Hopfield layer' and an output buffer layer. Each layer has the same number of PE's, *Hopfield 1984; Hopfield and Tank 1986*.
  
- **Back-propagation (BP):** These are the most widely used type of network due to its versatility. Generally it consists of three layers an input, an output and at least one hidden layer, *Rumelhart 1986*.
  
- **Radial Basis Function (RBF):** These are three layered networks consisting of an input, output and one hidden layer. The hidden layer is used to cluster the inputs of the network. Although they train faster than BP NNWs they are not as versatile, *Schalkoff 1997*.
  
- **Adaptive Resonance Theory (ART):** These networks consist of two fully interconnected layers. They store a set of patterns in such a way that when the network is presented with a new pattern it will either match it to a previous pattern or store it as a new pattern if entirely different from the patterns already stored. There are two general classes, one devised for classifying binary input patterns the other for analogue patterns, *Carpenter and Grossberg 1988, 1987*.
  
- **Kohonen or self-organising maps (SOM):** are two layer networks that transform n-dimensional input patterns into an ordered z-dimensional map. Data are formed into clusters where similar patterns are projected onto points in close proximity to one another, *Kohonen 1989*.

Another major advantage of NNW's is that it is not strictly necessary to understand the solution of the problem for which the network is being applied to. Traditional computer programming requires a greater understanding of the problem so that the correct inputs, algorithms, and outputs can be implemented. A NNW on the other hand is shown examples of the correct output for a corresponding input. However, failure to include some critical inputs will result in the network failing to converge on the correct solution, *NeuralWare 1996, Bishop 1995, Muller 1995, Stergiou 1998*.

### **3.3.3. APPLICATIONS OF NEURAL NETWORKS**

Neural networks offer ideal solutions to a variety of classification problems such as speech, character and signal recognition, as well as functional prediction and system modelling where the physical processes are not understood or are highly complex. The advantage of NNW's lies in their resilience against distortions in the input data and their capability for learning. They are often good at solving problems that are too complex for conventional technologies. They have been incorporated into many genres including: Financial Prediction, *Davalos et al. 1999, Moshiri et al. 1999, Wittkemper & Steiner 1996*; General Science, *El-Din et al. 2002, Abdul-Wahab et al. 2002, Adams et al. 2001, Meusinger & Moros 2001, Murvai et al. 2001, Fariselli et al. 1999, Hierlemann et al. 1995, Wienke et al. 1995*; Robotics, *Ozkan et al. 2000, Dauffenback 1999*; Manufacturing, *Liu Y et al. 2001, Huang et al. 1999, Quan et al. 1998* and in Medical diagnosis, *Sardari et al. 2002, Gogou et al. 2001, Williamson et al. 1997, Gardner et al. 1996*.

### 3.3.4. NETWORK DESIGN

The key to designing a successful neural network is to follow four basic steps:

*McCollum 1998.*

☞ ***Step 1. Purpose:***

To have a definitive task for the neural network to perform. The performance can be compromised if the task or the data presented is not clearly defined.

☞ ***Step 2. Training:***

Training examples are divided into inputs and target outputs. Network performance can be altered by changing a number of variables within the neural network architecture (discussed later).

☞ ***Step 3. Testing:***

The best network performance during the training phase may not essentially be the best when presented with new data. Therefore, to be sure that you have the optimal network, it is necessary to present it with previously unseen data for a truer interpretation of its performance. If the results remain good, then the network is ready to use. If not, then retraining and retesting have to be repeated.

☞ ***Step 4. Utilising:***

Once the optimal neural network has been designed it is then ready to be integrated into a working environment.

### 3.3.5. SELECTING A NETWORK ARCHITECTURE

The choice of which type architecture to use is dependent upon the problem to be solved and the data available. Back-propagation neural networks (BP NNW) are widely used due to their versatility. They can be applied to areas relating to data modelling, classification, forecasting, control, and pattern recognition. However, they are only practical in certain situations and when the correct data is available.

Below is a list of guidelines for when it would be more sensible to use an alternative approach to solving the problem:

- ⌘ If a flow chart or formula can provide an accurate representation of the problem then traditional programming methods are more appropriate.
- ⌘ If it is not possible to easily generate a significant number of input/output examples for the desired problem then it will be impossible to train a NNW to do anything.
- ⌘ If the solution to the problem is very discrete then it may be more practical to develop a suitably sized look-up table, which would be much simpler and more accurate.
- ⌘ If the desired output were to be a precise numeric value then a NNW would not be practical as they are not good at giving precise numeric answers.

Conversely, there are some situations where a BP NNW would be of advantage, for example when:

- ⌘ A large amount of input/output data is available, but it is difficult to simply relate it to the output.
- ⌘ The problem appears to have overwhelming complexity, but there is clearly a solution.
- ⌘ The solution to the problem may change over time, within the bounds of the given input and output parameters (i.e., today  $2+2=4$ , but in the future we may find that  $2+2=3.8$ ).
- ⌘ Outputs can be fuzzy, or non-numeric.

### 3.3.6. THE BACK-PROPAGATION ALGORITHM

The typical back-propagation network is a multi-layer perceptron (MLP) consisting of: *Stergiou & Siganos 1998*.

- ∅ An input layer, with nodes representing the input variables to the problem.
- ∅ An output layer, where the nodes represent the dependent variables and what the output value should be.
- ∅ And one or more hidden layers, with nodes to help capture the non-linearity in the data. There is no theoretical limit to the number of hidden layers to be used.

Each layer and its corresponding processing element(s) are fully connected to the succeeding layer and its associated PE(s), (*Fig 3.6b*).

For a neural network to be successfully trained in performing a specific task, the weights of each unit must be adjusted in order to minimise the error between the desired output and the actual output. This process requires the neural network to calculate how the error changes as each weight is increased or decreased slightly (*EA*).

Each connection has an associated real number, which is called the weight of the connection  $W_{ij}$  and is the weight of the connection from unit  $u_i$  to unit  $u_j$ . The pattern of connectivity characterises the architecture of the network and is represented by a weight matrix  $W$  whose elements are the weights  $W_{ij}$ . Two types of connection are usually distinguished: excitatory and inhibitory. A positive weight represents an excitatory connection whereas a negative weight represents an inhibitory connection.

A unit in the output layer determines its activity by following a two-step procedure:

First, it computes the total weighted input  $x_j$ , using the formula:

$$X_j = \sum_i y_i W_{ij}$$

where  $y_i$  is the activity level of the  $j$ th unit in the previous layer and  $W_{ij}$  is the weight of the connection between the  $i$ th unit and the  $j$ th unit.

Next, the unit calculates the activity  $y_j$  using some function of the total weighted input. Typically using the sigmoid function (transfer function):

$$y_j = \frac{1}{1 + e^{-x_j}}$$

Once the activities of all output units have been determined, the network computes the error  $E$ , which is defined by the expression:

$$E = \frac{1}{2} \sum_i (y_i - d_i)^2$$

Where  $y_j$  is the activity level of the  $j$ th unit in the top layer and  $d_j$  is the desired output of the  $j$ th unit.

The back-propagation algorithm consists of four steps:

The first stage is to compute how fast the error changes as the activity of an output unit is changed. This error derivative ( $EA$ ) is the difference between the actual and the desired output:

$$EA_j = \frac{\partial E}{\partial y_j} = y_j - d_j \dots\dots\dots \text{Step 1}$$

Secondly, it computes how fast the error changes as the total input received by an output unit is changed. This quantity ( $EI$ ) is the answer from Step 1 multiplied by the rate at which the output of a unit changes as its total input is changed:

$$EI_j = \frac{\partial E}{\partial x_j} = \frac{\partial E}{\partial y_j} \times \frac{dy_j}{dx_j} = EA_j y_j (1 - y_j) \dots\dots\dots \text{Step 2}$$

Thirdly, computes how fast the error changes as a weight on the connection into an output unit is changed. This quantity ( $EW$ ) is the answer from Step 2 multiplied by the activity level of the unit from which the connection emanates.

$$EW_{ij} = \frac{\partial E}{\partial W_{ij}} = \frac{\partial E}{\partial x_j} \times \frac{\partial x_j}{\partial W_{ij}} = EI_j y_i \dots\dots\dots \text{Step 3}$$

And finally, to compute how fast the error changes as the activity of a unit in the previous layer is changed. This is the crucial step as it allows back propagation to be applied to multilayer networks. When the activity of a unit in the previous layer changes, it affects the activities of all the output units to which it is connected. To compute the overall effect on the error all the separate effects on output units are added together. Each effect is simple to calculate, by multiplying the answer in Step 2 with the weight on the connection to that output unit.

$$EA_i = \frac{\partial E}{\partial y_i} = \sum_j \frac{\partial E}{\partial x_j} \times \frac{\partial x_j}{\partial y_i} = \sum_j EI_j W_{ij} \dots\dots\dots \text{Step 4}$$

Therefore, by using Steps 2 & 4, the  $EA$ 's of one layer of units are converted into  $EA$ 's for the previous layer. This procedure can be repeated to get the  $EA$ 's for as many previous layers as desired. Once the  $EA$  of a unit is known, Steps 2 & 3 can be used to compute the  $EW$ 's on its incoming connections. A back-propagation network is a known adaptive network as it is one which is able to change its weights, ie  $dW/dt$  not= 0.

### 3.3.7. TRAINING THE NETWORK

The development of a neural network to perform a specific task successfully requires careful planning and design. Overall there are several phases which should be followed to achieve this, (Fig 3.7.).

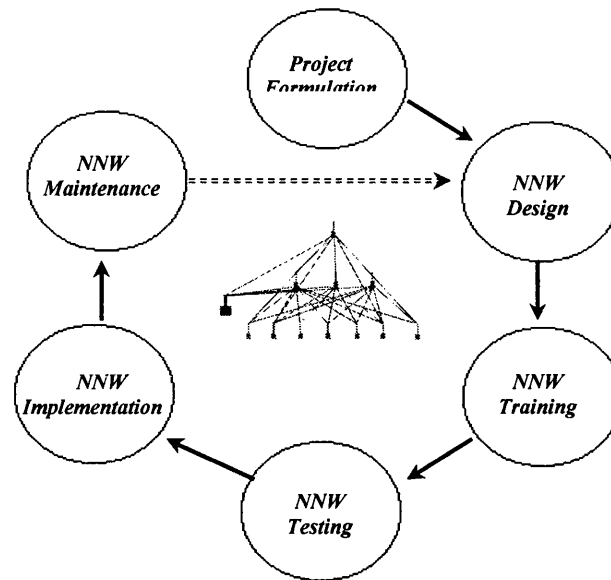


Fig 3.7. Developmental cycle for a neural network.

Once the initial problem has been identified the next stage is to construct a neural network with the appropriate architecture to achieve that task. In this phase the number of PE's for each layer is determined in addition to how the units are connected to one another, and the initialisation of the weights. The connections determine whether it is possible for one unit to influence another, while the weights specify the strength of that influence.

A three-layer network can be taught to perform a particular task by using the following procedure:

- ⌘ Presenting the network with training examples which consist of a pattern of activities for the input units together with the desired pattern of activities for the output units.

- ↻ Determining how closely the actual output of the network matches the desired output.
- ↻ Changing the weight of each connection so that the network produces a better approximation of the desired output.

By adjusting the weights on the connections between layers, the NNW output can be trained to match a desired output. If there is a difference between the actual and the desired outputs, the weights are adjusted on the adaptive / hidden layer to produce a set of outputs closer to the desired values. This training procedure is repeated until the network's performance no longer improves. At this point, it has either successfully learned the desired output or it has failed to learn all of the answers correctly.

There are specific features of a network that have a direct effect upon network performance for example the transfer function, the learning rule, the number and arrangement of hidden units and the number of training iterations. Preliminary investigations were performed altering these different variables and analyses carried out to determine the optimum parameter settings that would yield the optimum network performance in terms of its sensitivity and specificity, see Section 3.4.

### 3.3.7.1. TRANSFER FUNCTION

The transfer function is the component of a processing element through which the sum is passed to create the output. Some functions are designed to indicate only whether a PE can fire regardless of the magnitude of the net excitation by comparing this value to the PE threshold value. Typically there are three categories:

- ↻ **Linear** (or ramp)

The output activity is proportional to the total weighted output.

☞ **Threshold**

The output is set at one of two levels. Depending on whether the total input is greater than or less than this constant threshold value then some action takes place i.e. a neuron is fired.

☞ **Sigmoid**

The output varies continuously but not linearly as the input changes. Sigmoid units bear a greater resemblance to real neurones than linear or threshold units, but all three must be considered rough approximations. The sigmoid function is a smooth version of a (0,1) step. Any smooth function can be used: the hyperbolic tangent (TanH) has a step of (-1,1) and has been utilised as a reliable alternative, (Fig 3.8).

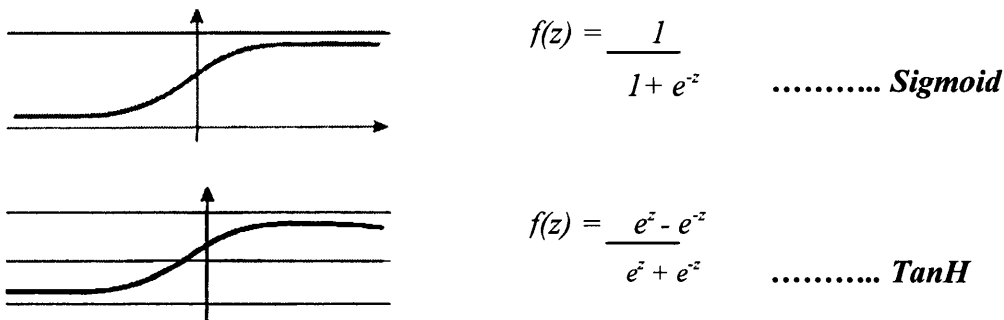


Fig 3.8. Sigmoid and hyperbolic tangent transfer functions for back-propagation. Adapted from NeuralWare 1996.

Most applications using a back propagation technique utilise a sigmoid function.

**3.3.7.2. LEARNING RULE**

The learning rule enables the network to configure itself so as to achieve an output as close to the desired value as possible. There are four standard types of learning rule:

#### ❧ **Error Correction**

The calculated arithmetic difference or error between the desired solution and the networks solution at any stage during training is used to modify the connection weights so as to gradually reduce the global network error. The update of the weight matrix can take place after every example or can be accumulated over the whole example set followed by a single update: this is referred to as cumulative or epoch update.

#### ❧ **Hebbian**

Hebbian learning is where a connection weight on an input path to a processing element is incremented only if both the input and the desired output are high.

#### ❧ **Boltzmann**

The Boltzmann learning rule is similar in theory to the error-correction technique, however each processing element generates an output based on a Boltzmann statistical distribution. Thus learning tends to be slower.

#### ❧ **Competitive**

In competitive learning the processing elements are forced to compete amongst themselves. The PE that generates the strongest response in relation to the given input in a particular iteration invokes a change in the weights attached to it so that it becomes more like the input.

### **3.3.7.3. HIDDEN LAYER**

In general one hidden layer has been found to be sufficient in the construction of a NNW when applied to function approximation problems, *Basheer 2000*. The selection of the optimal number of hidden units within the layer is one of the most critical tasks within the neural network design. For the input and output layer the number of PE's required is predefined by the problem to be solved and the data provided. The number of PE's in the hidden layer can be varied to produce

conflicting results. A network constructed with too few hidden PE's would be incapable of differentiating between complex patterns leading to only a linear estimation of the actual trend. However a network with too many hidden processing elements would over generalise the task at hand. Furthermore, the greater the number of PE's used the longer the network takes to train.

There are two general rules of thumb for determining the optimal number of hidden units required. The first is based upon the relationship between the number of training examples and the number of inputs given by the equation below:

$$H = \frac{\text{\# of training cases}}{5(m + n)}$$

Where:

- ◇ cases are the number of records in the training file.
- ◇ m is the number of PE's in the output layer.
- ◇ n is the number of PE's in the input layer.
- ◇ H is the number of PE's in the hidden layer.

The second is a trial and error approach. This involves training the network many times where each time the number of hidden units is incremented by a predefined factor until the new network achieves a poorer performance than the previous training phase. The incremental factor is then reduced and the number of hidden units decreased again until the network performance becomes worse. This process of increasing and decreasing the number of PE's in the hidden layer is repeated until the optimal network performance is achieved. It is therefore good practise to combine these two techniques, firstly by calculating the estimated optimal number of PE's in the hidden layer, then by adjusting the number of PE's around this value until the best network performance is obtained.

#### **3.3.7.4. TRAINING ITERATIONS**

The number of epochs or times an example is presented to successfully train a NNW is determined by trial and error. Training for too long only serves to produce a network that is no better than a lookup table. If a network is larger than need be with respect to the training data set and as a result is trained on a relatively small number of data examples, over-training can result. Such networks are said to have memorized their training data and lack the ability to generalise.

The training examples can be presented to the network in one of two modes. The first mode is example-by-example training; where the weights are updated immediately after each example. On presentation of the first example the BP network applies both feed-forward and backward sweeps until either the error between the desired output and the calculated output falls to an acceptable level or until a specified number of iterations have been completed. Once this example has been learned the process is repeated for the next example and so on. The second method is to apply a batch training technique where all the examples are presented in a single iteration. The error is then calculated as an average of the global error and then back propagated accordingly. Again this process is repeated according to the number of training iterations; this is controlled by the epoch value.

There are advantages and disadvantages for both these techniques. In the example-by-example method one of its main advantages is that it requires smaller storage space for the weights compared to batch training, which requires a larger storage space. However, this does allow batch training to calculate a better estimate of the error with a more representative calculation of the required weight change. The performance of both method can be affected by poor examples; for batch training this can be alleviated by randomising the training examples between each epoch.

We used a commercial system for developing our networks (NeuralWare, NeuralWorks Professional II/Plus) as it offers a range of pre-programmed learning rules and transfer functions.

### **3.4. ASSESSING PERFORMANCE OF A DIAGNOSTIC TEST**

The performance of a diagnostic test can be expressed as its ability to accurately detect those with disease against its ability to accurately detect those without disease. One method that is widely used in the medical literature is Receiver Operating Characteristic (ROC) curves, *Zweig et al. 1993, Hanley & McNeil. 1983.*

#### **3.4.1. RECEIVER OPERATING CHARACTERISTIC CURVE**

An ROC curve is a plot of the true positive ratio (*Sensitivity*) against the false positive ratio (*1-specificity*) for each value of the diagnostic test, *Hanley et al. 1982, Metz 1978.*

An ROC curve demonstrates several things:

- ⌘ It shows the trade-off between sensitivity and specificity (any increase in sensitivity is generally accompanied by a decrease in specificity).
- ⌘ The closer the curve follows the left-hand border and then the top-border of the ROC space, the more accurate the test.
- ⌘ The closer the curve comes to the 45-degree diagonal of the ROC space, the less accurate the test.
- ⌘ The area under the curve is a measure of test accuracy.

While considering the results of a particular test in two populations, *a* corresponds to a positive identification of a disease state (in this case the presence of sight threatening aspects of DR), and *b* corresponds to a negative identification (i.e. there are no sight threatening features of DR). It is rare to observe a perfect separation between the two groups. Indeed, the distribution of the test results will overlap, (*Fig 3.9.*).

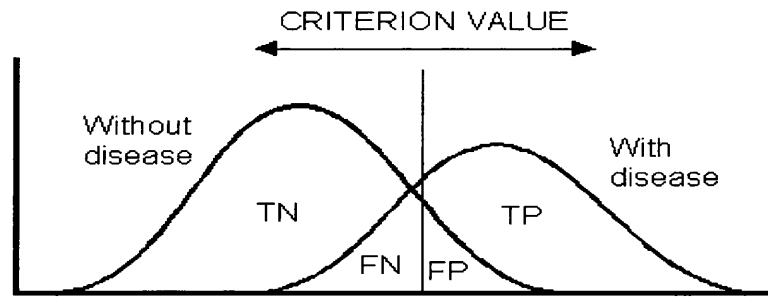


Fig 3.9. ROC cut-off criterion distribution curves. Adapted from ROC curve analysis 1993.

For every possible cut-off point selected to discriminate between the two populations, there will be some cases with the disease correctly classified as positive (TP = True Positive fraction), but some cases with the disease will be classified negative (FN = False Negative fraction). On the other hand, some cases without the disease will be correctly classified as negative (TN = True Negative fraction), but some cases without the disease will be classified as positive (FP = False Positive fraction).

The characteristics of an individual test relative to its gold standard are quantified through the *sensitivity* and *specificity*. Where:

☞ *Sensitivity*: is the probability that a test result will be positive when the disease is present (true positive rate, expressed as a percentage).

☞ *Specificity*: is the probability that a test result will be negative when the disease is not present (true negative rate, expressed as a percentage).

The two measures are inversely related; an increase in sensitivity will often result in a decrease in specificity and vice versa. The optimum cut-off level depends on the diagnostic strategy. If the primary objective is to identify a disease meaning false negatives are to be minimised and a limited number of false positives is acceptable, a system with a high sensitivity and good specificity is required. If on the other hand, the objective is to make sure that every test positive is truly diseased (meaning no

false positives, but limited amount of false negatives acceptable), the diagnostic system should have a high specificity and good sensitivity. The sensitivity and specificity can be calculated by:

<b>SENSITIVITY</b>	$= \frac{a}{a + b}$	<b>SPECIFICITY</b>	$= \frac{d}{c + d}$
<b>Positive Likelihood Ratio</b>	$= \frac{\text{Sensitivity}}{1 - \text{Specificity}}$	<b>Negative Likelihood Ratio</b>	$= \frac{1 - \text{Sensitivity}}{\text{Specificity}}$
<b>Positive Predictive Value</b>	$= \frac{a}{a + c}$	<b>Negative Predictive Value</b>	$= \frac{d}{b + d}$

Table 3.1. Calculation equations for sensitivity and specificity

Where:  $a$  = correct identification of an abnormal feature.  
 $b$  = wrong identification of abnormal feature.  
 $c$  = correct identification of normal feature.  
 $d$  = wrong identification of normal feature.

∅ *Positive likelihood ratio*: is the ratio between the probability of a positive test result given the *presence* of the disease and the probability of a positive test result given the *absence* of the disease, i.e.

$$\frac{\text{True Positive rate}}{\text{False Positive rate}}$$

∅ *Negative likelihood ratio*: ratio between the probability of a negative test result given the *presence* of the disease and the probability of a negative test result given the *absence* of the disease, i.e.

$$\frac{\text{False Negative rate}}{\text{True Negative rate}}$$

- ⌘ *Positive predictive value (PPV)*: probability that the disease is present when the test is positive (expressed as a percentage).
  
- ⌘ *Negative predictive value (NPV)*: probability that the disease is not present when the test is negative (expressed as a percentage).

It is essential to use good quality images when testing and training a diagnostic test. Poor quality images reduce the tests ability to accurately classify features thus the overall performance of the system results in a low sensitivity and specificity.

### **3.5. SUMMARY**

Image processing techniques have the advantage of being able to manipulate images by deriving algorithms that allow the detection of discrete lesions associated with diabetic retinopathy. The benefits that arise from neural networks are that instead of just being able to detect lesions they can also be trained to identify discrete patterns. Thus they further provide a method of grading the progression of the disease.

Neural networks and conventional algorithmic computers are not in competition but complement each other. There are tasks more suited to an algorithmic approach like arithmetic operations and tasks that are more suited to neural networks. In essence, neural networks are mathematical constructs that emulate the processes people use to recognize patterns, learn tasks, and solve problems.

It would seem that the grading of DR images is such a widely varied task that a marriage between image processing techniques and neural networks should offer an efficient automated grading tool.

## **CHAPTER 4 - IMAGE DATA SET FORMULATION**

### **4.1. IMAGE ACQUISITION**

Digital imaging is a broad term applied to the recording of images electronically where what we perceive as different hues of colour are converted into a set of numbers. These numbers can then be manipulated through computer software programmes. This opens up the opportunity for images to be transmitted across computer networks.

#### **4.1.1. DIGITAL FUNDUS PHOTOGRAPHY**

Digital images are assigned numbers that correlate to the traditional black and white scale tonal values as taken from a photograph. Each tonal area is known as a pixel which is represented by a fixed number of bytes. Hence, the greater the number of pixels the greater the amount of computer storage required. When defining a pixel as a single byte grey scale value, white is represented by a value of 255 and black 0. The grey tones in between are divided into 255 equal steps. Similarly, when considering colour images these tonal steps are viewed in terms of the three primary colours (red, green and blue) the contribution of each again is expressed in the range of 0..255. Consequently, a colour pixel requiring 24 bits of computer storage space can be expressed as a value in the range of 0..16777215: depending upon the relative contribution of the RGB values.

#### **4.1.2. PHOTOGRAPHIC PROTOCOLS**

Digital photography has been outlined as the preferred modality for supplying a cost-effective national screening strategy for diabetic retinopathy between departments within the United Kingdom, *National Screening Committee 2004*.

It was proposed that a digital photographic modality should conform to the standards set by the EURODIAB protocol that requires 2 x 45 (or 50) degree fields of the retina to be acquired, *Aldington SJ et al. 1995, ETDRS 1991*.

The limitation on resolution in a digital system is determined by the physical size and quantity of pixels per degree. To record information, a feature needs to cover more than half the pixel, ideally covering several pixels for a more accurate representation to be recorded, *National Screening Committee 2004*.

#### **4.1.3. DIGITAL FUNDUS CAMERA SPECIFICATIONS**

A review of the available leading manufacturers digital fundus cameras was undertaken at the outset of the project. The fundamental specifications at this time included:

##### **✎ *Camera resolution and Field of View:***

- ✧ Does the camera provide enough resolution, which would allow the screener to identify the smallest of lesions that they would have detected had they been viewing through a direct ophthalmoscope?
- ✧ Does the camera's field angle encompass the angles recommended in the current standards?

##### **✎ *PC platform:***

- ✧ Does it support Windows thus enabling custom written software to be installed and run independently on the camera's PC for the automatic image classification after acquisition?
- ✧ Can the systems be networked allowing images to be reviewed at a single site by one ophthalmologist?

##### **✎ *Software handling:***

- ✧ Is there an archival system to be used for storing patient information details and photographic record data?

- ✧ Source Code. Does the system provide access to the raw data files for the images thus permitting low level image processing algorithms to be applied to the images?

The available cameras assessed at this time were:

☞ ***OCULab / Zeiss FF 450IR Fundus camera:***

- ✧ In this system the images were automatically digitised through an attached Sony three-chip CCD digital camera. The fundus camera can acquire images covering a field of either 50°, 30° or 20° with a resolution of 1534x1024 pixels in addition to a viewing magnification of 11x, 19x and 30x.

The OCULab system provides a range of image enhancement and pre-processing features alongside an inbuilt patient information database. Archiving can be achieved through either CD or MOD (magneto optical disc). Furthermore the OCULab system allows access to the ASCII data files thus allowing the transfer of raw data to be imported in spreadsheets, databases or indeed other software applications and has full Windows support for peripheral devices.

☞ ***IMAGEnet / Topcon TRC-NW6 series Fundus camera:***

- ✧ Images can be digitised through the integration of either a Nikon or Fuji CCD digital camera, therefore pixel resolution would be defined by the chosen camera's specifications. The fundus camera offers two fields of view, 45° or 30°.

IMAGEnet accompanying software provides a range of image enhancement programs and panoramic imaging of the retina through the application of its mosaic tool. It supports the acquisition, storage (via CD-ROM), retrieval and analysis of a variety of ophthalmic images. Operates with Windows 95 onwards and has Network capabilities installed.

❧ **RIS / Clement Clarke Canon CR6-45N Digital Fundus camera**

- ❖ Images can be digitised through the integration of a Canon CCD digital camera, therefore pixel resolution would be defined by the chosen camera's specifications. The fundus camera offers two fields of view, 45° or 30°.

RISLite (Retinal Imaging Solutions) is a digital imaging software platform which acquires, stores, retrieves and provides image analysis solutions specifically designed to interface with the Canon fundus camera.

The OCULab system was finally chosen as it had the added advantage that it provided direct access to the low level software, (Fig 4.1.)



*Fig 4.1. OCULab digital fundus camera system at GGH.*

## 4.2. IMAGE HANDLING

Images were acquired by the two trained Ophthalmic photographers at the Diabetic Review Clinic, Tennent Institute of Ophthalmology based in Gartnavel General Hospital, Glasgow UK. A purpose written software programme was developed using Borland Delphi for the integration of the digital fundus images with Neural Networks. The *Diabetic Retinopathy Image Classification Programme* (DRIC) was custom written to incorporate pre-processing image enhancement algorithms and designed with the overall prospect of providing an automated classification result for the patient being reviewed. Details of the features developed within the DRIC programme are described in this chapter; in addition a test version is also included along with the program source code (*see attached disc*).

### 4.2.1. BORLAND DELPHI

Delphi is a high level programming language that supports structured and object-oriented design. Its benefits include easy-to-read code, quick compilation, and the use of multiple unit files for modular programming.

Delphi allows the creation of programmes and provides the capacity to quickly develop applications. Programmes are usually divided into source-code modules called units where each unit is stored and compiled separately. Thus large programmes can be divided into smaller modules that can be edited separately.

### 4.2.2. DIABETIC RETINOPATHY IMAGE CLASSIFICATION PROGRAMME

The DRIC programme was developed as a robust system which would be able to offer image processing algorithms and neural network classifications. This involved designing a system that would be capable of extracting, classifying and retaining information from the images. Constructing datasets for training and testing purposes. Finally allowing comparison between any feature enhancement algorithms that may

be applied to the images. The source code written for the programme was the author's own work.

The current programme consists of 17 interconnecting Units, 1 parent form and 7 child forms, (Fig 4.2.). A summary of each unit's function can be seen in Table 4.1.

**DIABETIC RETINOPATHY IMAGE CLASSIFICATION PROGRAMME  
FUNCTIONCHART**

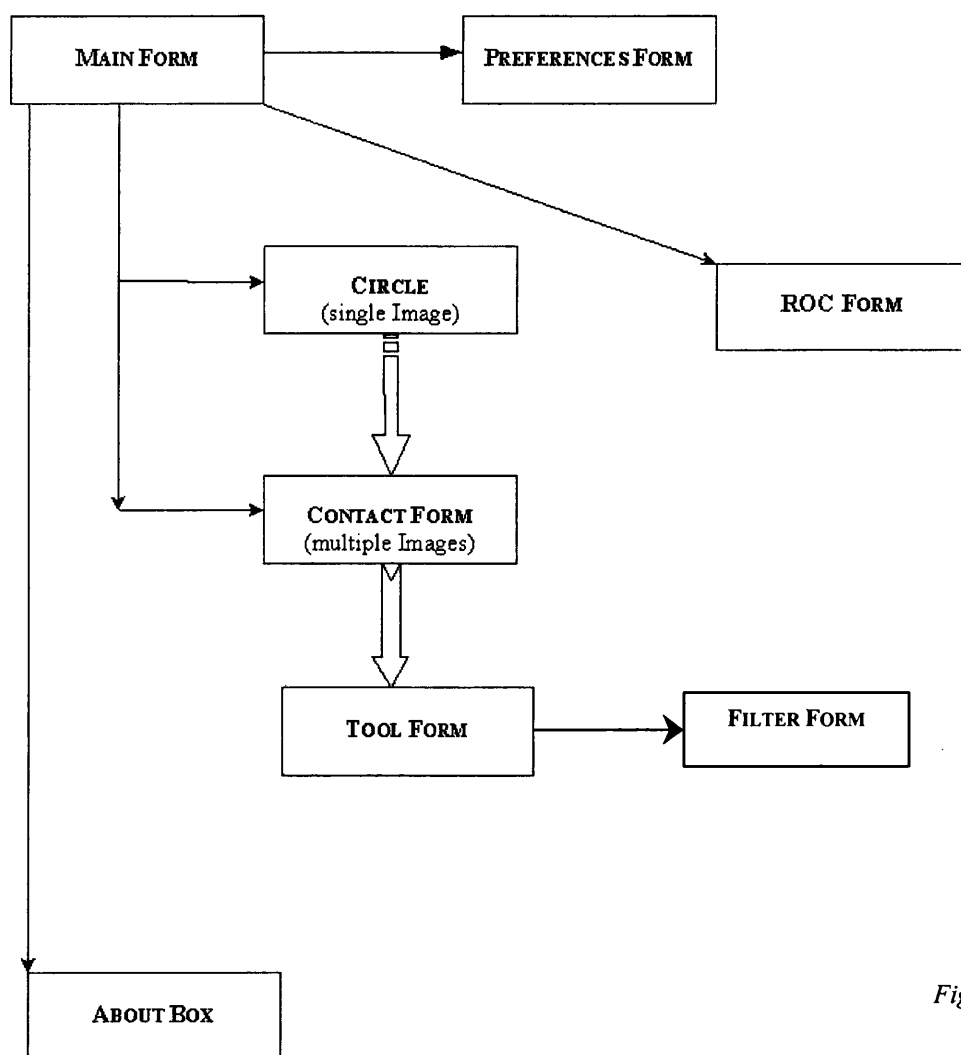


Fig 4.2 a).

### DIABETIC RETINOPATHY IMAGE CLASSIFICATION PROGRAMME PREFERENCES FUNCTIONS CHART

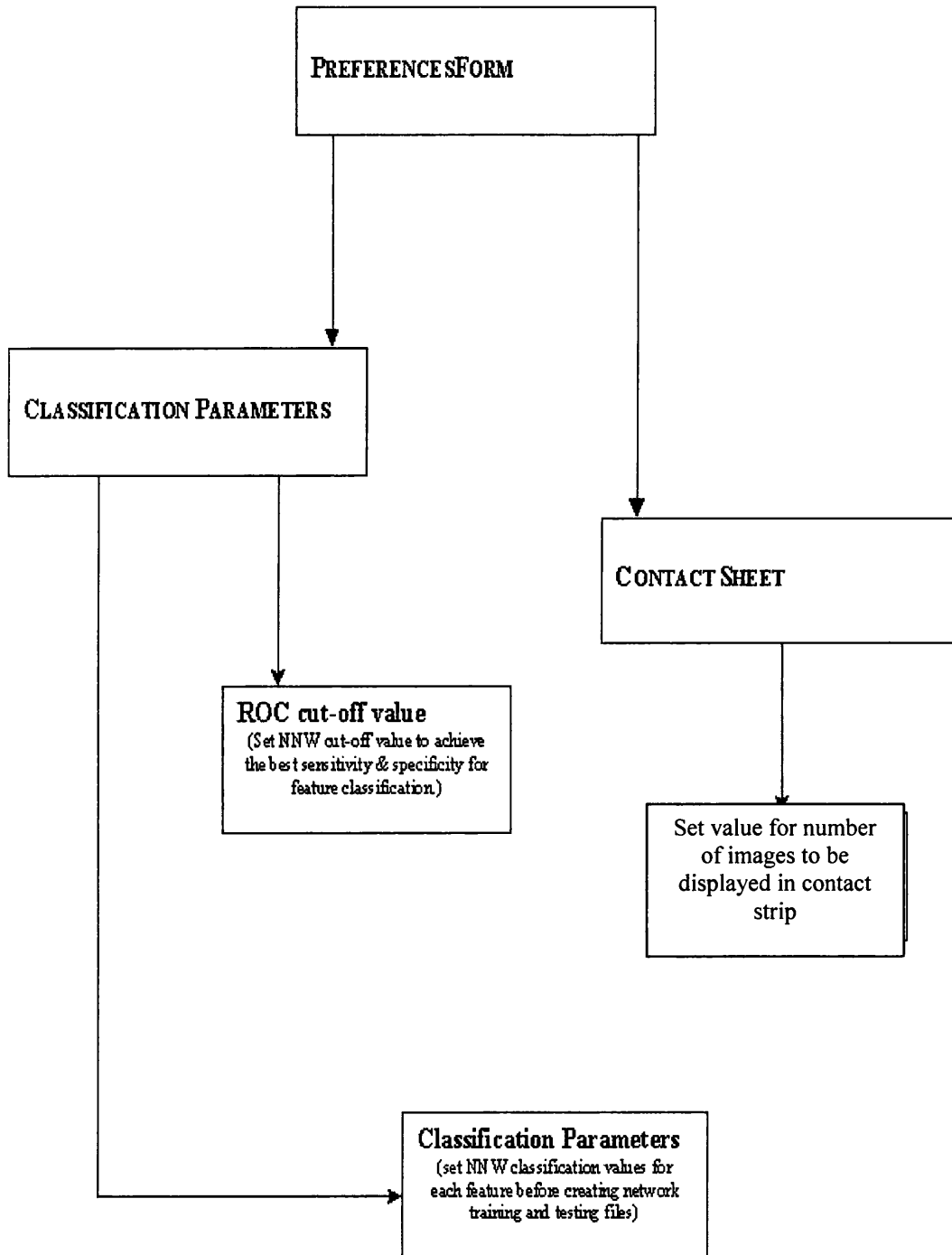


Fig 4.2b.

**DIABETIC RETINOPATHY IMAGE CLASSIFICATION PROGRAMME**

**TOOL FORM FUNCTIONS CHART**

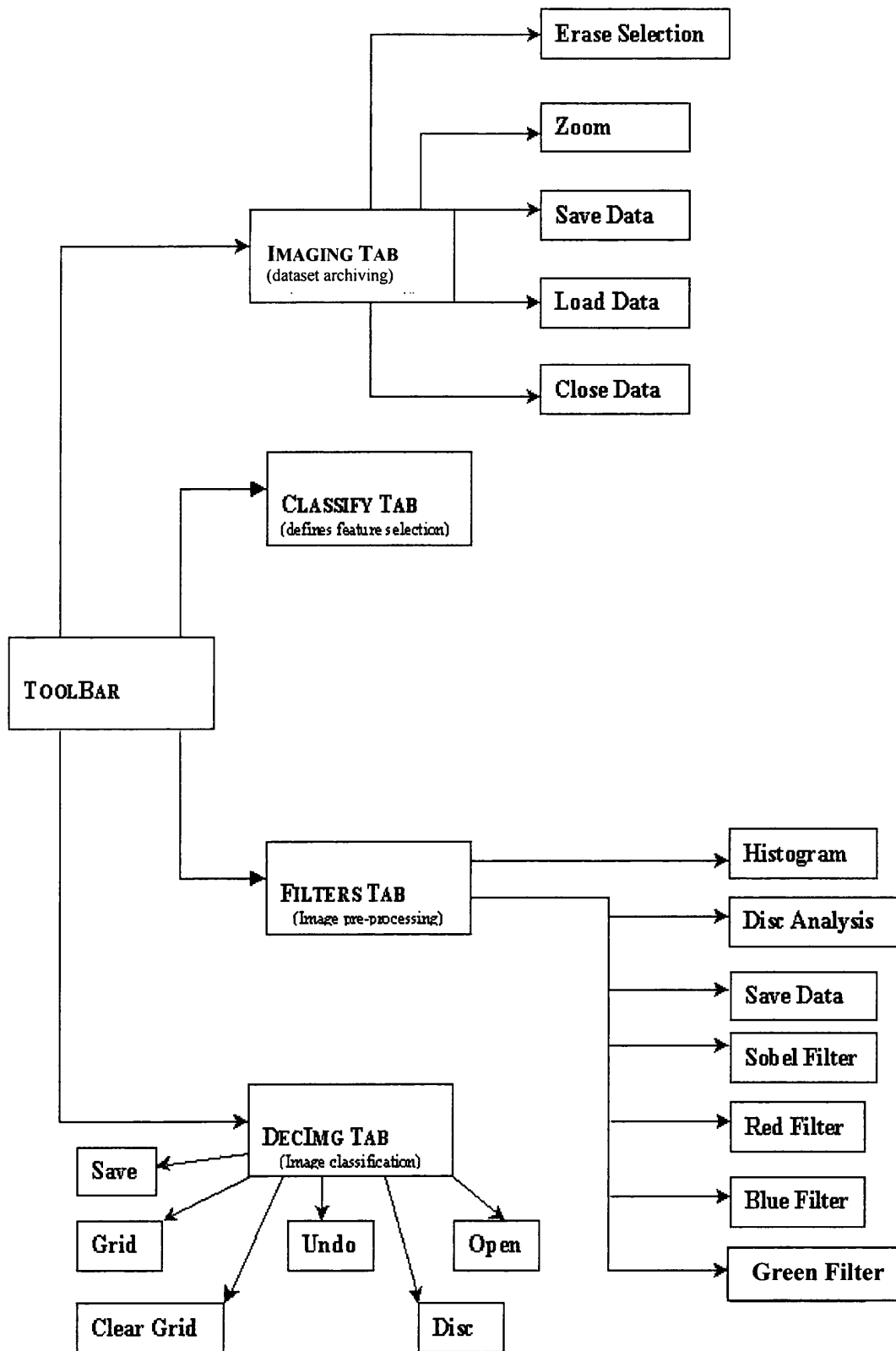


Fig 4.2c.

<i>Unit Name</i>	<i>Form Name</i>	<i>Purpose of Unit</i>
<b>About</b>	<b>AboutBox</b> (Child Window)	Contains procedures for the creation /closing and running of the AboutBox display.
<b>Circle</b>	<b>ChildWindow</b>	Holds child window global variables/ types, creates display boxes on mouse down events, responsible for opening current image.
<b>Contact</b>	<b>ContactForm</b> (Child Window)	Contains procedures which create/closes & highlights an image in the contact form. New procedure for batch filtering throughout all images in the contact.
<b>DataFuction</b>		Open NNW test set and results file to pull back image and find problem areas for the network.
<b>DecimateImage</b>		Dissects fundus images into 20x20 sequential boxes for full image classification.
<b>DiscAnalysis</b>		Creates an array to store the circumferential pixel values around the disc at interchangeable diameters, for later analysis of normal discs against discs exhibiting new vessel growth.
<b>Filter</b>		Contains procedures for performing image-processing filters on a selected image.
<b>FilterDisplay</b>	<b>FilterForm</b> (Child Window)	Creates and closes histogram form for the display of RGB colour distribution throughout a selected image.
<b>ImageArchive</b>		Contains Save/Load/SaveASCII Data procedures, which allow the saving and loading of dimension (*.dim) files to be used for the creation of neural network training and testing (*.nna) files.
<b>ImageFunction</b>		Extracts pixel RGB info from image within a selected cell, the classification & its top left XY co-ordinates and stores the entire information including image name in arrays with 9 variations of the cell.
<b>MainForm</b>	<b>Main</b> (ParentWindow)	Create child form applications, hold global variables, reacts to mouse movement on screen.

<i>Unit Name</i>	<i>Form Name</i>	<i>Purpose of Unit</i>
<b>OpDisplay</b>		Contains all display procedures from previously saved dim & nna files, redraws classified cells and NNW misclassified cells back onto its associated image.
<b>OpticDisc</b>		Calculates the location of the Optic Disc and macula for each fundus image.
<b>Preferences</b>	<b>frmPreferences</b> <i>(Child Window)</i>	Creates and closes pref. form. Factors that can be altered, no. of images per row in contact strip, classification value (must be changed when saving nna), NNW cut-off value k.
<b>ROCUnit</b>	<b>ROCform</b> <i>(Child Window)</i>	Contains the code to draw a ROC curve graph. Plots the sensitivity & specificity of a trained network & outputs the results on the graph.
<b>TiffToBmp</b>		Converts Oculab tiff images to bitmaps.
<b>Tools</b>	<b>ToolForm</b> <i>(Child Window)</i>	Contains all shortcuts to each feature that you wish to perform on an image from classifying images to saving test and dim files.

Table 4.1. Diabetic Retinopathy Image Classification Program unit summary

#### 4.2.2.1. MAIN / PARENT FORM

At the outset the user is presented with a blank form providing them with menu options for the links to the tasks available through the programme, (Fig 4.3.). The key areas of interest are housed within the ‘File’ and ‘Preferences’ dropdown menus.

The programme allows the user to review a single image at a time or multiple images. The number of images displayed on each row of the contact strip is governed by the preferences form accessed via ‘Show\_Preferences’.

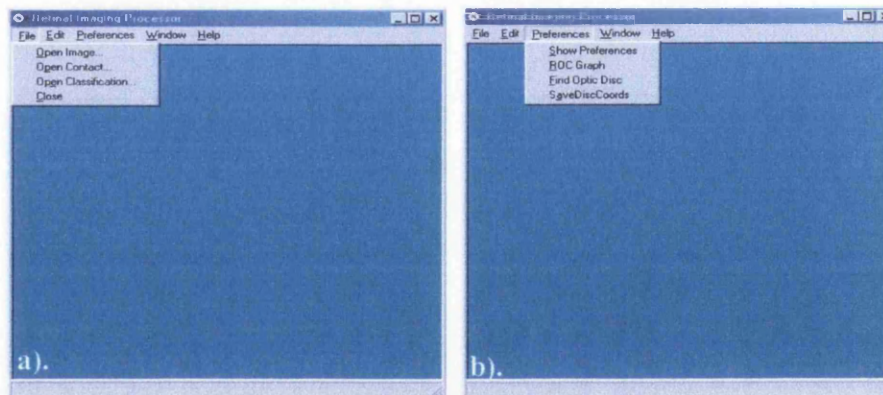


Fig 4.3. Screenshot of main form displaying options in a). File menu. b). Preferences menu.

#### 4.2.2.2. PREFERENCES FORM

The preferences form provides the user with the option of manually changing the default values and saving those changes if so desired, (Fig 4.4.). Changing the value to a higher or indeed a lower value via the spin-button can alter the number of images displayed on each row of the contact strip, bearing in mind that as the number of images in a row increases the thumbnail of the image displayed decreases.

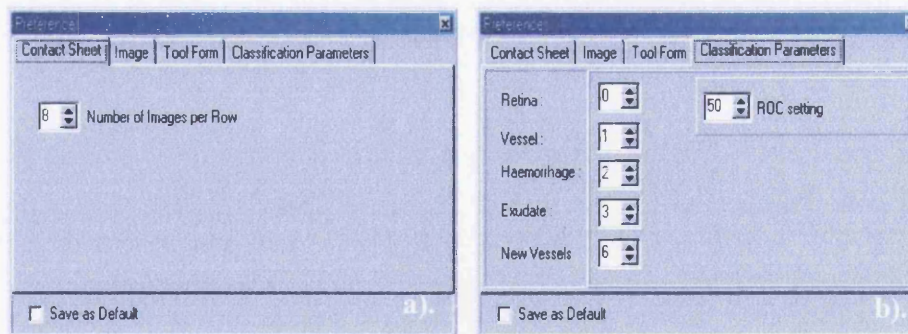


Fig 4.4. Screenshot of the two main option tabs in the preferences form a). sets the number of images displayed in each row of the contact strip. b). Offers the option to change the default feature identification tag and the default neural network cut-off values (which assumes anything below the set value is a normal feature and anything above is abnormal).

In addition feature identification tags can be altered from their default values for NNW training purposes. For simplicity it is better to work between normal (0) and abnormal (1) classification tags when training the NNW. Therefore when creating

neural network training files (\*.nna) these default values can be altered if necessary. During the training and testing process the NNW assumes that anything over a value of 0.5 is an abnormal feature and anything under is normal. However, this may not strictly be the best value in terms of achieving the best network performance. Therefore the Receiver Operator Curve (ROC) spin button allows the optimum cut-off value to be reset after ROC analysis, Chapter 3.4.1.

#### 4.2.2.3. RECEIVER OPERATING CHARACTERISTIC CURVE

In order to assess the optimum cut-off value between a normal or an abnormal feature the relative sensitivity and 1-specificity of each trained network was plotted on an ROC curve. This feature was custom written into the DRIC programme and is accessed from the Main Menu / Preference / ROC Graph, (Fig 4.5.).

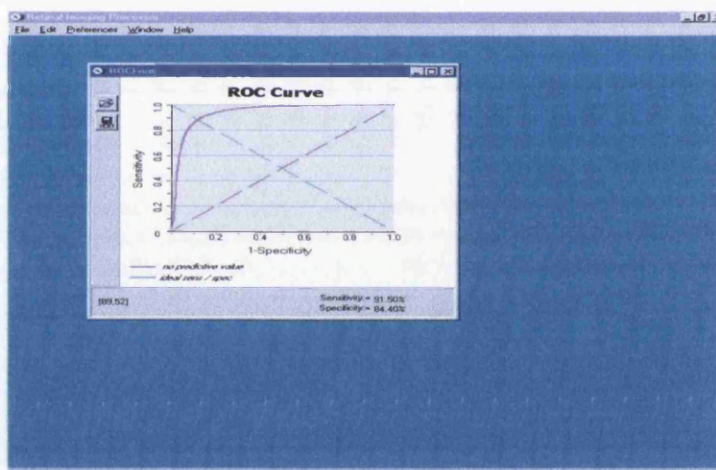


Fig 4.5. Screenshot of active ROC curve, displaying results taken from a trained neural network. The relative values of sensitivity/specificity are displayed in relation to the mouse position on the graph and outputted in the bottom right of the window. The complete range of sensitivity v specificity in 0.01 increments can be calculated and saved via the 'text' button.

The relative values for each point along the curve are displayed on screen corresponding to the current mouse position as it traces along the line of the curve. The optimum cut-off value is determined when the curve directly crosses the diagonal line plotted between  $y = 1$  &  $x = 1$  (green dashed line depicted in graph). Thereafter, the specificity begins to fall and the test becomes more unreliable. In

practical terms this would mean that a larger number of patients who were not displaying sight-threatening features of DR would be unnecessarily referred.

In addition to the visual display of the ROC curve, the calculated values for both the sensitivity and specificity at each cut-off value from 0 to 1 in increments of 0.01 is saved as a separate text file. The analysis of these files allows the operator to assess the optimum cut-off value to yield the highest sensitivity and specificity for specific features.

#### 4.2.2.4. CHILDWINDOW / CONTACTFORM – DISPLAYING AND PROCESSING IMAGES

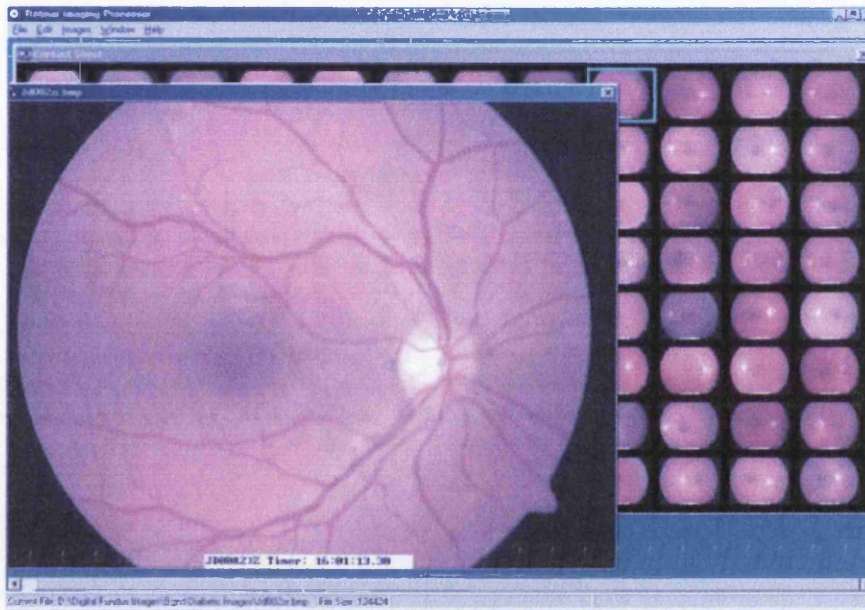


*Fig 4.6. Screenshot of contact strip and overlying image chosen for assessment. Green hotspot depicts which image is chosen.*

The units that directly govern the ChildWindow and ContactForm are circle.pas and contact.pas. These units provide code relevant to the selection and manipulation of the selected image(s).

Once the user has selected the file location of their fundus images to be viewed / analysed, the images are displayed on screen, (Fig 4.6.). From the contact strip only



☞ **Classify** tab:

This allows the random selection of the key features such as retina, vessel, exudates, haemorrhage etc. By clicking the left mouse button on the image the user is then identifying that central pixel and the surrounding pixels (covering an area of 20 x 20) as being a specific feature. A record of how many features have been selected is also displayed beside each one. The position of the mouse pointer is outputted at the bottom of the form.

☞ **Filters** tab:

Commencing with the buttons at the top, the first option is for the display of a histogram depicting the RGB colour distribution throughout the selected image. The second histogram style button is for saving the radial pixel colour information of the optic disc for analysis purposes. The third button is for saving individual neural network ASCII files (\*.nna), however this is more as a debug feature. The 'S' button performs a Sobel filter on the current image. Finally the last four buttons enable the image to be viewed in terms of its red, green and blue components or returned to its original RGB combined state.

☞ **DecImg** tab:

This provides the option for dividing the image into 20 x 20 pixel width boxes by superimposing a grid over the top of the image. In addition, there is an option to toggle between the original image and the 'grid' image without losing any of the selected cell information. The choice of which normal and diabetic retinal feature to be classified has to be pre-selected before classifying each cell. A cell to be associated with whichever feature selected at that time is chosen by highlighting that cell with the hotspot. There is also an undo button, which will delete the last selected cell. Each time a cell is classified the numerical display is updated keeping a tally of how many cells have been classified under the umbrella of each specific feature. Feature classification \*.dim files can be created and saved. The position of the mouse pointer is outputted at the bottom of the form.



### 4.3. DIGITAL FUNDUS IMAGES

Digital fundus images were acquired from the Diabetic review clinic based in the Tennent Institute of Ophthalmology at Gartnavel General Hospital (GGH) and were representative of random age populations. The attending ophthalmologist initially graded each image and completed a classification form for each patient they referred (*Fig 4.10.*). Details recorded included the patient name and hospital number solely for image retrieval purposes, a classification of the severity of the disease for each eye and whether the patient had undergone previous photocoagulation treatment. The images were subsequently graded by a specialist consultant ophthalmologist to address inter observer variability. These classifications can be seen in Appendix I.

Of the patients referred who had previously undergone laser treatment, only untreated areas displaying neovascularisation were extracted for training purposes: treated areas were not included in the data set. The effects of laser photocoagulation are illustrated in *Fig 4.11.*, initially the treated areas appear as brown circular lesions, (*Fig 4.11a.*). As the retina begins to heal the lesion fades. However the retina never returns to its original hue as when the laser beam interacts with the retinal tissue in addition to being absorbed by the retinal haemoglobin supply a certain amount of the beam is absorbed by and hence destroys the retinal pigment, thus leaving these areas hypo pigmented. Therefore the laser burns remain as pale lesions which could be misclassified as areas of exudates or cotton wool spots, (*Fig 4.11b.*).

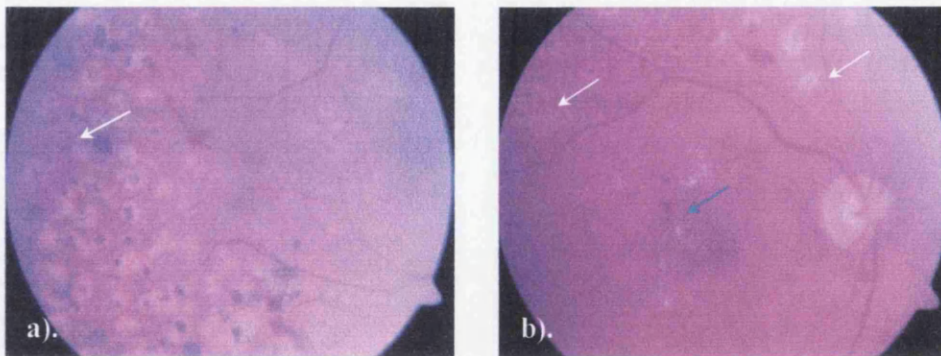
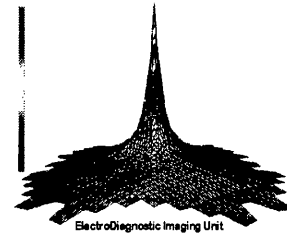


*Fig 4.11. a). Peripherally laser treated retina, dark brown lesions are areas recently photocoagulated. b). White arrows indicate areas of retina which have undergone photocoagulation treatment. At the outset the burns appear as brownish lesions, as they heal they become paler and could be mistaken for a cotton wool spot or exudates (blue arrow) by a neural network.*

# BRITISH DIABETIC ASSOCIATION

## *Diabetic Retinopathy Study*



ElectroDiagnostic Imaging Unit

**Ophthalmologist:** \_\_\_\_\_

**Date:** \_\_\_\_\_

**Affix Patient Details**

**NAME:**

**HOSPITAL NO.:**

**DOB :**

***Please send Patient for photography if they have:***

	<b>R</b>	<b>L</b>
<b><i>Maculopathy</i></b>	<input type="checkbox"/>	<input type="checkbox"/>
<b><i>New Vessels at Disc</i></b>	<input type="checkbox"/>	<input type="checkbox"/>
<b><i>New Vessels Elsewhere</i></b>	<input type="checkbox"/>	<input type="checkbox"/>
<b><i>Pre-Proliferative Retinopathy</i></b>	<input type="checkbox"/>	<input type="checkbox"/>
<b><i>Proliferative Retinopathy</i></b>	<input type="checkbox"/>	<input type="checkbox"/>
<b><i>Background Retinopathy</i></b>	<input type="checkbox"/>	<input type="checkbox"/>
<b><i>Has had previous laser treatment?</i></b>	<b>Y/N</b>	

Fig 4.10.

#### 4.4. FORMULATION OF DATA SETS

To make the training process faster each image was dissected into 1110 boxes, each of which was 20 x 20 pixels, (Fig 4.12.,4.13.). If the NNW were to be trained on the full image the overall training period would take days due to the large number of inputs and multiple outputs required. This would result in poorer sensitivities and specificities due to the large variance in features associated between individuals. Therefore it was decided to apply a multiple NNW approach and to dissect the image into localised areas. Each box would contain enough information to identify a feature while at the same time not requiring too many inputs that would slow the overall NNW training time. Boxes around the circumference of the retina and those containing the dark background were excluded from the data set; these areas accounted for 228 boxes. The remaining 882 boxes were manually classified as being *normal retina (0)*, *normal vessel (1)*, *haemorrhage (2)*, *exudate (3)*, *cotton wool spot (4)*, *venous abnormalities (5)* and *new vessels elsewhere (6)*.

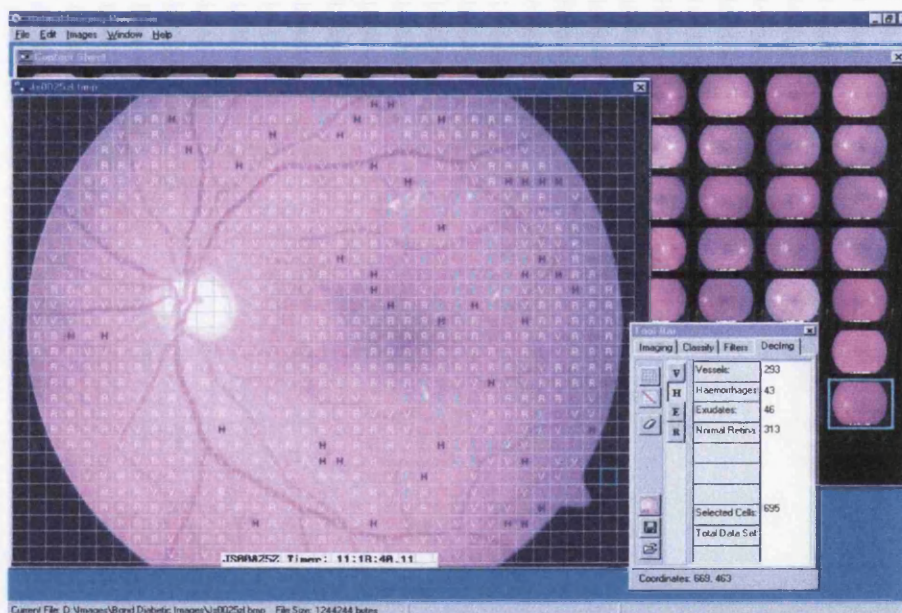


Fig 4.12. Each image is dissected into 20 x 20 pixel cells. The cells are then classified and assigned a character to show which type of feature resides within that area.

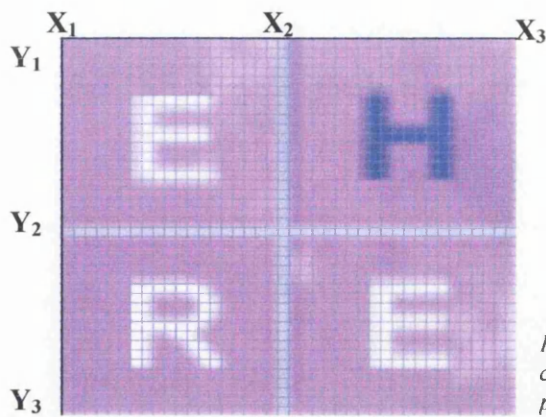


Fig 4.13. Magnified view of four classified cells. Each cell contains 400 individual pixels.

The co-ordinates and classification codes for each feature were saved as dimension files (\*.dim) for each image, hence permitting this information to be recalled at a later date for the construction of the neural network files.

Table 4.2. illustrates the number of images and the number of features collectively identified within these images. These images were used to form the NNW training and testing data sets and the final system validation. At this stage we concentrated our efforts on detecting the more abundant features associated with diabetic retinopathy.

<b>System Training &amp; Testing</b>		
<i>Number of Images &amp; Classification</i>	<i>Feature</i>	<i>Number of features</i>
<b>NNW training data set:</b>		
normal digital fundus images: 70 diabetic retinopathy digital fundus images: 70	Retina	8864
	Vessel	28533
	Exudate	3900
	Haemorrhage	8228
	New Vessels	334
<b>NNW test data set:</b>		
normal digital fundus images: 30 diabetic retinopathy digital fundus images: 30	Retina	3799
	Vessel	12228
	Exudate	1671
	Haemorrhage	3526
	New Vessels	143
<b>System Validation</b>		
<i>Number of Images &amp; Classification</i>	<i>Feature</i>	<i>Number of features</i>
Maculopathy: 11	Retina	4834
New Vessels at optic disc: 17	Vessel	4456
Background diabetic retinopathy: 28	Exudate	1207
Normals: 58	Haemorrhage	1072

Table 4.2. No of images collected for each classification

NNW training and testing files were generated through the batch function procedure which opened the associated \*.dim files for each image in the contact strip. The information incorporated in the neural network ASCII files were the 400 pixel colour values as the network input variables and the classification code used as the network output value; an example of a single classified feature can be seen in Appendix II. A comment line is included which is invisible to the network but provides the name of the image and the feature co-ordinates for later use.

#### **4.5. SUMMARY**

This chapter provides details of the specifications of the digital fundus camera selected and the collection and integration of images acquired. Details are provided of the custom written Diabetic Retinopathy Image Classification programme. This programme was developed to enable training and learning data sets to be automatically created in a syntax that was translatable to Neural Networks. In order to assess the optimum cut-off value between a normal or an abnormal feature the relative sensitivity and 1-specificity of each trained neural network a receiver operating characteristic curve feature was also incorporated into the DRIC programme. Other features of the DRIC programme include pre-processing image enhancement algorithms and the automated identification of the optic disc and macula. These will be discussed in detail in Chapter 5.

## CHAPTER 5 - PERFORMANCE TESTING ON MAIN RETINAL COMPONENTS

The benefits and procedures for diagnosing and the screening of diabetic retinopathy have been well recognized and guidelines have been set, *ETDRS 1991*.

The main objective when assessing the progression of DR is to identify the key features associated with the disease and to weigh up the severity of these features through their quantity and location. Therefore it is important to be able to identify normal retinal features i.e. the macula, optic disc and vessels as well as the abnormal features such as exudates and haemorrhages.

### 5.1. NORMAL BACKGROUND RETINA

If laid flat the normal human background retina is fairly uniform in colour and tone. However, in-vivo, the retina is technically not spherical it is a thin layer on the surface of a sphere and as such its uniformity is affected by discrepancies in illumination. Consequently, this may affect the performance of feature recognition algorithms. To minimise the adverse effects of this a Sobel matrix was applied to the green plane of images within the test and training data sets. This enhanced the features within the image (*Fig 5.1.*).

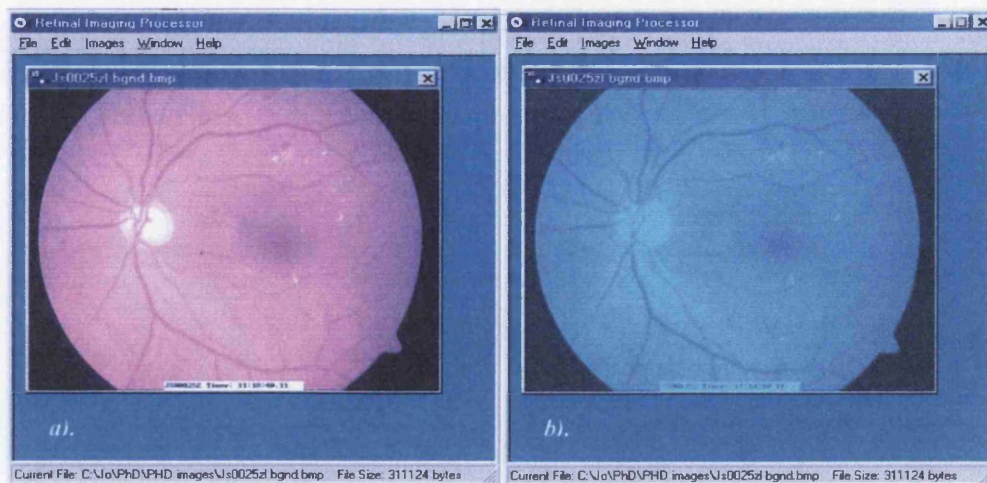


*Fig 5.1. a). RGB digital fundus image before processing. b). Post processed image with Sobel filter on green plane.*

## 5.2. LOCATING THE OPTIC DISC

Anatomically, the human optic disc is elliptical in shape and although it varies in size from person to person it has a typical vertical diameter of 1.5mm. In order to standardise the size of the optic disc as captured by the digital camera a random selection of 50 fundus images were analysed from the group of 100 normal images.

For each of the 50 images chosen the relative widths and heights were calculated by subtracting the  $x$  and  $y$  co-ordinates obtained by positioning the mouse pointer at the four widest points of the optic disc, (Fig 5.2.).

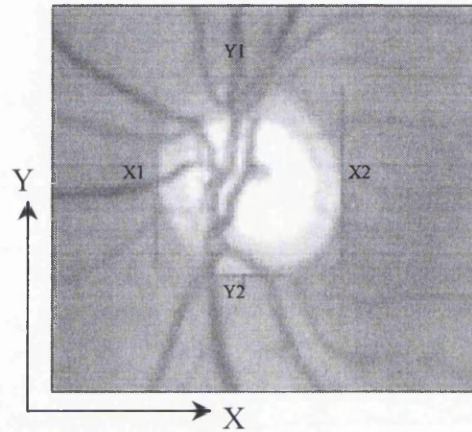


Fig 5.2. Calculating average dimension of optic disc taken from four widest points.

Therefore:  $Width = X_2 - X_1$   
&  $Height = Y_2 - Y_1$

The average width, height and standard deviation was calculated, the resultant optic disc region of interest (ROI) had a diameter of 90 pixels. We applied two approaches to automatically detect the optic disc, both techniques were based on taking advantage of the brighter hue of the disc against the more uniform orange of the retina. The first approach was by custom writing a piece of code in Delphi, the second was to employ a commercial pre-processing system Aphelion™.

### 5.2.1. METHOD 1 – CUSTOM WRITTEN SOFTWARE

An optic disc detection feature was written into the DRIC programme, (Fig 5.3.). In each image a sub box of equivalent dimensions to the optic disc (OSq) was scanned across the image in 20 pixel increments. For each stopping pixel (P) the TopLeft  $(i_1, j_1)$  & BottomRight  $(i_2, j_2)$  co-ordinates were stored in an array in addition to the corresponding 8100 RGB pixel colour values of the image: the position of the OD was initialised with  $OSq_{RMS} = 0$  and  $P_{(i_1, j_1)}, P_{(i_2, j_2)}$  co-ordinates of (0,0), (0,0). The

location of the optic disc was determined by calculating the root mean square (RMS) value of the associated box:

$$OSq_{RMS} = \text{SQRT} (\Sigma P_{RGB} / 8100)$$

For each subsequent box the location of the optic disc was altered only if the  $OSq_{RMS}$  value was greater than the preceding value. Thus the remaining values contained within the  $OSq_{RMS}$  array corresponded to the location of the OD.

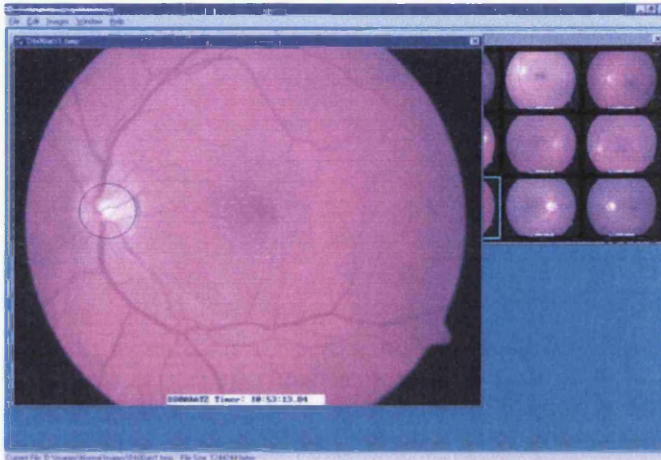


*Fig 5.3. Screenshot taken from DRICP, location of the optic disc is highlighted by encircling it with a blue ring for visual confirmation.*

### 5.2.2. METHOD 2 – COMMERCIAL SOFTWARE

The second method was to employ a commercial image-processing package (Aphelion™ 2.2 developer): the source code can be viewed in Appendix III.

Initially the RGB images were converted to HIS, next the intensity image was extracted and the image ID label excluded from the bottom. An optic disc ROI of 90x90 pixels was scanned across the image within a predefined area with a starting point of  $(80_{x1}, 80_{y1})$  and ending at  $(619_{x2}, 419_{y2})$ . The location of the OD was identified as the region with the highest percentage threshold based on the (max-min) value within the ROI, (Fig 5.4.).

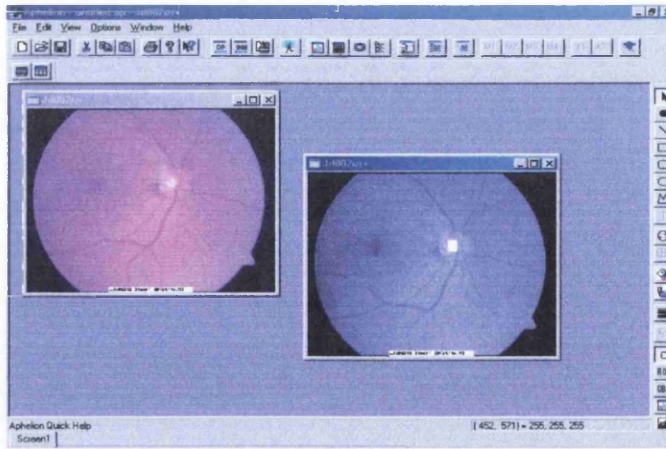


Fig 5.4. Screenshot taken from Aphelion™ disc detection macro where the white rectangle illustrates the ROI in relation to the centre of the disc.

### 5.2.3. AUTOMATED OPTIC DISC FINDINGS

A collection of fundus images were classified into two subgroups by an experienced ophthalmologist, G1 ~ normals, G2 ~ background DR. There were 100 posterior pole views ensuring good definition of the optic disc and macula in each group. G1 contained a 57 / 43 mix of left and right eyes, while G2 had a 53 / 47 split. The actual location of the disc was manually depicted and co-ordinates saved by a mouse-down function incorporated into the DRICP. The accuracy of each technique, Tables 4.1. & 4.2., was expressed as a result of the difference between the actual co-ordinates ( $i_d, j_d$ ) and the automated co-ordinates ( $i_1, j_1$ ):

$$r = \text{SQRT} ((i_1 - i_d)^2 + (j_1 - j_d)^2)$$

OD's in Normal Images										
I No.	Actual Co-ords		DRICP			Aph				
	ld	jd	i1	j1'	r1	i2	j2	r2	Mean r	r1-r2
1	225	124	231	139	16	232	135	13	14.5	3
2	189	96	191	102	6	190	101	5	5.5	1
3	228	82	225	89	8	231	87	6	7	2
4	211	141	219	144	9	219	143	8	8.5	1
5	226	121	217	123	9	235	121	9	9	0
6	212	519	209	513	7	211	512	7	7	0
7	145	127	137	140	15	149	138	12	13.5	3
8	235	174	227	185	14	231	184	11	12.5	3
9	290	169	291	171	2	291	169	1	1.5	1
10	244	488	249	481	9	248	482	7	8	2
11	269	103	271	107	4	273	109	7	5.5	-3
12	260	477	257	441	36	250	443	35	35.5	1
13	248	152	255	164	14	253	162	11	12.5	3
14	198	559	181	546	21	180	548	21	21	0
15	244	479	253	467	15	247	471	9	12	6
16	293	86	297	92	7	297	92	7	7	0
17	209	509	203	471	38	210	472	37	37.5	1
18	251	107	254	143	36	251	142	35	35.5	1
19	255	160	242	163	13	259	168	9	11	4
20	217	491	211	490	6	210	490	7	6.5	-1
21	226	479	229	476	4	230	475	6	5	-2
22	212	100	218	101	6	217	97	6	6	0
23	233	420	217	412	18	228	402	19	18.5	-1
24	235	213	222	223	16	243	225	14	15	2
25	226	170	205	183	25	235	174	10	17.5	15
26	239	530	233	522	10	233	522	10	10	0
27	248	116	257	125	13	255	123	10	11.5	3
28	236	114	235	123	9	235	122	8	8.5	1
29	181	520	157	521	24	179	526	6	15	18
30	229	113	231	111	3	235	117	7	5	-4
31	205	392	207	393	2	207	390	3	2.5	-1
32	187	516	184	510	7	184	510	7	7	0
33	227	101	233	109	10	231	107	7	8.5	3
34	266	411	261	398	14	262	398	14	14	0
35	186	89	203	101	21	197	107	21	21	0
36	214	458	217	454	5	217	455	4	4.5	1
37	236	200	251	191	17	251	188	19	18	-2
38	208	151	209	161	10	211	153	4	7	6
39	212	515	195	511	17	216	516	4	10.5	13
40	233	494	212	478	26	210	477	29	27.5	-3
41	212	99	219	121	23	220	119	22	22.5	1
42	201	549	183	554	19	197	535	15	17	4
43	217	189	228	191	11	227	188	10	10.5	1
44	271	564	284	549	20	283	548	20	20	0
45	291	153	299	163	13	299	162	12	12.5	1
46	251	208	253	220	12	253	219	11	11.5	1
47	188	538	197	530	12	195	529	11	11.5	1
48	236	524	249	510	19	249	510	19	19	0
49	203	521	213	490	33	212	490	32	32.5	1
50	251	103	259	135	33	259	112	12	22.5	21
51	209	462	205	453	10	205	453	10	10	0
52	215	180	211	187	8	211	185	6	7	2
53	209	515	215	510	8	215	510	8	8	0
54	183	79	183	110	31	185	94	15	23	16
55	223	517	235	495	25	233	495	24	24.5	1
56	251	128	257	142	15	257	142	15	15	0
57	247	162	251	173	12	252	180	19	15.5	-7
58	231	107	230	128	21	228	124	17	19	4
59	240	105	235	113	9	235	113	9	9	0
60	242	466	241	455	11	239	455	11	11	0

61	194	85	195	119	34	192	117	32	33	2
62	248	500	244	469	31	244	469	31	31	0
63	215	158	217	127	31	217	126	32	31.5	-1
64	206	140	209	150	10	209	150	10	10	0
65	213	99	211	109	10	209	104	6	8	4
66	241	469	237	466	5	235	464	8	6.5	-3
67	200	534	206	522	13	208	521	15	14	-2
68	252	188	257	232	44	260	213	26	35	18
69	229	119	221	119	8	220	118	9	8.5	-1
70	210	155	209	167	12	209	166	11	11.5	1
71	202	145	183	181	41	185	180	39	40	2
72	256	524	258	523	2	255	520	4	3	-2
73	238	145	233	152	9	233	146	5	7	4
74	265	181	261	195	15	268	187	7	11	8
75	257	441	267	420	23	262	419	23	23	0
76	196	119	194	128	9	194	128	9	9	0
77	232	540	229	503	37	235	505	35	36	2
78	171	93	195	123	38	188	121	33	35.5	5
79	211	529	211	520	9	217	506	24	16.5	-15
80	225	87	229	83	6	233	79	11	8.5	-5
81	195	492	193	488	4	194	487	5	4.5	-1
82	220	119	203	87	36	201	85	39	37.5	-3
83	217	499	225	494	9	223	491	10	9.5	-1
84	227	156	227	168	12	228	167	11	11.5	1
85	229	425	229	412	13	227	412	13	13	0
86	245	116	243	123	7	245	116	0	3.5	7
87	217	537	209	532	9	216	540	3	6	6
88	196	153	203	170	18	203	169	17	17.5	1
89	198	528	191	520	11	196	520	8	9.5	3
90	222	152	223	154	2	222	151	1	1.5	1
91	249	218	252	236	18	251	234	16	17	2
92	223	440	211	431	15	217	428	13	14	2
93	226	72	225	85	13	227	81	9	11	4
94	212	130	229	161	35	229	151	27	31	8
95	253	137	251	142	5	252	141	4	4.5	1
96	272	102	266	128	27	265	127	26	26.5	1
97	294	513	299	512	5	299	512	5	5	0
98	197	543	195	521	22	207	527	19	20.5	3
99	242	454	228	453	14	227	454	15	14.5	-1
100	255	555	263	543	14	264	544	14	14	0
	Mean		226.7	291.7	15.6	228.6	289.9	13.9	14.8	1.8
	SD		29.4	175.4	10.7	28.0	176.4	9.54	9.6	4.86

Table 5.1. Automatic optic disc findings on normal retinal images. *r* values depict how close in pixels the automated techniques placed the optic disc in comparison to its actual location when tested on 100 normal digital fundus images.

OD's in Diabetic Images										
I No.	Actual Co-ords		DRICP			Aph				
	Id	jd	i1	j1'	r1	i2	j2	r2	Mean r	r1-r2
1	73	185	91	171	18	81	197	14	16	4
2	565	220	553	217	12	548	222	17	14.5	-5
3	416	220	408	213	8	407	211	13	10.5	-5
4	172	204	181	192	9	186	203	14	11.5	-5
5	518	302	501	306	17	500	305	18	17.5	-1
6	531	181	528	183	3	527	186	6	4.5	-3
7	105	236	117	233	12	117	233	12	12	0
8	454	213	420	215	34	351	429	239	136.5	-205
9	495	145	89	301	406	471	160	28	217	378
10	467	241	459	250	8	457	248	12	10	-4
11	425	208	414	207	11	413	206	12	11.5	-1
12	84	222	93	234	9	91	233	13	11	-4
13	196	229	206	237	10	203	237	11	10.5	-1
14	485	241	474	248	11	475	245	11	11	0
15	486	188	479	191	7	474	193	13	10	-6
16	195	188	195	181	0	198	179	9	4.5	-9
17	437	273	430	255	7	427	268	11	9	-4
18	183	217	189	209	6	188	219	5	5.5	1
19	76	222	118	225	42	105	222	29	35.5	13
20	461	227	478	391	17	486	364	139	78	-122
21	433	228	420	231	13	420	228	13	13	0
22	88	221	93	205	5	88	209	12	8.5	-7
23	478	249	466	229	12	472	255	8	10	4
24	76	255	83	250	7	78	261	6	6.5	1
25	461	210	452	201	9	451	204	12	10.5	-3
26	115	236	120	229	5	116	237	1	3	4
27	513	247	506	243	7	506	243	8	7.5	-1
28	148	232	158	241	10	156	238	10	10	0
29	491	307	481	307	10	483	308	8	9	2
30	149	253	159	246	10	159	245	13	11.5	-3
31	105	262	115	267	10	113	265	9	9.5	1
32	164	220	166	205	2	173	213	11	6.5	-9
33	120	239	152	269	32	1	103	181	106.5	-149
34	100	191	136	194	36	136	195	36	36	0
35	233	223	267	225	34	268	223	35	34.5	-1
36	143	235	152	243	9	152	243	12	10.5	-3
37	108	286	119	291	11	117	290	10	10.5	1
38	481	265	479	259	2	480	259	6	4	-4
39	591	200	572	209	19	575	205	17	18	2
40	97	250	108	243	11	105	251	8	9.5	3
41	490	147	483	147	7	483	151	8	7.5	-1
42	38	218	57	218	19	51	217	13	16	6
43	197	254	196	241	1	203	255	6	3.5	-5
44	128	223	129	215	1	129	223	1	1	0
45	464	274	457	259	7	457	269	9	8	-2
46	413	222	413	243	0	412	243	21	10.5	-21
47	560	285	143	293	417	141	291	419	418	-2
48	47	276	57	281	10	57	282	12	11	-2
49	393	239	380	234	13	377	234	17	15	-4
50	531	262	529	273	2	529	273	11	6.5	-9
51	197	234	216	242	19	213	245	19	19	0
52	152	196	155	203	3	154	202	6	4.5	-3
53	532	238	531	239	1	531	239	1	1	0
54	403	250	437	265	34	436	265	36	35	-2
55	97	217	102	226	5	101	226	10	7.5	-5
56	581	272	583	275	2	583	274	3	2.5	-1
57	73	213	80	209	7	75	208	5	6	2
58	71	224	102	219	31	102	219	31	31	0
59	453	201	440	203	13	438	201	15	14	-2
60	165	211	383	89	218	176	205	13	115.5	205
61	457	246	456	221	1	449	231	17	9	-16

62	167	182	188	181	21	188	181	21	21	0
63	42	237	58	228	16	57	232	16	16	0
64	113	222	124	207	11	123	223	10	10.5	1
65	490	237	448	245	42	448	245	43	42.5	-1
66	509	223	496	213	13	492	227	17	15	-4
67	136	265	144	257	8	143	262	8	8	0
68	110	216	113	211	3	118	221	9	6	-6
69	436	185	434	185	2	431	184	5	3.5	-3
70	533	221	515	215	18	515	224	18	18	0
71	104	202	123	189	19	107	202	3	11	16
72	459	213	457	203	2	522	450	245	123.5	-243
73	182	215	198	203	16	197	210	16	16	0
74	521	227	503	226	18	506	226	15	16.5	3
75	142	194	147	199	5	147	199	7	6	-2
76	523	237	215	220	308	213	220	310	309	-2
77	127	257	129	237	2	141	254	14	8	-12
78	89	226	110	233	21	110	231	22	21.5	-1
79	186	221	194	223	8	192	221	6	7	2
80	476	249	468	253	8	466	251	10	9	-2
81	176	225	185	211	9	181	229	6	7.5	3
82	24	260	39	259	15	33	257	9	12	6
83	500	224	492	233	8	492	233	12	10	-4
84	193	223	240	217	47	227	221	34	40.5	13
85	170	280	191	281	21	188	281	18	19.5	3
86	516	237	515	249	1	515	249	12	6.5	-11
87	66	170	76	173	10	73	173	8	9	2
88	472	177	465	173	7	464	173	9	8	-2
89	78	299	94	307	16	92	305	15	15.5	1
90	412	242	379	227	33	397	237	16	24.5	17
91	112	267	122	271	10	121	271	10	10	0
92	55	213	428	279	373	399	304	356	364.5	17
93	108	207	380	339	272	379	339	301	286.5	-29
94	217	228	225	239	8	221	236	9	8.5	-1
95	447	258	406	251	41	436	261	11	26	30
96	425	204	418	187	7	415	204	10	8.5	-3
97	491	198	453	213	38	455	215	40	39	-2
98	189	252	198	259	9	196	259	10	9.5	-1
99	487	230	484	231	3	483	232	4	3.5	-1
100	530	264	522	265	8	525	265	5	6.5	3
	Mean		293.3	232.3	31.9	292.6	348	34.1	33.0	-2.2
	SD		170.6	40.2	79.0	173.7	47.9	75.5	71.8	57.5

Table 5.2..Automatic optic disc findings on diabetic retinopathy images. *r* values depict how close in pixels the automated techniques placed the optic disc in comparison to its actual location when tested on 100 background retinopathy digital fundus images.

From the 100 normal images assessed the DRICP successfully identified 98% of the OD's within a 40 pixel deviance while the technique applied using the Aphelion™ software correctly located 100%. Of the 100 background diabetic retinopathy images DRICP located 90% of the OD's within 40 pixels, while Aphelion™ located 91%. This range is further illustrated, (Fig 5.5.).

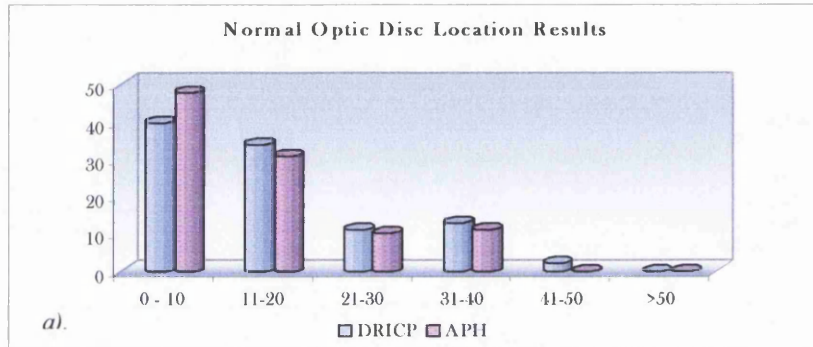


Fig 5.5. a) Histogram of results from 100 normal retinal images displayed within pixel accuracy to the actual disc location.

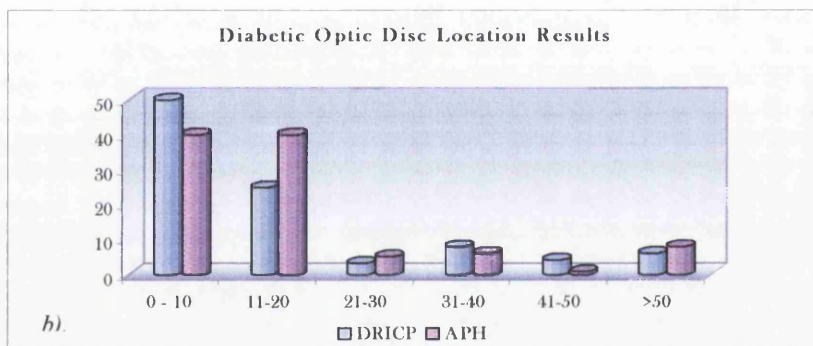


Fig 5.5. b) Histogram of results from 100 retinal images displaying background retinopathy features, results displayed within pixel accuracy to the actual disc location.

To assess the statistical correlation of both methods for detecting the optic disc the results were plotted on a series of Bland and Altman charts, *Bland and Altman 1986*. In the first instance the x co-ordinates and y co-ordinates are plotted from the DRICP along the x-axis and the results from Aphelion™ along the y axis. The results are displayed for both the normal and diabetic groups of images, (Fig 5.6. a & b). The plots show good linear correlation between both techniques for identifying the x ( $r = 0.97761$ ) & y ( $r = 0.99962$ ) co-ordinates in the normal images with poorer correlation shown in the diabetic images (x,  $r = 0.96196$ ; y,  $r = 0.56747$ ). However these plots only display the correlation between each technique and not the accuracy with which

each technique locates the optic disc. Therefore the high correlation between both techniques in identifying the individual x and y co-ordinates does not indicate the accuracy of these co-ordinates in comparison with the true values.

To determine the accuracy with which each technique located the OD with respect to the actual location the mean difference between the actual co-ordinates and the detected co-ordinates of each technique was calculated (r values Table 5.1. & 5.2.) Again the results were plotted for both groups of images, (*Fig 5.6 c & d*). The correlation between each technique was  $r = 0.882$  for the normal group and  $0.724$  for the diabetic group of images. In addition to displaying the correlation between both techniques this chart shows the accuracy with which each technique locates the optic disc where the closer the value to the origin the more accurate the co-ordinates.

Finally the mean difference of each technique against the difference of each technique in relationship to the actual co-ordinates is displayed within confidence intervals of 2SD, (*Fig 5.6, e & f*). In the normal group 7 optic discs were identified out with 2SD of the mean. However the location of these OD's were still within  $\frac{1}{2}$  disc diameter of the actual disc location. Six of optic discs identified in the diabetic group lay outside 2SD of the mean ( $r > 100$ ). In these instances a cluster of exudates were wrongly identified as being the optic disc.

The difference between the accuracy with which each method locates the optic disc arises from the technique applied. In the first method the optic disc location is solely reliant on the identification of the maximal pixel RGB intensity value. The second method identifies the OD as the region with the highest percentage threshold based on the (max-min) value within a region of interest.

The accuracy with which the optic disc was located was improved when combining the maximal volume intensity with the maximal pixel intensity value. Hence this was the preferred method for detecting the optic disc.

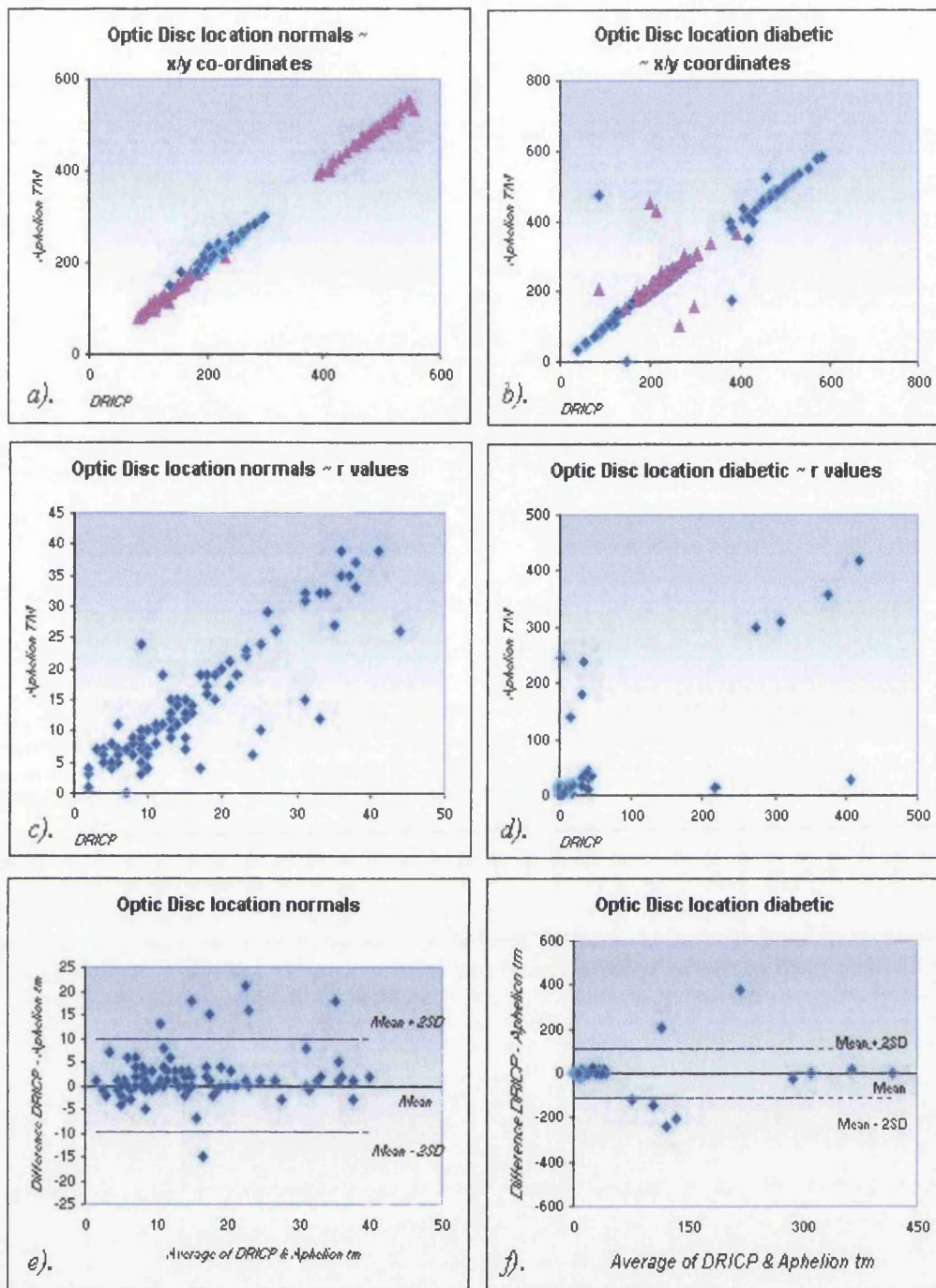


Fig 5.6. Statistical correlation plots for comparison of both techniques in the identification of the optic disc ~ a) shows good linear correlation between both techniques in the identification of the x & y co-ordinates in the normal group, b) shows slightly poorer linear correlation in the diabetic group, c),d) shows the correlation between each technique when calculated as the difference between the actual co-ordinates and the identified co-ordinates in the normal and diabetic groups respectively, e), f) shows the mean difference of each technique.

### **5.3. LOCATING THE MACULA**

The typical human macula is comparable in size to the optic disc. Its position within the retina is approximately 4mm temporal (or 2 ½ disc diameters to the left) and 0.8mm inferior to the centre of the optic nerve head.

The same two groups of images used in the detection of the optic disc were also used for the identification of the macula. In contrast to the optic disc, which is the object with the brightest hue object within the retina, the macula tends to be the darkest but with a comparable intensity to that of the vessels. A similar technique combining the optic disc location and minimum pixel intensity values were investigated for the identification of the macula.

The DRICP program looks for a minimum average intensity within the 90x90 pixel area and determines the location of the macula relative to the OD. Thus if the OD  $i_j$  co-ordinate is  $<360$  then the macula is on the disc's right hand side and on the left if  $>360$ . Similarly, in the Aphelion™ system macula detection uses the previously determined OD LLX & LLY: if the OD is on the right of the image (LLX $>360$ ), look for the minimum point in the region (OD LLX - 250,OD LLY - 100,OD LLX - 150,OD LLY + 100). If however, the OD is on the left of the image (LLX $<360$ ), look for the minimum in the region (OD LLX + 150,OD LLY - 100,OD LLX + 250,OD LLY + 100). The analysis was performed initially in 10 pixel steps for the ROI coordinates, then in one-pixel steps over the first maximum volume -10 to +10. The Aphelion™ system macula detection code can be seen in Appendix IV.

The macula detection results are displayed in Tables 5.3. & 5.4..

Macula's in Normal Images										
I No.	Actual Co-ords		DRICP			Aph				
	Im	jm	i1	j1'	r1	i2	j2	r2	Mean r	r1-r2
1	367	243	335	197	32	358	234	13	22.5	19
2	281	227	295	223	14	280	211	16	15	-2
3	282	255	295	223	13	311	221	45	29	-32
4	364	243	353	253	11	387	228	27	19	-16
5	319	226	322	248	3	317	227	2	2.5	1
6	295	259	292	253	3	292	243	16	9.5	-13
7	330	202	333	205	3	316	205	14	8.5	-11
8	414	281	333	205	81	411	292	11	46	70
9	406	284	333	205	73	404	267	17	45	56
10	255	283	250	211	5	256	283	1	3	4
11	321	294	314	197	7	322	294	1	4	6
12	252	281	186	215	66	246	293	13	39.5	53
13	380	262	186	215	194	381	256	6	100	188
14	339	215	331	213	8	319	196	28	18	-20
15	254	251	264	221	10	242	249	12	11	-2
16	314	299	334	199	20	326	297	12	16	8
17	312	239	188	245	124	307	229	11	67.5	113
18	307	272	339	209	32	305	256	16	24	16
19	376	289	354	206	22	376	283	6	14	16
20	272	260	280	247	8	268	241	19	13.5	-11
21	254	273	215	195	39	246	290	19	29	20
22	328	215	320	249	8	325	217	4	6	4
23	188	262	191	253	3	188	252	10	6.5	-7
24	439	252	191	253	248	476	236	40	144	208
25	397	259	191	253	206	388	247	15	110.5	191
26	293	274	221	201	72	300	274	7	39.5	65
27	350	288	327	203	23	346	305	17	20	6
28	338	266	341	203	3	340	256	10	6.5	-7
29	283	210	292	201	9	284	210	1	5	8
30	350	273	327	199	23	343	246	28	25.5	-5
31	180	233	182	241	2	163	226	18	10	-16
32	300	227	286	221	14	303	221	7	10.5	7
33	308	239	334	201	26	296	232	14	20	12
34	183	243	184	230	1	166	260	24	12.5	-23
35	327	205	323	234	4	313	199	15	9.5	-11
36	250	277	237	253	13	248	258	19	16	-6
37	413	260	237	253	176	437	268	25	100.5	151
38	383	232	352	253	31	378	232	5	18	26
39	279	247	273	243	6	246	230	37	21.5	-31
40	255	281	253	251	2	248	267	16	9	-14
41	321	265	335	251	14	321	238	27	20.5	-13
42	333	246	347	231	14	329	221	25	19.5	-11
43	391	223	347	231	44	411	212	23	33.5	21
44	360	291	319	207	41	354	288	7	24	34
45	385	323	354	228	31	387	315	8	19.5	23
46	424	286	354	228	70	441	289	17	43.5	53
47	327	231	337	231	10	313	227	15	12.5	-5
48	306	242	202	195	104	296	227	18	61	86
49	285	230	284	244	1	314	226	29	15	-28
50	348	231	345	223	3	325	233	23	13	-20
51	262	247	257	251	5	256	238	11	8	-6
52	403	235	257	251	146	387	229	17	81.5	129
53	283	232	280	247	3	298	233	15	9	-12
54	278	250	354	219	76	289	209	42	59	34
55	302	234	241	195	61	297	228	8	34.5	53
56	358	286	334	197	24	373	305	24	24	0
57	396	262	334	197	62	404	260	8	35	54
58	331	252	337	197	6	326	254	5	5.5	1
59	328	255	334	199	6	327	248	7	6.5	-1
60	252	278	205	197	47	248	278	4	25.5	43
61	298	220	310	226	12	299	221	1	6.5	11

62	280	242	272	213	8	293	235	15	11.5	-7
63	402	268	354	249	48	385	255	21	34.5	27
64	348	259	346	249	2	350	255	4	3	-2
65	302	231	304	242	2	308	226	8	5	-6
66	248	267	231	195	17	246	256	11	14	6
67	295	220	295	237	0	291	213	8	4	-8
68	430	268	295	237	135	447	261	18	76.5	117
69	344	247	338	252	6	348	231	16	11	-10
70	369	248	338	252	31	373	246	4	17.5	27
71	356	230	338	252	18	375	204	32	25	-14
72	300	284	286	199	14	296	305	21	17.5	-7
73	350	261	346	201	4	361	248	17	10.5	-13
74	396	253	346	201	50	400	250	5	27.5	45
75	228	277	224	207	4	228	261	16	10	-12
76	338	220	333	225	5	352	226	15	10	-10
77	303	256	256	195	47	301	241	15	31	32
78	323	216	322	226	1	322	213	3	2	-2
79	310	257	319	251	9	309	241	16	12.5	-7
80	308	250	343	197	35	309	239	11	23	24
81	298	255	288	253	10	287	248	13	11.5	-3
82	354	241	352	241	2	344	239	10	6	-8
83	319	266	352	241	33	317	249	17	25	16
84	370	242	352	241	18	372	244	3	10.5	15
85	214	253	188	197	26	200	262	17	21.5	9
86	304	255	334	199	30	300	244	12	21	18
87	332	255	333	247	1	320	242	18	9.5	-17
88	369	242	333	247	36	374	232	11	23.5	25
89	315	249	317	249	2	308	246	8	5	-6
90	385	237	317	249	68	385	202	35	51.5	33
91	449	281	317	249	132	472	277	23	77.5	109
92	221	271	220	253	1	225	262	10	5.5	-9
93	317	255	220	253	97	321	261	7	52	90
94	344	260	354	196	10	349	243	18	14	-8
95	379	276	342	201	37	370	261	17	27	20
96	319	277	333	203	14	327	255	23	18.5	-9
97	309	337	278	229	31	309	341	4	17.5	27
98	317	233	314	241	3	310	232	7	5	-4
99	238	287	235	197	3	244	272	16	9.5	-13
100	320	297	256	195	64	319	288	9	36.5	55
	Mean		295.8	224.9	34.7	322	248.2	14.9	24.8	19.9
	SD		60.8	21.5	59.8	84.7	48.3	56.9	25.2	47.1

Table 5.3. Automatic macula detection on normal retinal images. *r* values depict how close in pixels the automated techniques placed the macula in comparison to its actual location when tested on 100 normal retinal digital fundus images.

Macula in Diabetic Images										
I No.	Actual Co-ords		DRICP			Aph			Mean r	r1-r2
	Im	jm	i1	j1'	r1	i2	j2	r2		
1	314	230	311	233	3	309	229	5	4	-2
2	324	242	319	251	5	325	244	2	3.5	3
3	206	256	192	245	14	205	251	5	9.5	9
4	393	264	192	245	201	390	254	10	105.5	191
5	300	295	257	237	43	296	299	6	24.5	37
6	320	233	327	237	7	311	225	12	9.5	-5
7	324	226	337	201	13	322	218	8	10.5	5
8	241	249	192	253	49	610	486	439	244	-390
9	258	214	285	213	27	265	212	7	17	20
10	258	258	190	217	68	229	252	30	49	38
11	182	242	177	245	5	143	116	132	68.5	-127
12	312	267	336	201	24	328	264	16	20	8
13	422	253	336	201	86	462	257	40	63	46
14	243	290	186	201	57	216	280	29	43	28
15	273	212	276	225	3	252	197	26	14.5	-23
16	410	229	276	225	134	419	233	10	72	124
17	222	301	188	197	34	207	272	33	33.5	1
18	420	231	188	197	232	432	229	12	122	220
19	292	229	188	197	104	288	242	14	59	90
20	245	242	251	242	6	233	274	34	20	-28
21	202	243	225	195	23	201	239	4	13.5	19
22	296	270	293	253	3	295	259	11	7	-8
23	265	270	185	195	80	257	252	20	50	60
24	310	295	316	195	6	300	291	11	8.5	-5
25	230	247	228	249	2	212	242	19	10.5	-17
26	349	265	348	197	1	335	269	15	8	-14
27	285	290	256	195	29	289	292	4	16.5	25
28	372	244	353	205	19	351	244	21	20	-2
29	276	302	185	253	91	290	309	16	53.5	75
30	360	277	350	209	10	351	266	14	12	-4
31	316	277	348	225	32	322	273	7	19.5	25
32	374	261	348	225	26	366	247	16	21	10
33	323	293	348	210	25	255	182	130	77.5	-105
34	313	210	340	232	27	325	213	12	19.5	15
35	460	238	340	232	120	462	243	5	62.5	115
36	375	282	348	205	27	373	269	13	20	14
37	338	308	347	247	9	336	312	4	6.5	5
38	262	307	272	209	10	259	306	3	6.5	7
39	360	233	353	247	7	362	231	3	5	4
40	292	246	310	195	18	295	245	3	10.5	15
41	290	199	184	199	106	292	196	4	55	102
42	279	233	276	252	3	277	258	25	14	-22
43	414	297	276	252	138	440	305	27	82.5	111
44	365	279	327	249	38	364	281	2	20	36
45	222	276	183	197	39	221	271	5	22	34
46	177	232	177	207	0	163	232	14	7	-14
47	334	282	350	253	16	363	283	29	22.5	-13
48	291	285	273	209	18	289	283	3	10.5	15
49	195	246	187	201	8	107	313	111	59.5	-103
50	310	268	276	220	34	313	244	24	29	10
51	393	285	276	220	117	410	285	17	67	100
52	382	207	348	239	34	368	214	16	25	18
53	304	208	333	197	29	314	200	13	21	16
54	181	308	177	217	4	166	300	17	10.5	-13
55	323	259	352	195	29	307	229	34	31.5	-5
56	348	283	343	225	5	337	277	13	9	-8
57	291	243	288	251	3	298	230	15	9	-12
58	302	231	309	250	7	308	233	6	6.5	1
59	233	244	233	251	0	218	236	17	8.5	-17
60	400	252	233	251	167	402	245	7	87	160
61	208	249	200	253	8	213	251	5	6.5	3

62	421	234	200	253	221	447	91	145	183	76
63	284	252	310	197	26	277	248	8	17	18
64	337	246	334	251	3	321	244	16	9.5	-13
65	257	263	222	213	35	253	266	5	20	30
66	300	293	225	249	75	290	295	10	42.5	65
67	354	293	340	219	14	361	296	8	11	6
68	334	244	325	245	9	329	241	6	7.5	3
69	210	225	198	235	12	217	225	7	9.5	5
70	309	255	304	253	5	296	303	50	27.5	-45
71	340	219	334	221	6	318	230	25	15.5	-19
72	265	246	266	251	1	252	360	115	58	-114
73	404	257	266	251	138	404	247	10	74	128
74	293	259	268	195	25	298	246	14	19.5	11
75	363	224	354	234	9	378	216	17	13	-8
76	306	236	354	234	48	363	237	57	52.5	-9
77	362	268	320	197	42	400	284	41	41.5	1
78	306	234	303	199	3	294	238	13	8	-10
79	404	250	303	199	101	404	235	15	58	86
80	253	253	215	217	38	251	245	8	23	30
81	420	258	215	217	205	440	265	21	113	184
82	252	277	351	215	99	253	273	4	51.5	95
83	279	201	261	197	18	268	228	29	23.5	-11
84	421	251	261	197	160	412	247	10	85	150
85	398	320	261	197	137	413	321	15	76	122
86	296	271	237	209	59	296	261	10	34.5	49
87	294	188	290	205	4	293	187	1	2.5	3
88	250	216	250	225	0	253	211	6	3	-6
89	319	318	349	215	30	307	323	13	21.5	17
90	194	261	188	195	6	176	253	20	13	-14
91	357	306	337	195	20	372	324	23	21.5	-3
92	282	248	227	235	55	238	241	45	50	10
93	338	220	183	235	155	109	418	303	229	-148
94	439	238	183	235	256	473	220	38	147	218
95	219	238	211	215	8	207	224	18	13	-10
96	196	241	186	241	10	197	236	5	7.5	5
97	232	240	236	251	4	241	236	10	7	-6
98	411	253	236	251	175	431	254	20	97.5	155
99	256	218	276	195	20	274	225	19	19.5	1
100	298	267	281	213	17	298	237	30	23.5	-13
	Mean		271.6	222.8	47.3	307.5	255.2	28.2	37.7	19.2
	SD		60.8	21.5	59.8	84.7	48.3	56.9	43.9	77.0

Table 5.4. Automatic macula detection on diabetic retinopathy images. *r* values depict how close in pixels the automated techniques placed the macula in comparison to its actual location when tested on 100 background retinopathy digital fundus images.

The accuracy of each technique is defined by its ability to locate the macula within a 40 pixels distance of its actual position. Of the 100 normal images assessed the DRICP identified 74% while the technique applied using the Aphelion™ software identified 98% within this range. For the 100 background diabetic retinopathy images DRICP identified 69% and Aphelion™ identified 89%. The range of deviance from the actual macula location is displayed, (Fig 5. 7).

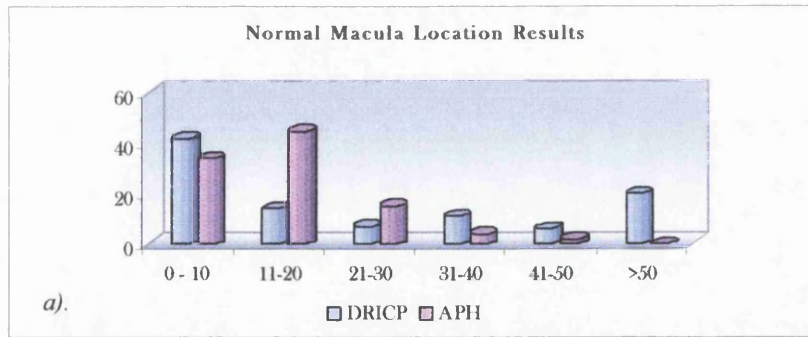


Fig 5.7. a) Histogram of results from 100 normal retinal images, results displayed within pixel accuracy to the actual macula location.

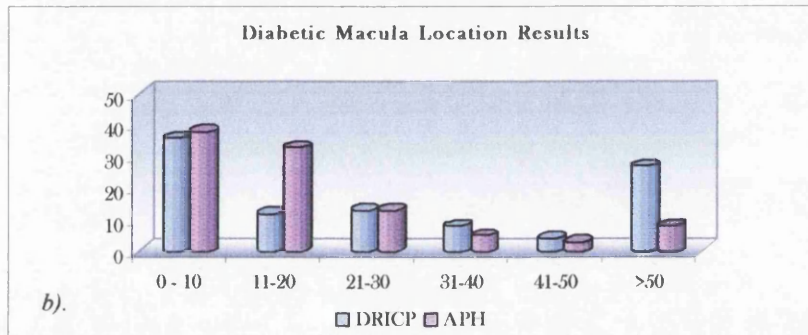


Fig 5.7. b) Histogram of results from 100 retinal images displaying background retinopathy features, results displayed within pixel accuracy to the actual macula location.

Again the statistical correlation of both methods for detecting the macula were assessed and displayed on a series of Bland and Altman charts, *Bland and Altman 1986*. The first graph displays the x co-ordinates and y co-ordinates of the DRICP plotted along the x axis and the results from Aphelion™ technique plotted along the y axis for the same group of normal and diabetic images, (*Fig 5.8. a & b*). The linear correlation between both techniques was  $r = 0.512$  &  $0.378$  for the x co-ordinates of both groups of images respectively and  $r = 0.309$  &  $0.048$  for the y co-ordinates. Unlike the results for the optic disc there is less of a correlation between the two techniques in macula identification.

Therefore to evaluate the accuracy of each technique in identifying the macula with respect to its true location the mean difference between the actual co-ordinates and the detected co-ordinates was calculated (r values Table 5.3. & 5.4.) and plotted for both groups of images, (*Fig 5.8 c & d*). The correlation between each technique was  $r = 0.178$  and  $0.130$  for the normal and diabetic group of images respectively. In

addition to displaying the correlation between both techniques this chart shows the accuracy with which each technique locates the macula where the closer the value to the origin the more accurate the co-ordinates.

Finally the mean difference of each technique was plotted within confidence intervals of 2SD, (*Fig 5.8, e & f*). Only 12 images lay out with 2SD of the combined test images.

Once again the method by which each technique locates the macula differs but this time producing a more striking difference between the results. There was only a slight difference between the two techniques performance in locating the optic disc: the Aphelion<sup>TM</sup> method was only marginally superior by 2% in the normal group and 1% in the DR group of images. However it outperformed the DRICP by 24% and 20% in the normal and DR groups respectively when applied to the task of identifying the macula.

One reason for the poor performance of the DRICP method is due to its dependency upon successful detection of the optic disc. If the disc is wrongly located then it is highly unlikely that the macula will correctly be identified as the programme is designed to find the lowest intensity pixel value in a predefined ROI from the disc location. Although correctly identifying the minimal pixel within that ROI it does not necessarily correspond to the overall minimal pixel intensity value that would be located within the centre of the macula.

The preferred method for detecting the macula was once again the technique using the Aphelion<sup>TM</sup> software system. It combined volume intensity values with the minimal pixel intensity value and used the optic disc location only as a guide as to whether the macula will be on the right or left of the image.

The overall purpose of being able to identify the optic disc and the macula region is that it enables localised analysis of these key retinal regions to be performed. For example once the optic disc has been located analysis of its vessel appearance can be

performed to determine if there is evidence of new vessel formation. Similarly we can analyse the macular region for features associated with diabetic maculopathy.

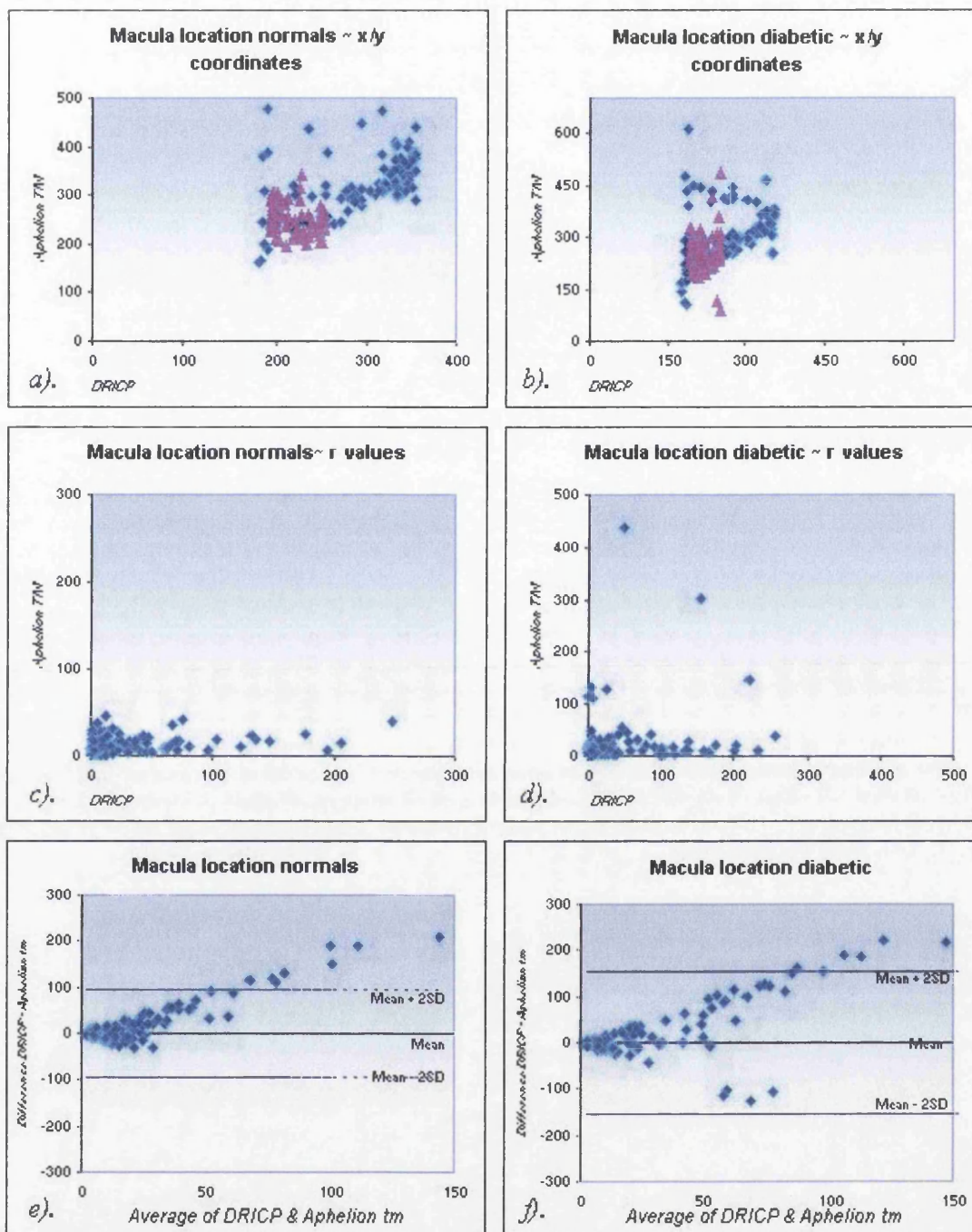


Fig 5.8. Statistical correlation plots for comparison of both techniques in the identification of the macula ~ a), b) shows the linear correlation between both techniques in the identification of the x & y coordinates in the normal and diabetic groups respectively, c), d) shows the correlation between each technique when calculated as the difference between the actual co-ordinates and the identified co-ordinates in the normal and diabetic groups respectively, e), f) shows the mean difference of each technique.

#### 5.4. RETINAL VASCULATURE RECOGNITION

One method of making vessels more distinguishable from background retina is by extracting only the information from the green plane as the red and blue planes provide very little additional information. To further enhance the visual distinction between background retina with vessels, new vessels, haemorrhages & exudates a Sobel edge detection filter was applied to the images to emphasise feature edges see Chapter 4.2.1, (Fig 5.9.).

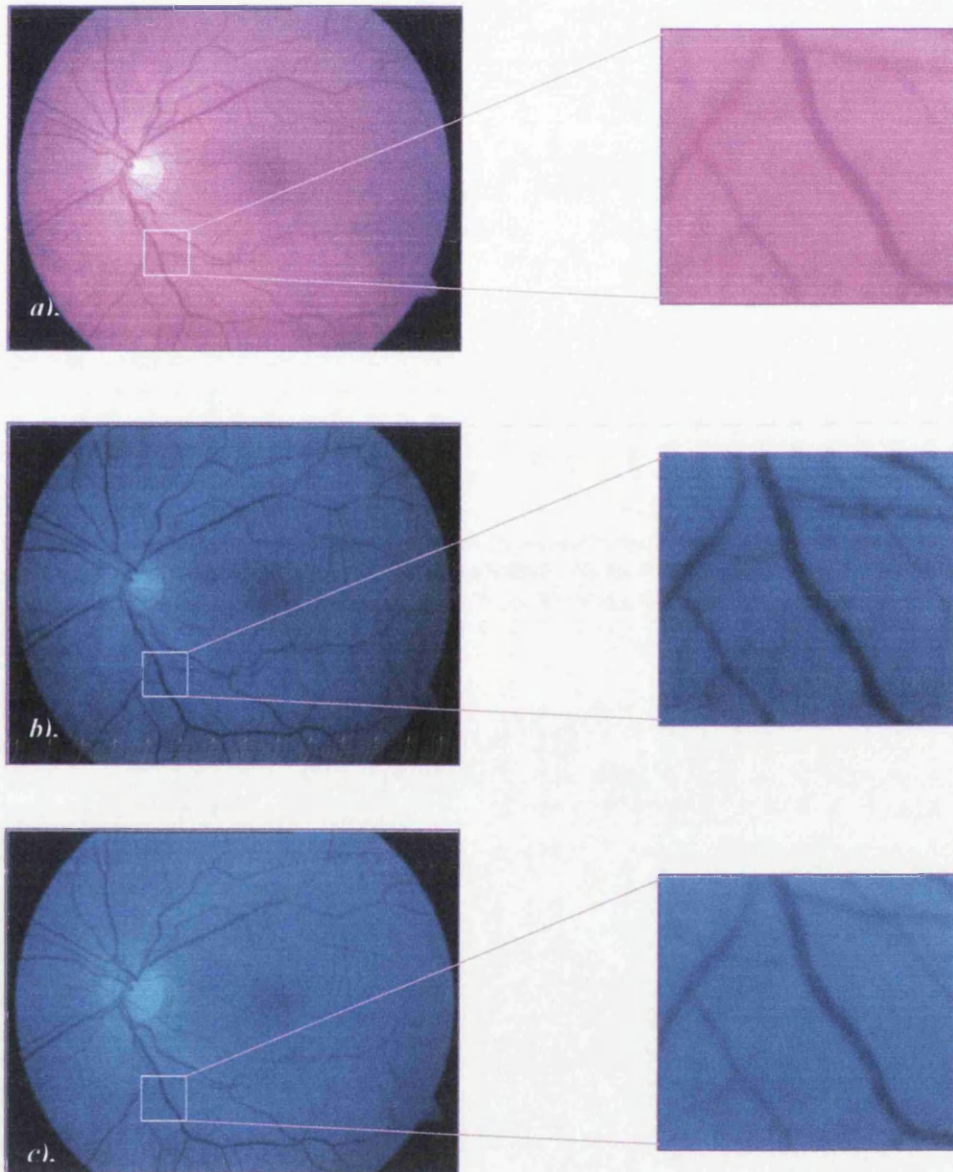


Fig 5.9. a) Original image. b) Green plane information. c) Sobel enhanced image, clearer visual definition of vessels.

Trials were executed to identify the optimal back-propagation NNW architecture for the identification of vessels by varying the number of hidden units and training iterations. From the available set of images we were able to construct datasets that contained 12663 normal background retina examples and 40761 vessels; 70% of the examples were used for NNW training the other 30% for testing NNW performance.

Each NNW comprised of 400 inputs corresponding to the individual pixel colour values contained within the classified 20x20 pixel box and one output. The NNW was trained to find the optimal number of training iterations and hidden units using feature examples compiled from Sobel enhanced images, see neural network architecture Chapter 3.3.7. The NNW result files were exported to the DRIC program where Receiver Operator Curves were plotted to identify the optimal cut off value that would yield the best network performance in terms of sensitivity and specificity, Table 5.5., (Fig 5.10), Chapter 4.2.2.3.

Retina vs Vessel										
Iterations → ↓ Hidden	50,000		100,000		150,000		200,000		250,000	
	Sens	Spec	Sens	Spec	Sens	Spec	Sens	Spec	Sens	Spec
5	75.01	74.86	85.91	85.75	86.22	85.99	89.13	88.87	85.95	86.04
10	84.21	83.63	88.68	88.7	88.51	88.71	89.03	88.97	88.82	88.95
15	82.7	82.65	89.2	89.42	89.81	89.68	89.64	89.76	89.68	90.01
20	82.43	81.8	88.51	88.48	89.74	89.74	91.45	91.32	89.98	90.04
10/10	73.4	77.26	90.53	90.42	90.6	90.68	90.15	90.06	90.7	90.55
7/7	74.58	73.63	83.64	84.72	84.51	83.52	88.55	88.42	84.62	84.52

Table 5.5. NNW performance for varying training iterations and hidden units – to find optimal network structure for the identification of vessels.

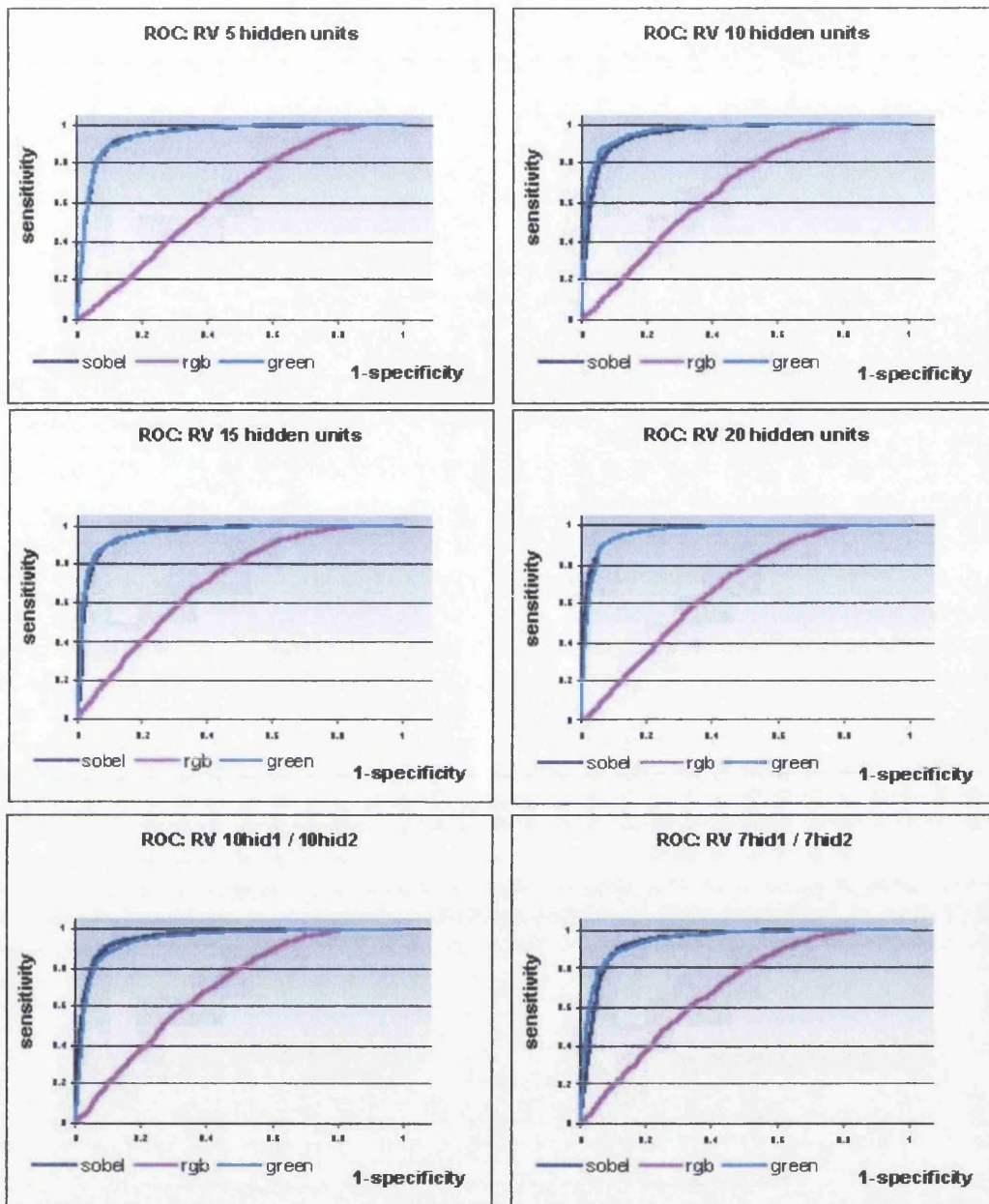


Fig 5.10. ROC analysis of NNW performance to find optimal number of hidden units. The graphs show that NNW's trained and tested on green plane images and pre-processed using a Sobel filter performed better than NNW's trained on images with no processing and full RGB pixel colour information.

To quantify the subjective visual enhancement of the features after the application of the Sobel filter, two further NNW were trained on the optimal number of iterations of 200,000 but this time without the Sobel filter pre-processing. Using the same data set of examples, the first NNW was trained using information provided only by the green plane, the second trained on the full RGB colour information for each pixel, Table 5.6..

Iteration →	200,000			
	Green		RGB	
Hidden ↓	Sens	Spec	Sens	Spec
5	88.82	88.58	59.66	57.76
10	89.91	90.17	60.44	60.11
15	89.5	89.8	60.39	63.43
20	89.64	89.76	62.6	62.3
10/10	88.62	88.46	62.46	64.03
7/7	88.17	88.36	62.19	64.4

*Table 5.6. NNW performance for hidden units – for comparison, when green plane without Sobel filter and full RGB pixel colour information is used.*

The optimum network architecture for the detection of vessels trained on Sobel enhanced images was one with 20 hidden units and trained for 200,000 iterations, yielding a sensitivity of 91.45% and specificity of 91.32%.

These results displayed an increase of 1.81% in sensitivity and 1.56% in specificity compared to the NNW trained on green plane information. A more significant increase was noted, 28.85% in sensitivity and 29.29% in specificity, when results were compared to a NNW with the same architecture trained on full RGB information.

These results agree with the visual findings that the application of a Sobel filter to the image increases the distinction between vessels and background retina. Although only marginally better than the NNW trained on the original green plane image, there is a significant increase in sensitivity and specificity when compared to the full RGB image. Fundamentally, this significant difference is a consequence of the amount of information the NNW has to learn to enable it to determine the correct association between pixel colour values and the feature which these values represent. When

trained on full RGB information the NNW is effectively presented with redundant information from the red and blue plane; that is to say the NNW has to learn to differentiate between more disperse numerical ranges. For example a single pixel on the green plane can only range from 0 to 255 numerically, however that same pixel on full RGB information can range from 0 to 16777215, thus introducing greater uncertainty.

Therefore for a NNW to achieve its optimal performance it has to be presented with the simplest and most appropriate information applicable to the problem. In this situation the primary contributing information is best provided by the Sobel enhanced green plane image.

## **5.5. SUMMARY**

In this chapter analysis of the digital fundus images for the detection of normal retinal features are described. Two techniques were applied to the detection of the optic disc and the macula. The first used custom written software by the author to identify the location of the centre of the optic disc as being the pixel with the highest intensity colour value on the RGB plane. The second technique was a commercial system which similarly looked for the highest intensity value on the HIS plane. In contrast the macula is the darkest notable region of the retina and therefore its identification was based on the minimal pixel value located within a ROI placed relative to the optic disc.

Results were obtained from a cohort of 100 normal and 100 background retinopathy fundus images. The custom written software successfully identified 98% of the OD from the normal images and 90% from the background retinopathy images within 40 pixels. The commercial system correctly located 100% of the OD's in the normal images and 91% of the background retinopathy images. For the identification of the macula both techniques were applied to the same group of images and identified 74%, 98% of the maculas in the normal images and 69%, 89% of the maculas in the diabetic retinopathy images respectively.

The results showed that the accuracy with which the optic disc was located was improved when combining the maximal volume intensity with the maximal pixel intensity value. Similarly, combining the volume intensity values with the minimal pixel intensity value and using the optic disc location only as a guide as to whether the macula will be on the right or left of the image produced superior results. Therefore this strategy was the preferred method for detecting the optic disc and macula within a standard posterior pole view of the retina.

The other standard recognisable normal feature of a retinal fundus image is a blood vessel. Trials were executed to identify the optimal back-propagation NNW architecture in terms of hidden units and training iterations for the identification of vessels from normal background retina. In addition, the neural network was also presented with three different types of pixel information. These included training and testing the NNW's performance when presented with full RGB pixel colour information, only the information contributed by the green plane information and finally information contributed by pre-processed green plane information.

The results showed that the optimum network architecture for the detection of vessels was one with 20 hidden units and trained for 200,000 iterations, yielding a sensitivity of 91.45% and specificity of 91.32%. These results were achieved from the pre-processed pixel information test set. This set displayed an increase of 1.81% in sensitivity and 1.56% in specificity compared to the NNW trained on green plane information and an increase of 28.85% sensitivity and 29.29% in specificity compared to a NNW with the same architecture trained on full RGB information. It was postulated that the performance of the NNW trained on the RGB pixel information reduced as a consequence of presenting it with redundant information contributed by the red and blue planes. Furthermore the application of a Sobel filter enhanced the feature edges thus enabling the NNW to better distinguish between vessels and background retina.

## **CHAPTER 6 – PERFORMANCE TESTING – THE DIABETIC RETINA**

### **6.1. HAEMORRHAGES**

Haemorrhages have the same colour as retinal vasculature and differ only in shape and size. It can often be difficult to distinguish smaller haemorrhages from background retina due to the similarities in their hue. One method of making them more distinguishable is by extracting only the information from the green plane, (*Fig 6.1.*). To further emphasis feature edges and enhance the visual distinction between background retina and vessels, new vessels, haemorrhages & exudates a Sobel edge detection filter was applied to the images, see Chapter 3.2.

A series of investigations were performed to identify the optimal back-propagation NNW architecture for the identification of haemorrhages. This was achieved by varying the number of hidden units and also the number of training iterations. From the available set of images feature data sets were constructed, they contained 12663 normal background retina examples and 11754 haemorrhages; 70% of the examples were used for NNW training the other 30% for testing NNW performance. Each NNW comprised of 400 inputs and one output, and was trained upon Sobel enhanced images, see neural network architecture Chapter 3.3.7. The NNW result files were exported to the DRIC program where Receiver Operator Curves Chapter 4.2.2.3., were plotted to identify the optimal cut off value that would yield the best network performance in terms of sensitivity and specificity, (*Fig 6.2.*).

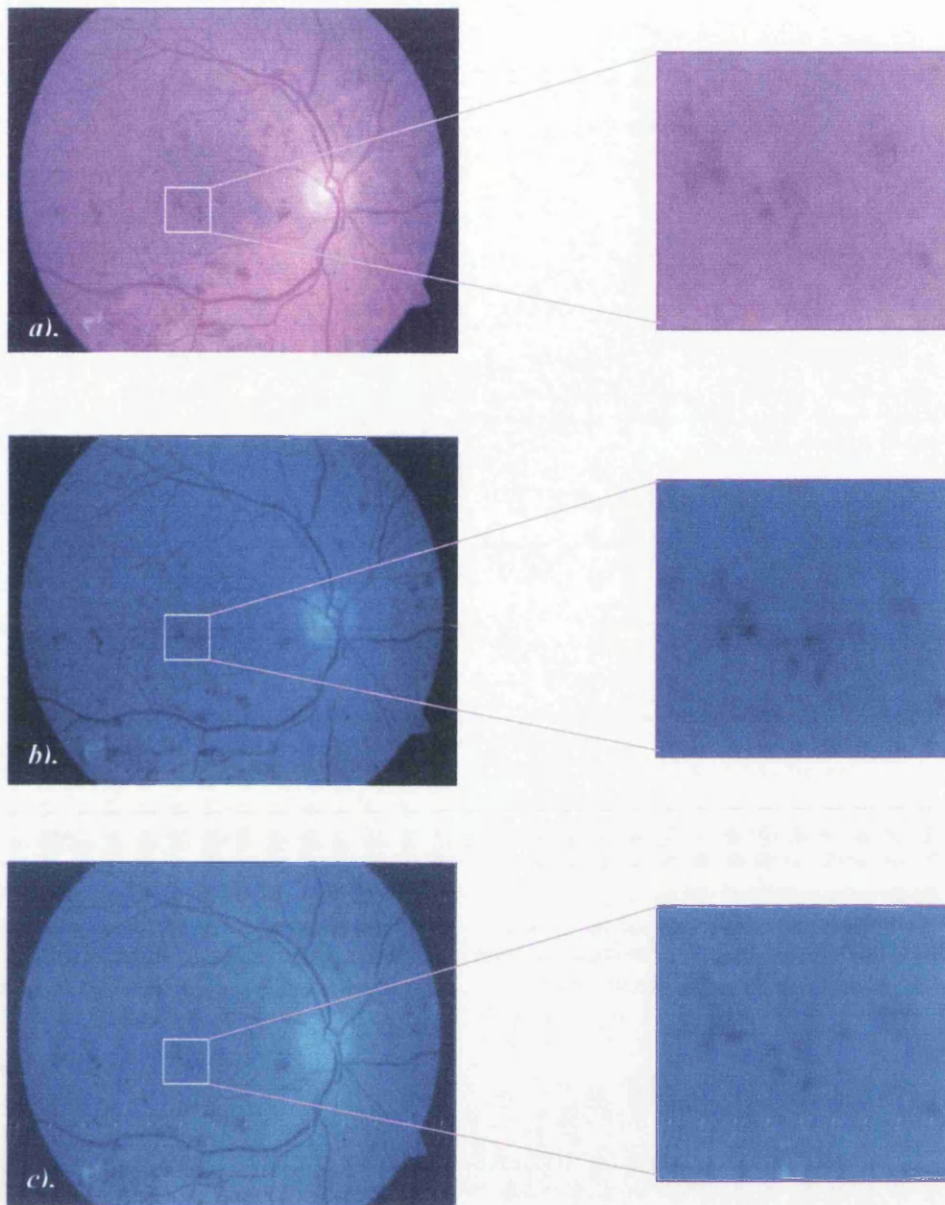


Fig 6.1. a) Original image. b) Green plane information. c) Sobel enhanced image, clearer visual definition of haemorrhages.

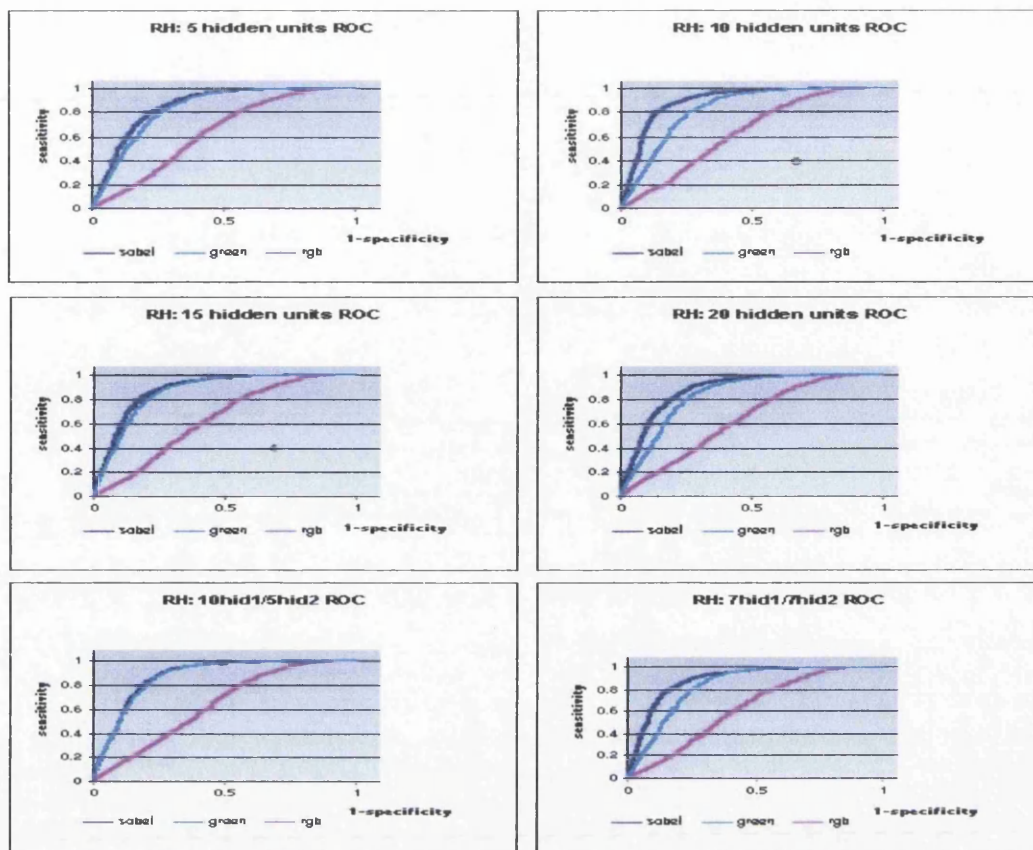


Fig 6.2. ROC analysis of NNW performance to find optimal number of hidden units. The graphs show that NNW's trained and tested on images using the green plane information and pre-processed using a Sobel filter performed better than NNW's trained on images with no processing and those using full RGB pixel colour information.

The results of each network's performance when trained and tested with different numbers of hidden units, multiple hidden layers and training iterations are displayed in Table 6.1.

Retina vs Haemorrhage										
Iterations →	50,000		100,000		150,000		200,000		250,000	
Hidden ↓	Sens	Spec	Sens	Spec	Sens	Spec	Sens	Spec	Sens	Spec
5	63.25	63.23	78.05	77.91	79.73	79.77	79.83	79.98	79.73	80.11
10	74.56	74.3	83.21	83.08	84.58	84.31	84.92	85.2	85.23	85.11
15	76.55	76.72	81.47	81.26	83.18	83.29	83.15	83.33	83.56	83.25
20	71.01	71.67	80.34	79.94	81.57	81.76	86.36	86.13	81.91	81.42
10/5	80.55	78.37	80.34	80.07	82.26	82.1	82.26	81.85	82.09	81.93
7/7	72.58	73.03	81.64	81.72	84.51	84.31	84.55	84.48	84.62	84.52

Table 6.1. NNW performance for varying training iterations and hidden units – to find optimal network structure for the identification of haemorrhages.

To quantify the subjective visual enhancement of the features after the application of the Sobel filter, two further NNW were trained for 200,000 iterations and incorporated the same array of hidden units. The first one used information provided only by the green plane, the second one was trained on the full RGB colour information for each pixel, Table 6.2.

Iterations → Hidden ↓	200,000			
	Green		RGB	
	Sens	Spec	Sens	Spec
5	76.68	75.49	58.97	59.37
10	75.9	75.36	58.63	59.08
15	79.52	78.97	59.25	58.91
20	82.91	83.08	58.36	57.93
10/5	79.28	79.26	58.29	57.21
7/7	76.07	76.29	58.80	59.46

Table 6.2. NNW performance for hidden units – for comparison when green plane and full RGB pixel colour information are used as opposed to Sobel enhanced green bit information.

The optimum network architecture for the detection of haemorrhages comprised 20 hidden units and training for 200,000 iterations, thus yielding a sensitivity of 86.36% and specificity of 86.13%. this was an increase of 3.45% in sensitivity and 3.05% in specificity compared to the green plane trained NNW. A more significant increase

was noted in sensitivity 28% and specificity 28.2% when results were compared to a NNW with the same architecture trained on full RGB information.

As previously discussed in Chapter 5.3, error or confusion between features within the learning process can be minimised by training the NNW on information at its most concise level. Therefore the NNW performs better when the edges between features are enhanced and information contained within the red and blue planes is excluded because they provide surplus information.

## 6.2. EXUDATES

Exudates appear as randomly shaped yellow deposits and it is this difference in hue which makes them easily distinguishable from other retinal features such as vessels and haemorrhages. Scattered in small numbers across the retina they do not dramatically affect a person's visual acuity. As clusters of exudates increase small blind spots in a person's vision can be noted, however, it is not until these features begin to encroach within the macular region that vision can be affected, *Hamilton et al. 1996*.

Conventional digital fundus photography provides a 2-D solution to the detection of maculopathy; the other primary contributing factor to the loss of visual acuity is a thickening (oedema) of the macula caused by capillary leakage. The identification of exudates within 1 disc diameter of the fovea is indicative of a higher potential for that patient to experience severe visual impairment, *ETDRS 1991*. Therefore, the detection and more importantly the ability to identify the position of exudates within the retina is of particular importance.

Once exudates have been located within the macular region the operator could then be prompted to provide additional information on a patient's visual acuity and whether oedema is present, thus providing a more accurate diagnosis. Therefore when considering a viable approach to the detection of exudates it is necessary to include a method which will provide positional information also. As discussed in

Chapter 4 all NNW data sets contained location information at the time of construction.

Trials were executed to find the optimal network structure for the identification of exudates. Maintaining the same background retina data set as previously used in the haemorrhage trials, the new series of neural networks were trained and tested on a total number of 5571 exudates using 400 inputs and 1 output. Once again the feature data sets were assembled with full RGB pixel colour information, green plane only and green plane information from Sobel enhanced images. An example of an image containing multiple exudates displayed in each of the states above can be visually assessed in *Fig 6.3*. From the example highlighted in the RGB and green plane images, the edges around the exudates appear fuzzy. In comparison the edges of the same exudates in the Sobel enhance image appear more defined.

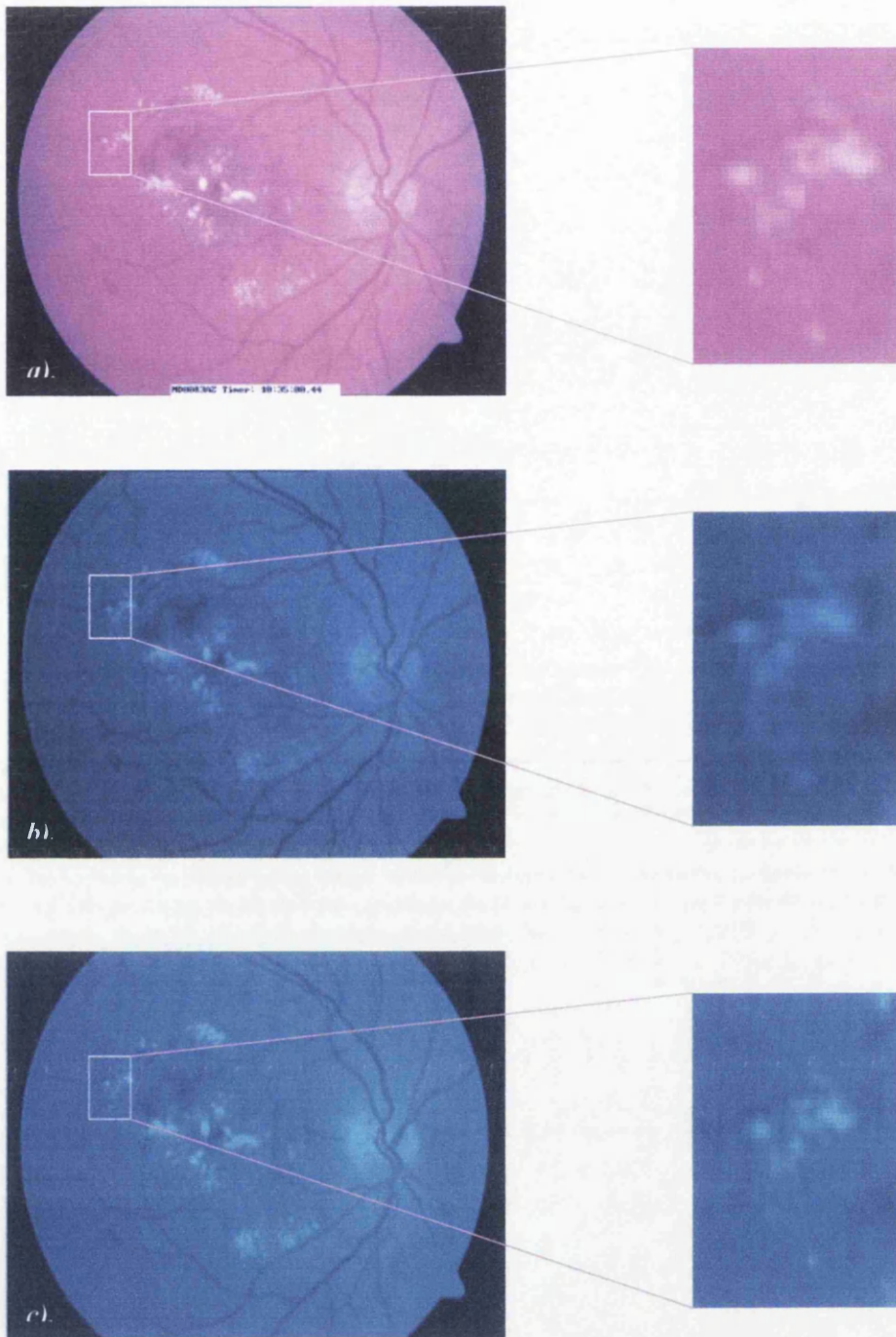


Fig 6.3. a) Original image. b) Green plane information. c) Sobel enhanced image, clearer visual definition of exudates.

To corroborate this visual enhancement of exudate edges ROC analysis was performed to identify each network's optimal performance (Fig 6.4.). The results are displayed in Table 6.3. & 6.4.

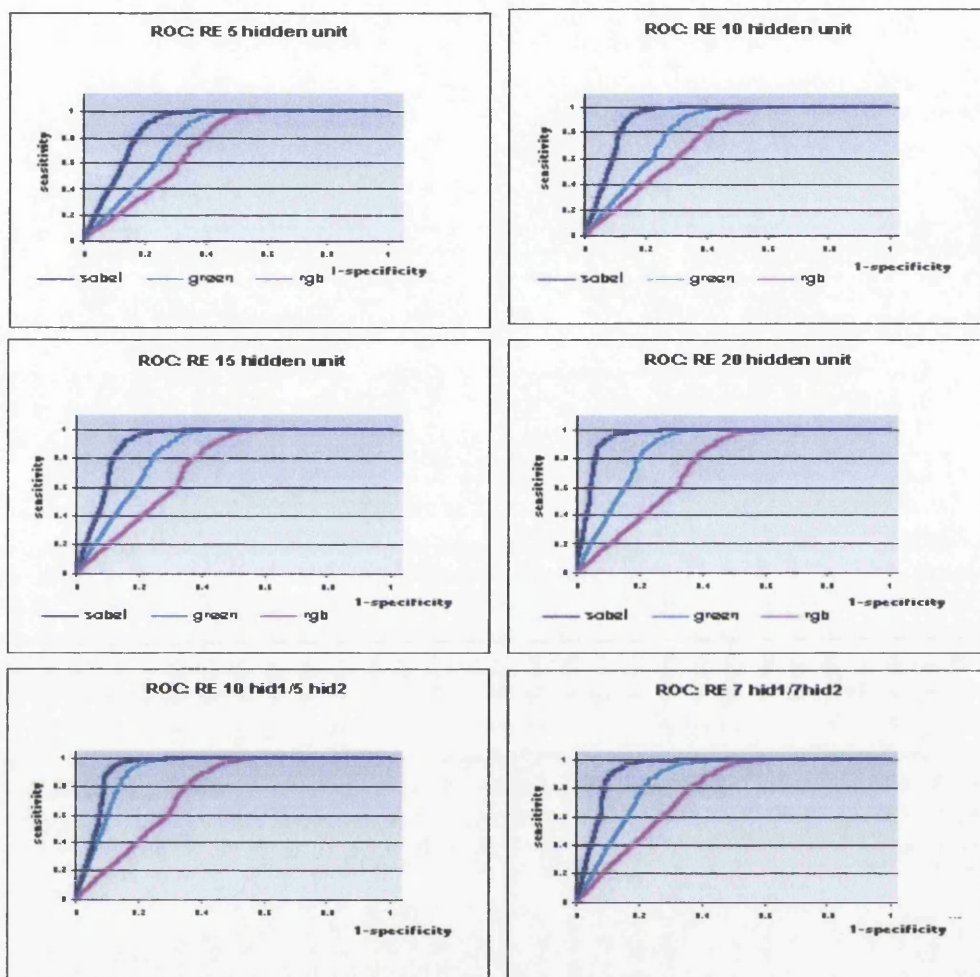


Fig 6.4. ROC analysis of NNW performance to find optimal number of hidden units. The graphs show that NNW's trained and tested on images of the green plane information and pre-processed using a Sobel filter performed better than NNW's trained on images with no processing and those using full RGB pixel colour information.

Retina vs Euxdate										
Iterations → Hidden ↓	50,000		100,000		150,000		200,000		250,000	
	Sens	Spec	Sens	Spec	Sens	Spec	Sens	Spec	Sens	Spec
5	75.59	75.5	81.57	82.05	83.18	83.76	83.83	83.62	83.97	83.62
10	82.26	81.98	86.5	86.47	87.28	86.61	86.36	86.61	86.15	86.75
15	91.56	74.57	85.61	85.83	89.16	89.1	89.5	89.17	89.16	89.32
20	90.63	77.92	90.94	90.81	91.9	92.02	91.9	92.09	91.97	92.09
10/5	85.47	82.69	89.23	89.1	87.59	88.11	88.03	87.89	88.14	87.82
7/7	90.09	80.77	88.34	88.89	89.5	89.1	88.92	89.32	89.13	89.17

Table 6.3. NNW performance for varying training iterations and hidden units – to find optimal network structure for the identification of exudates.

Iterations → Hidden ↓	200,000			
	Green		RGB	
	Sens	Spec	Spec	Spec
5	82.94	81.7	65.91	66.45
10	86.5	86.47	68.14	65.31
15	86.8	85.53	66.46	66.45
20	89.94	89.81	65.85	66.17
10/5	87.22	86.13	68.00	67.81
7/7	86.34	86.87	78.91	63.46

Table 6.4. NNW performance for hidden units – for comparison when full RGB pixel colour information is used as opposed to Sobel enhanced green bit information.

The optimal network performance for the identification of exudates from normal background retina on Sobel enhanced data sets comprised of 20 hidden units and trained for 200,000 iterations yielding a sensitivity/specificity of 91.90% & 92.09% respectively. This was an increase of 1.96% in sensitivity and 1.28% in specificity compared to the green plane trained NNW. A more significant increase was noted in sensitivity 26.05% and specificity 24.92% when results were compared to a NNW with the same architecture trained on full RGB information. These results verify that applying a Sobel filter to the images increases the definition of exudate edges and thus improves the NNW’s performance in identifying these features.

Once the NNW has been trained to successfully recognise exudates their positional information can be extracted and analysed. We incorporated the location of exudates

relative to the macula to provide a method for identifying maculopathy, this technique is detailed in Chapter 7.3.

### 6.3. SIGHT THREATENING DIABETIC RETINOPATHY

The Scottish Executive has reported that there are nearly 120,000 people in Scotland who have been diagnosed as having diabetes. Of this population 2 - 3% (2,400 – 3,600 people) will go on to develop sight threatening features of DR requiring automatic referral to a consultant ophthalmologist for treatment. The Greater Glasgow region accounts for approximately 12.2% (609,370) of the Scottish population, *General Register Office 2000*. Assuming there is an equal distribution of the diabetic population between all regions we can postulate that an estimated 366 people with sight threatening features of DR would be referred to the diabetic review clinic at Gartnavel General Hospital if it were the sole centre.

However, not all diabetic patients attend their routine eye examinations, some through ignorance of the associated risk of diabetic related eye disease, others through logistical complications or just poor health. In consequence this causes a direct reduction in the number of presenting examples of sight threatening features of DR. In addition, GGH is not the only Glasgow site which has direct screening access to all diabetic patients in the Greater Glasgow Region, in fact on average the department has a throughput of approximately 3200 patients a year. Thus we would expect to obtain 60 – 100 cases (since the progression of sight threatening DR can be unilateral). Unfortunately other exclusion criteria come into play reducing this number further, for example:

- ⌘ People presenting with additional non-diabetic related eye disease pathology e.g. age related macular degeneration (ARMD) and Drusen – as it becomes difficult to differentiate from maculopathy or cotton wool spots in the early stages. These are relatively common diseases in the elderly. Glaucoma – high intraocular pressure (IOP) can result in flame shaped haemorrhages; these can be confused with DR lesions. Inherited retinal dystrophies or Maculopathies

such as Stargardts or Retinitis Pigmentosa (RP) or Best's disease cause conflicting or additional retinal lesions, *Kanski 1984*.

- ⌘ Post laser photocoagulated proliferative retinopathy with reoccurrence in new areas of the retina – much of the retina is contaminated with scarring, thus confusing the network with conflicting normal retina examples.
  
- ⌘ Cataracts – the opaque lens diffuses the light entering the eye and prevents a clear image from being captured, *Kanski 1984*.

Most of these conditions, with the exception of Drusen are symptomatic. Thus most patient's would go to their optician or GP complaining of a reduction in vision, thereby bypassing the screening program because they have an appreciable problem in the eye.

Taking all this into account we were presented with relatively few images displaying sight threatening features of DR. Nonetheless with the collective number of examples available to us at this time we did attempt to address the identification of neovascularisation and maculopathy, see Chapter 7.

### **6.3.1. NEOVASCULARISATION ELSEWHERE ON THE RETINA**

In theory the retina's ability to regenerate the growth of new vessels would seem an ideal solution for conveying nutrients to areas that have been starved through damage incurred by capillary closure. However, in reality the new vessels are fragile and may bleed. When these haemorrhages occur the blood begins to disperse through the vitreous cavity, vision becomes blurred or dim and can result in severe visual impairment or blindness. It is for this reason that neovascularisation is one of the most sight threatening features of DR, however it is also the least common. We investigated the use of NNWs as a potential technique for identifying new vessels.

From the available set of images datasets were constructed, these contained 12663 examples of normal retina, 5571 exudates, 11754 haemorrhages and 477 new vessels. Three back-propagation NNW's were trained to identify new vessels from background retina and other recognisable features of diabetic retinopathy (exudates and haemorrhages). Data sets were compiled from green plane pixel colour information on Sobel enhanced images (*Fig 6.5*), Table 6.5.

New Vessels Elsewhere								
Hidden	R vs NVE		Hidden	E vs NVE		Hidden	H vs NVE	
	Sens	Spec		Sens	Spec		Sens	Spec
20	82.35%	51.85%	10	75.72%	77.38%	10	58.33%	41.27%

Table 6.5. Optimal NNW performances for the identification of new vessels against normal background retina (R), exudates (E) and haemorrhages (H).

From these datasets the NNW achieved a sensitivity and specificity of 82.4% / 51.8% respectively for the identification of normal retina against new vessels, 75.7% / 77.4% between exudates and new vessels and 58.3% / 41.3% against haemorrhages. Due to the small number of new vessel examples available and the relatively poor performance of the NNW we did not repeat RGB trials, as we did not feel that it would provide any further beneficial findings.

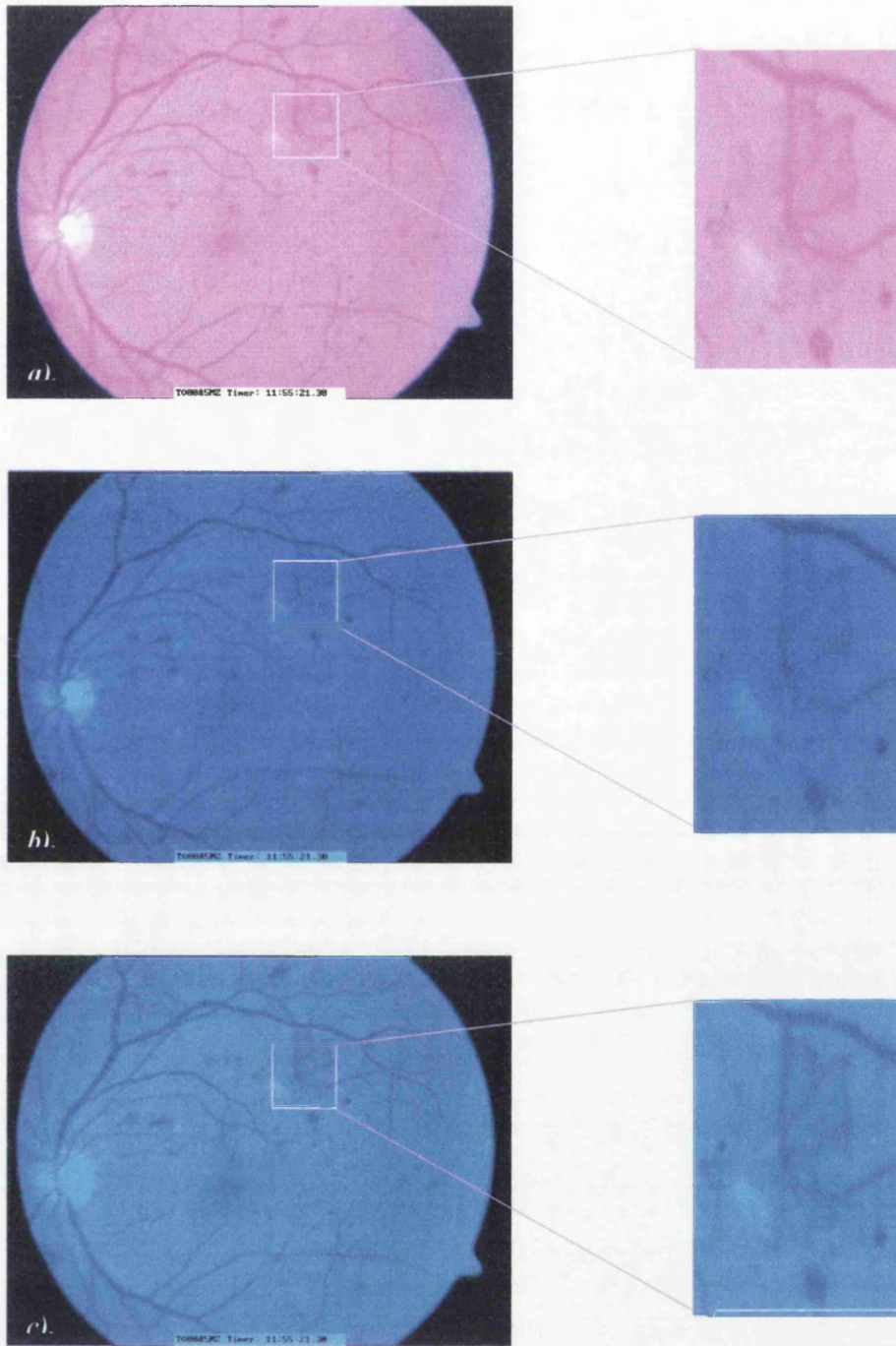


Fig 6.5. a) Original image. b) Green plane information. c) Sobel enhanced image clearer definition of new vessels.

### **6.3.2. NEOVASCULARISATION AT THE OPTIC DISC**

The optic disc (OD) is also susceptible to the growth of new vessels; therefore an essential requirement of any automated system is one that includes the ability to identify the growth of these new vessels as early in their developmental process as possible. As discussed in Chapter 5.2 we successfully derived a method for detecting the optic disc within a digital fundus image. At the time of detection the relative coordinates were saved thus permitting localised analysis to be performed on the optic disc area.

#### **6.3.2.1. CIRCULAR INTENSITY PROFILING**

Circular intensity profiling (CIP) is a method that was employed to analyse the optic disc for the detection of new vessels. Due to the limited number of examples available of new vessels at the optic disc the analysis was performed on a data set of 34 images (17 normal and 17 with new vessels at the optic disc). The normal OD has unique vascular structure where vessels and background optic disc can easily be identified by their differing hues. However new vessels at the OD are still difficult to detect as they are much finer than normal vessels and their hue is often only marginally darker than the normal optic disc background.

To enhance the vessel edges within the optic disc we applied a High Pass filter (Photoshop™) with a radius of 3.5 pixels. This enabled edge details to be retained, where sharp colour transitions occurred while suppressing the rest of the image, (*Fig 6.6.*). The filter effectively removes lower-frequency information. To further enhance the vessels the image contrast was raised to 75%.

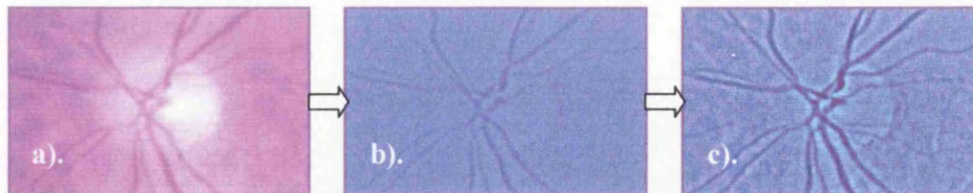


Fig 6.6. a) Normal optic disc, unprocessed. b) Image after the application of a High pass filter with radius set at 3.5 pixels to enhance vessel edges. c) Image contrast is increased to further enhance vessels.

The circular intensity profiles of the processed images were obtained from custom written code incorporated within the DRIC program, (Fig 6.7.).

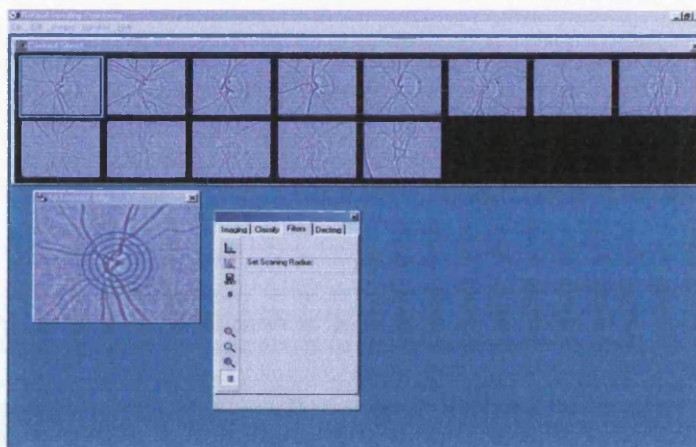


Fig 6.7. DRIC program, records the co-ordinates and pixel intensity values of the optic disc and outputs the values to a text file for analysis. The profile of each disc can be built up by varying the radius of the circle.

The information contained within the CIP data included the x, y co-ordinates and pixel intensity values. These were collated for a range of scanning ring radii. The files were then exported to MSExcel for subsequent analysis.

Vessels are reflected through a lower intensity value than the normal yellow hue associated with the OD background. When the intensity values are plotted these changes in intensity values are displayed as a series of peaks and troughs. The CIP plots illustrate vessel edges as troughs and the resultant peaks indicating the end of the vessel and a return to the higher intensity background. An example taken from a normal optic disc and one that has new vessel growth is shown in Fig 6.8. & 6.9.

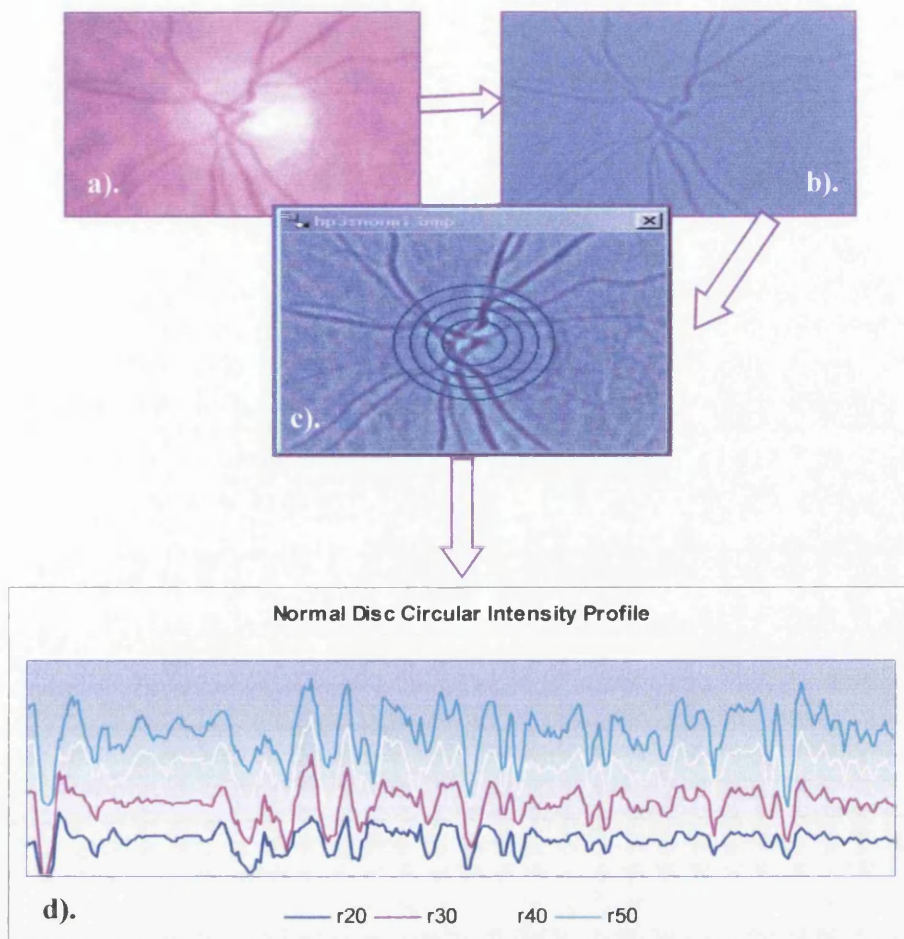


Fig 6.8. a) Typical normal optic disc. b) Normal image after the application of a high pass filter (3.5 pixel kernel using Adobe Photoshop). c) Contrast enhancement is applied to make vessels more prominent, before circular pixel intensity values are obtained with the DRIC program. d) Normal disc intensity profile plots for radius values of 20,30, 40 & 50 pixels

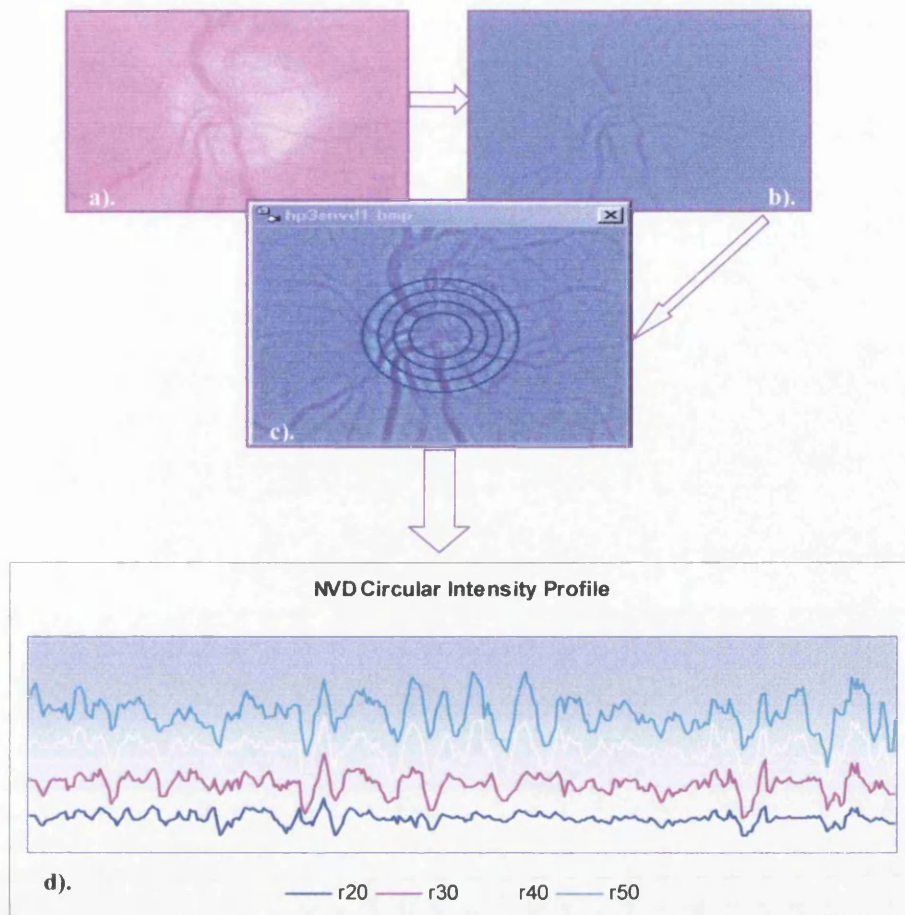
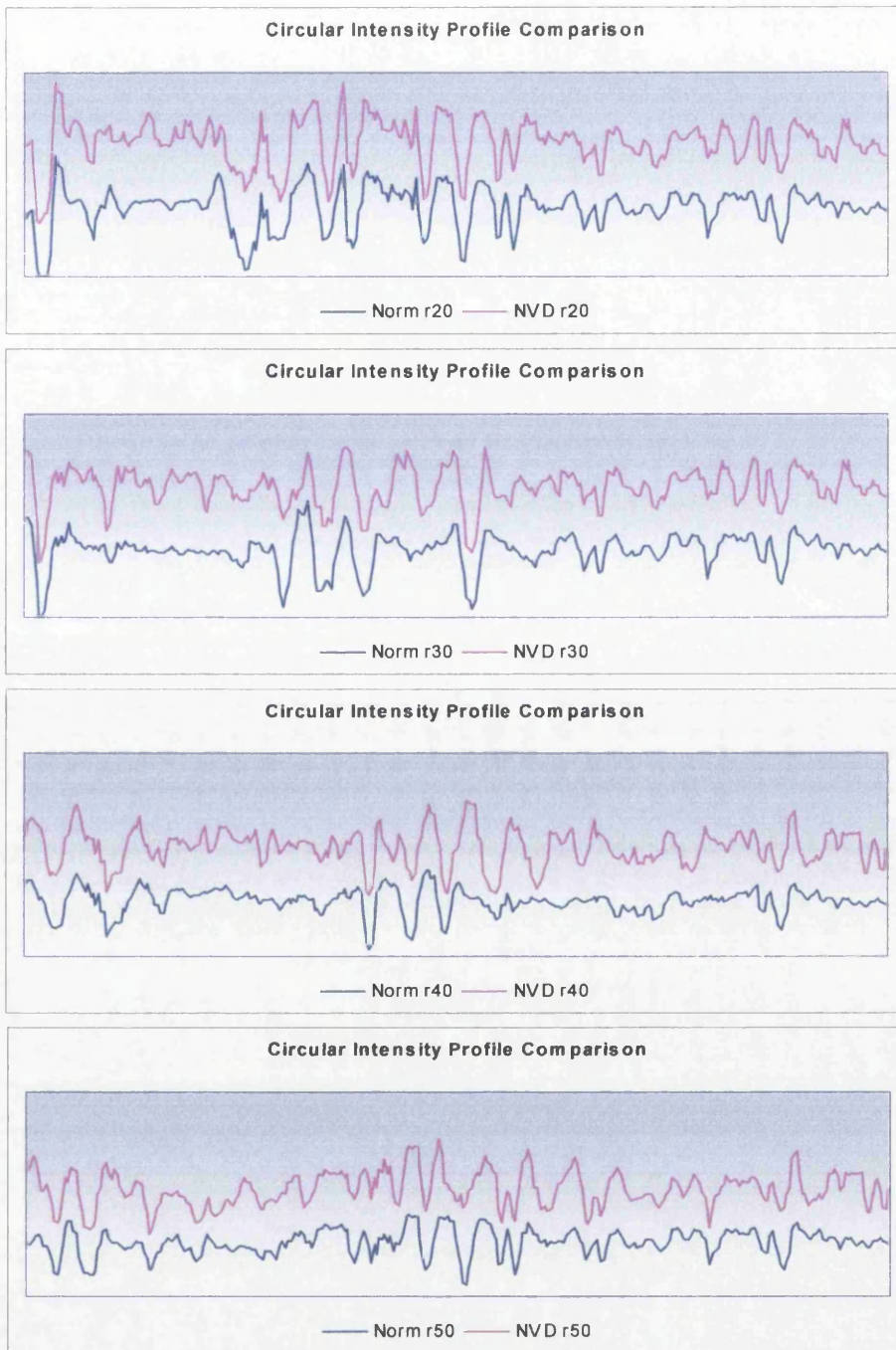


Fig 6.9. a) optic disc with new vessel growth. b) NVD image after the application of a high pass filter (3.5 pixel kernel using Adobe Photoshop). c) Contrast enhancement is applied to make vessels more prominent, before circular pixel intensity values are obtained with the DRIC program. d) NVD intensity profile plots for radius values of 20,30, 40 & 50 pixels.

On normal OD profiles the plateau between the major vessel edges remain fairly uniform, however on optic discs with new vessel growth the plateaus between major vessels exhibit an increase in the number of peaks suggesting the presence of further vessel activity. A direct comparison between the CIP plot for a normal optic disc and an optic disc with new vessels is shown in Fig 6.10. To further illustrate this, the CIP were segmented into four arcs, (Fig 6.11.).



*Fig 6.10. Circular intensity profiles taken from normal disc (blue) and a disc with new vessel growth (pink). The peaks indicate vessel edges, normal discs appear fairly uniform between vessels. There are areas of increased peaks on the NVD profile indicative of more vessel edge activity.*

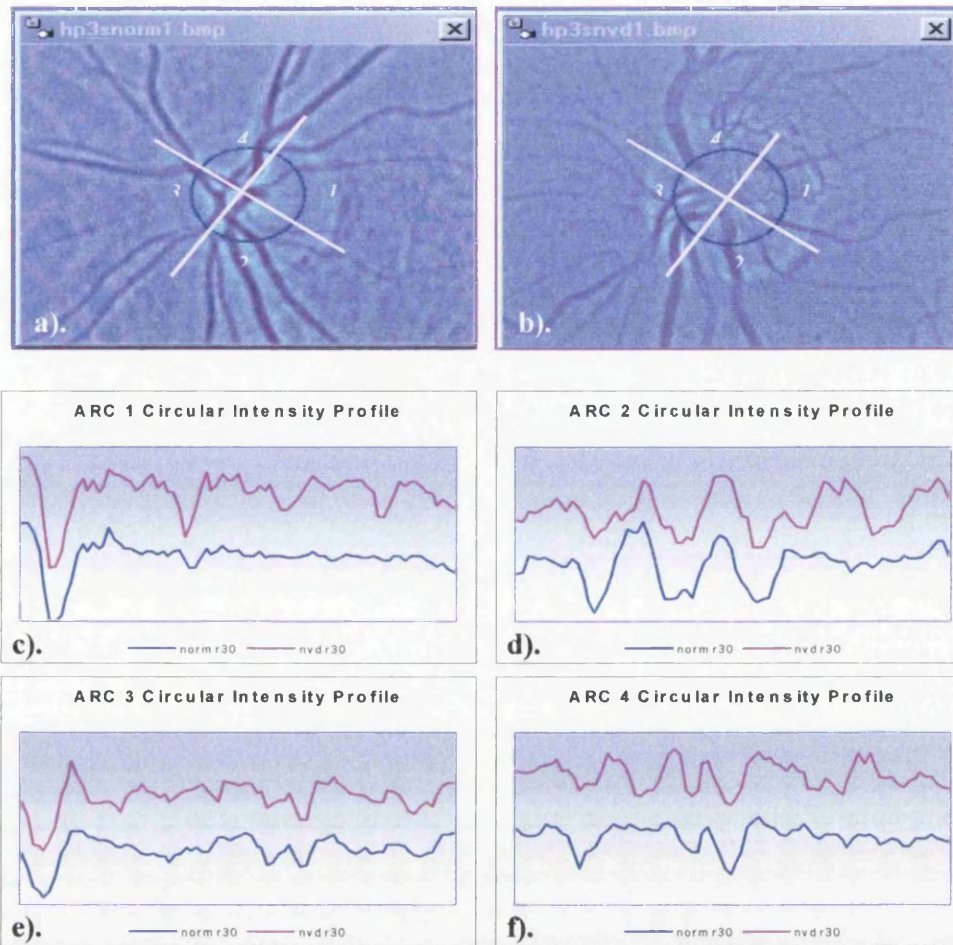


Fig 6.11. a) normal optic disc arc segmentation. b) Disc with new vessel growth arc profile. c,d,e,f). CIP are segmented into 4 arcs, the plots of the normal discs are shown in blue (bottom), the disc with new vessels in pink (top). The peaks represent the vessel edges, the normal image remains fairly uniform between major vessels while the disc with new vessels displays multiple peaks between major vessels indicating a great abundance of vessels.

To quantify the difference between the CIP's of OD's displaying normal retinal vasculature and OD's with new vessels we employed a method of counting the relative number of turning points across each plot. For this trial a selection of normal images and images with new vessels were assessed. There is a natural variance in hue across the vessels and the background of the optic disc which may give rise to false vessel edges. To minimise these discrepancies of non-uniformity and noise the CIP's were smoothed using nearest neighbour averaging. Where  $P$  is the pixel value and  $n$  is the  $n$ th pixel, the average calculated as:

$$P_n = \sum(P_n + P_{(n-1)} + P_{(n+1)})/3$$

It is necessary not to over smooth the data as this could result in the peaks created by the new vessels being averaged out. Hence the new vessels would not be identified.

A pixel was identified as a turning point (i.e. a peak or a trough) if the following conditions were met:

If  $(P_n > P_{(n-1)})$  AND  $(P_n > P_{(n+1)})$  or If  $(P_n < P_{(n-1)})$  AND  $(P_n < P_{(n+1)})$

The number of turning points was calculated for each image over differing radii and the results displayed in Table 6.6.

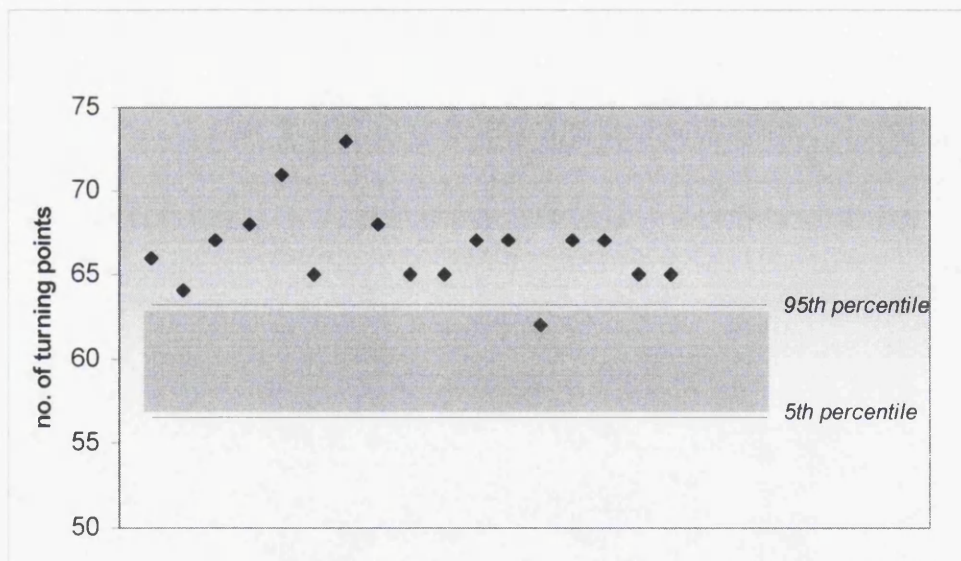
Radius 20		Radius 30		Radius 40		Radius 50	
Norm	NVD	Norm	NVD	Norm	NVD	Norm	NVD
35	37	55	54	61	66	63	63
34	33	63	62	59	64	63	61
28	33	64	56	60	67	59	58
34	41	52	66	63	68	65	62
30	40	58	60	55	71	65	60
33	37	52	52	62	65	61	62
29	41	60	58	63	73	65	71
34	40	59	60	58	68	65	72
33	31	58	62	61	65	59	61
33	29	59	66	59	65	65	61
36	31	60	62	57	67	63	61
38	39	63	62	64	67	67	64
33	35	56	56	58	62	67	63
41	39	64	64	57	67	67	54
36	33	53	67	59	67	67	69
33	34	64	65	60	65	63	73
35	34	58	54	60	65	53	72
AVG 33.82	AVG 35.71	AVG 58.71	AVG 60.35	AVG 59.76	AVG 66.58	AVG 63.35	AVG 63.94
SD 3.13	SD 3.84	SD 4.10	SD 4.66	SD 2.41	SD 2.57	SD 3.69	SD 5.48

Table 6.6. Number of turning points identified for each radii.

To establish if there is any statistical variation between the two groups of images, the number of turning points were analysed using a Mann-Whitney non-parametric test, Lyman Ott 1992. Analysis at 95% confidence intervals revealed no significant

variation between the number of turning points when the radius of the scanning circle was set at 20, 30 and 50 pixels ( $p = 0.1984$ ,  $p = 0.2837$ ,  $p = 0.6773$  respectively). At the smaller radii the vessels are still tightly packed together making it difficult to detect overlying new vessel formation. Similarly, at the boundary of the optic disc the vessels are more disperse and begin to branch out across the retina resulting in the introduction of greater numbers of normal vessels. This combined with the darker hue of the OD boundary contributes to the new vessels being less distinguishable as they merge into the background or overlie the normal vessels.

The optimal radius for identifying new vessel formation was a radius of 40 pixels. At this point the vessels begin to branch out and there is good separation between normal vessel edges and the brighter background hue of the OD. Thus the new vessels are easier to distinguish. There was a significant statistical variation between the number of identified turning points between normal optic discs (average 59.8, SD 2.41) and optic discs with new vessels (average 66.6, SD 2.58) at this radius where  $p < 0.001$ . To illustrate this the number of turning points in the NVD population was plotted against the 5<sup>th</sup> and 95<sup>th</sup> percentile range of the normal population, (*Fig 6.12.*).



*Fig 6.12. Distribution of turning points NVD vs normal radius 40. Blue diamonds represent NVD group.*

This clearly illustrates the difference between the number of turning points in each group. Of the 17 optic discs analysed only 1 image lay within the 95<sup>th</sup> percentile

range. On further inspection of this image the majority of the new vessels were superimposed upon the normal vessels.

#### **6.4. SUMMARY**

The identification of the primary features associated with diabetic retinopathy provides a good starting platform from which a fully automated system can be produced. Information relating to the number of features present and more importantly their location within the retina can all be weighted to provide an overall classification of the severity of retinopathy for a particular patient.

Three back-propagation neural networks were trained to identify the key features of micro-aneurysms, dot/blot haemorrhages, exudates and neovascularisation from normal background retina. The optimum networks achieved sensitivities of 86%, 92%, 82% and specificities of 86%, 91% and 52% for each NNW respectively.

Optic discs were analysed to differentiate between normal and optic discs with new vessel growth. This was achieved by extracting circular intensity profiles at varying radii from both groups. The comparing the number of turning points identified within the two groups we found that there was a significant difference  $p < 0.001$  between the average number of turning points on a normal optic disc (59.8, SD 2.41) with radius 40 pixels when compared to an optic disc which had new vessels (66.6, SD 2.58).

## CHAPTER 7 - PERFORMANCE TESTING OF THE DIABETIC RETINA

### 7.1. VALIDATION OF NEURAL NETWORK PERFORMANCES

In Chapter 6, methods for the optimisation of neural network performance in association with the main clinical features of the normal and diabetic retina were described. To ascertain the accuracy of the network performance the classification results from the network were compared to that of an experienced ophthalmic clinician. A random selection of images was selected from the Diabetic review clinic. These images had not previously been used in the training and testing phase. The images were segmented into boxes each containing 20 x 20 pixels and classified by the clinician as being normal background retina, normal vessel, hard exudate or dot / blot haemorrhage.

The previously optimised NNW's trained for the identification of vessels, exudates & haemorrhages from background retina were tested on the new test images and the results imported into the DRIC programme for analysis.

Quantification of the NNW's performance can be executed via the main menu, File > Open Classification in the DRIC programme. The user is prompted to input the neural network result file (\*.nnr) from which information relating to the associated test set file (\*.nna) can be accessed. This allows the classification results from the NNW to be directly compared to the original feature classification. If the NNW correctly classified a feature then that feature would be displayed in its original position on the image from which it was taken. If on the other hand the NNW incorrectly classified a feature it would then be displayed in black instead of its predefined colour coding: i.e. exudate:yellow, vessel:white, exudate:green, haemorrhage:blue, (*Fig 7.1.*).

The sensitivity values are calculated as a percentage of the number of abnormal features correctly classified by the NNW over the total number of that specific feature presented to the NNW. The specificity is calculated as 1- (the number of

normal features incorrectly classified by the NNW over the total number of normal features presented to the NNW) and expressed as a percentage.

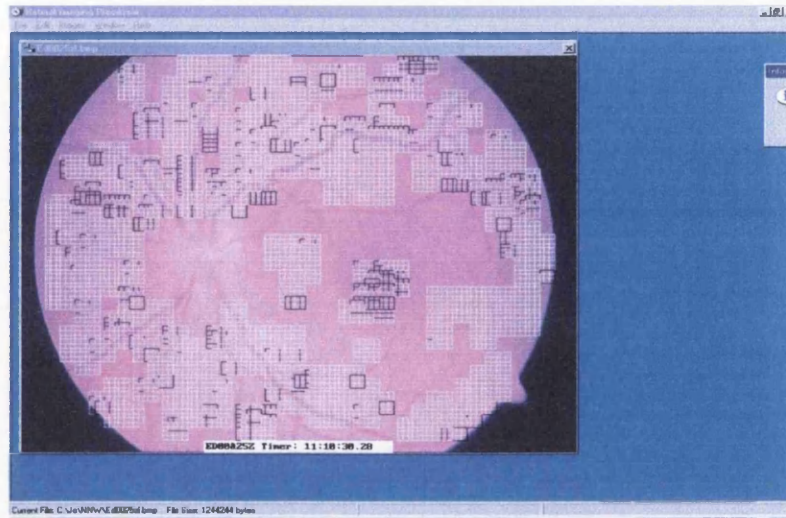


*Fig 7.1. Screenshot of neural network results file analysis through DRIC program. White boxes represent correctly classified vessels, yellow boxes represent correctly classified normal background retina. Features that were incorrectly classified by the NNW are displayed in black.*

#### **7.1.1. RECOGNITION OF VESSELS**

The clinician generated data sets were tested on data trained using the optimal neural network architecture as identified in the previous trials, Chapter 5.3 & 6. For the performance testing of vessels against normal background retina the NNW architecture included 400 inputs, 1 output, 1 hidden layer with 20 units, trained for 200,000 iterations and using the hyperbolic tangent learning rule. Included within the test set were 4456 examples of vessels and 1386 examples of normal retina taken from 20 images. For the new test set of images the neural network achieved an average sensitivity of 93% and specificity 84%. The individual breakdown from each image within the test set is displayed in Table 7.1.

Image	TF	IV	TV	IR	TR	sens	specs
1	883	8	648	21	235	99%	91%
2	171	16	99	8	72	84%	89%
3	108	0	0	19	108	n/a	82%
4	90	0	0	8	90	n/a	91%
5	423	6	360	21	63	98%	67%
6	432	47	306	4	126	85%	97%
7	477	10	360	15	117	97%	87%
8	369	27	306	4	63	91%	94%
9	198	24	171	0	27	86%	100%
10	162	3	153	2	9	98%	78%
11	288	5	235	22	53	98%	58%
12	45	3	45	0	0	93%	n/a
13	450	47	450	0	0	90%	n/a
14	171	14	153	7	18	91%	61%
15	279	17	180	17	99	91%	83%
16	441	27	378	11	63	93%	83%
17	18	0	0	0	18	n/a	100%
18	189	6	108	18	81	94%	78%
19	243	10	171	5	72	94%	93%
20	405	18	333	17	72	95%	76%
					Average	93%	84%

Table 7.1. . NNW performance testing of vessel recognition from normal retinal TF: total number of features, IV: number of incorrectly classified vessels, TV: total number of vessels to be identified, IR: number of incorrectly classified retina examples, TR: total number of retina examples to be identified

### 7.1.2. RECOGNITION OF HAEMORRHAGES

The optimum back-propagation network architecture for the detection of haemorrhages consisted of 400 inputs, 1 output, 1 hidden layer comprising of 20 units, trained for 200,000 iterations and using the hyperbolic tangent learning rule. The neural network was tested on a new set of 20 images, which collectively displayed 1072 examples of haemorrhages and 1452 examples of normal retina. Eight images included within the data set had no known diabetic retinopathy related pathology. The NNW achieved an average sensitivity of 81% and specificity 85%. The number of features and the performance of the NNW for each image are displayed in Table 7.2.

Image	TF	IH	TH	IR	TR	sens	specs
1	235	0	0	16	235	n/a	93%
2	39	0	0	3	39	n/a	92%
3	27	0	9	6	18	100%	67%
4	108	0	0	18	108	n/a	83%
5	126	1	36	5	90	97%	94%
6	90	0	0	24	90	n/a	73%
7	63	0	0	15	63	n/a	76%
8	243	29	117	2	126	75%	98%
9	117	0	0	9	117	n/a	92%
10	99	8	36	2	63	78%	97%
11	117	34	90	3	27	62%	89%
12	54	7	45	3	9	84%	67%
13	81	8	28	5	53	71%	91%
14	369	96	369	0	0	74%	n/a
15	135	5	36	14	99	86%	84%
16	63	0	0	13	63	n/a	74%
17	216	32	198	1	18	84%	94%
18	153	16	72	6	81	78%	92%
19	117	7	36	6	81	81%	92%
20	72	0	0	16	72	n/a	71%
					Average	81%	85%

Table 7.2 . NNW performance testing of haemorrhage recognition from normal retina.

TF: total number of features, IH: number of incorrectly classified haemorrhages, TH: total number of haemorrhages to be identified, IR: number of incorrectly classified retina examples, TR: total number of retina examples to be identified

### 7.1.3. RECOGNITION OF EXUDATES

For the performance testing of exudates against normal background retina the NNW protocol included 400 inputs, 1 output, 1 hidden layer comprising of 20 units, trained for 200,000 iterations and using the hyperbolic tangent learning rule. There were 27 images in the test set, containing 1207 examples of exudates and 1996 examples of normal retina. 7 images included in the test set had no known diabetic retinopathy related pathology. The NNW had achieved average sensitivity of 80% and specificity 98% for the identification of exudates against normal retina. The individual breakdown from each image within the test set is displayed in Table 7.3.

Image	TF	IE	TE	IR	TR	sens	specs
1	235	0	0	0	235	n/a	100%
2	115	7	36	6	79	81%	92%
3	81	0	0	1	81	n/a	99%
4	135	9	36	2	72	75%	97%
5	54	2	9	0	45	78%	100%
6	63	5	45	0	18	89%	100%
7	108	0	0	8	108	n/a	93%
8	90	0	0	1	90	n/a	99%
9	144	9	27	2	117	67%	98%
10	90	0	0	9	90	n/a	90%
11	186	4	9	0	177	56%	100%
12	63	0	0	4	63	n/a	94%
13	90	3	27	1	63	89%	98%
14	117	13	81	0	36	84%	100%
15	126	16	99	0	27	84%	100%
16	27	5	18	0	9	72%	100%
17	81	1	45	0	36	98%	100%
18	198	20	145	2	53	86%	99%
19	108	30	108	0	0	72%	n/a
20	27	1	9	1	18	89%	94%
21	162	0	0	6	162	n/a	96%
22	90	8	72	0	18	89%	100%
23	108	9	27	2	81	67%	97%
24	108	8	36	0	72	78%	100%
25	180	29	162	0	18	82%	100%
26	171	11	90	3	81	88%	96%
27	162	25	126	0	36	80%	100%
					Average	80%	98%

Table 7.3. NNW performance testing of exudate recognition from normal retinal.

TF: total number of features, IE: number of incorrectly classified exudates, TE: total number of exudates to be identified, IR: number of incorrectly classified retina examples, TR: total number of retina examples to be identified

## 7.2. MACULA ANALYSIS

For our central vision to function properly it is vital that the highly sensitive macula region remains disease free. The presence of exudates, new vessels and or haemorrhages within and immediately surrounding the macula region acts as a forewarning that if untreated normal vision will be affected. The detection of these features only serves as an indication that sight may become threatened; a prognosis of maculopathy or macula oedema cannot be made unless there has been a reduction in visual acuity and a thickening of the macula region.

As discussed in Chapter 5.3 we successfully derived a process for detecting the macula region on a digital fundus image. At the time of detection the relative co-ordinates are saved thus permitting localised analysis to be performed on this area.

By combining the co-ordinates of the macula with the co-ordinates of the features correctly classified as exudates by the NNW, we were able to grade an image as being diabetic maculopathy based on the assumption that there are multiple exudates within one disc diameter of the centre of the fovea, *National Screening Committee 2004*.

The performance of the NNW was tested against a consultant ophthalmologist who classified twenty-eight images: 11 as maculopathy the other 17 were classified as not having maculopathy Table 7.4. This technique correctly identified 10 out of the 11 fundus images with maculopathy and 12 of 17 with no maculopathy, giving an overall sensitivity and specificity of 91%, 71% respectively.

Image	exudate	EWMR	NNWC	CC	Image	exudate	EWMR	NNWC	CC
1	0	0	x	x	15	68	30	√	x
2	0	0	x	x	16	83	8	√	x
3	29	29	√	√	17	13	8	√	√
4	27	6	√	√	18	44	17	√	√
5	7	0	x	x	19	125	58	√	√
6	40	15	√	√	20	8	0	x	x
7	18	0	x	√	21	0	0	x	x
8	0	0	x	x	22	0	0	x	x
9	5	0	x	x	23	64	25	√	√
10	5	5	√	x	24	18	16	√	√
11	0	0	x	x	25	28	2	√	x
12	0	0	x	x	26	0	0	x	x
13	0	0	x	x	27	133	24	√	√
14	24	0	x	x	28	79	47	√	√

Sensitivity: 91%  
Specificity: 71%

Table 7.4. Detection of maculopathy.

EWMR: number of exudates within 1 disc diameter of macula, NNWC: neural network classification, CC: consultant ophthalmologist classification, x: no maculopathy present, √: maculopathy present.

### **7.3. FULL IMAGE CLASSIFICATION**

We have successfully trained three individual NNW's to identify the main components of the diabetic retina, namely, normal background retina, vessels, haemorrhages and exudates. Combining the results from the three networks and by extrapolating the position of exudates in relation to the macula region we were able to grade the digital fundus images as being:

- ⌘ Normal, no evidence of diabetic retinopathy: No identifiable haemorrhages or exudates related to diabetic retinopathy.
- ⌘ Background: Multiple haemorrhages and or exudates detected.
- ⌘ Maculopathy: Exudates detected within one disc diameter of the macula.

The performance of the NNW was tested against a consultant ophthalmologist who classified 25 randomly selected images from the image data set. The classification of each image by the NNW and the consultant ophthalmologist is shown in Table 7.6. (the individual numbers of features have already been shown in Tables 7.2. & 7.3.).

Image	haemorr	exudates	maculop	NNWC	CC
1	x	x	x	N	N
2	x	√	x	M	M
3	√	x	√	M	M
4	√	x	x	B	B
5	x	x	x	N	P
6	√	√	√	M	M
7	x	√	x	B	M
8	x	x	x	N	N
9	x	√	x	B	B
10	x	√	√	M	B
11	x	x	x	N	N
12	√	x	x	B	B
13	x	x	x	N	B
14	x	√	√	M	M
15	√	√	√	M	B
16	√	√	√	M	B
17	x	√	√	M	M
18	√	√	√	M	M
19	√	√	x	B	B
20	x	x	x	N	N
21	x	x	x	N	B
22	√	√	√	M	M
23	√	√	√	M	M
24	x	x	x	N	N
25	x	√	√	M	M

*Sensitivity: 85%*  
*Specificity: 100%*

*Table 7.5. Full image classification.*

*NNWC: neural network classification, CC: consultant ophthalmologist classification, x: no features present, √: features present, N: normal, B: background retinopathy, M: maculopathy.*

The consultant ophthalmologist classified 5 images as normal with no disease pathology and the remaining 20 as having features associated with diabetic retinopathy. The 20 images were then graded with respect to disease progression: 9 images displaying features associated with background diabetic retinopathy, 10 images with maculopathy and 1 image with regressive pre-proliferative retinopathy.

Using the results from the trained NNW we graded each image as being:

- ⌘ Normal – no evidence of diabetic retinopathy: If the NNW classified none of the features as being either haemorrhages or exudates.
- ⌘ Background diabetic retinopathy: If one or more features were correctly classified as being haemorrhages or exudates.
- ⌘ Maculopathy: If one or more exudates were correctly identified and located within one disc diameter of the macula.

The NNW correctly classified all 5 of the normal images (100%) and 17 / 20 of the images displaying features associated with diabetic retinopathy (85%). It incorrectly classified three images as being normal: the ophthalmologist graded two of the images as background retinopathy and the other pre-proliferative retinopathy.

Under the above criteria, the NNW correctly classified 9 out of the 10 images displaying features associated with maculopathy (90%) and 4 of the 9 images displaying features associated with background retinopathy (44%). Three of the 5 background images were classified as being maculopathy (33%), the other 2 as normal (22%).

The current guidelines recommend a sensitivity of >80% and specificity of >95% for a single modality screening process, *British Diabetic Association report 1997*. Overall our method of combining image pre-processing algorithms with neural networks fulfils this criteria by achieving a sensitivity of 85% and specificity of 100% for distinguishing between normal images and images containing features associated with diabetic retinopathy.

#### 7.4. SUMMARY

In this chapter the ability of the trained neural network in identifying the main clinical features associated with diabetic retinopathy was assessed. A consultant ophthalmologist classified individual segments (20 x 20 pixel boxes) in addition to the image as a whole.

Three individual NNWs were trained to identify normal vessels, haemorrhages and exudates from normal background retina. The performance of the NNW was tested against the classification provided by the ophthalmologist for each feature. For the identification of each feature from normal background retina the NNW achieved a sensitivity of 93% and specificity 84% for vessels, a sensitivity of 81% and specificity 85% for haemorrhages and a sensitivity of 80% and specificity 98% for exudates.

Full images were classified as being normal if the NNW correctly identified no exudates or haemorrhages being present within the field of view. A classification of background retinopathy was given if the NNW correctly identified multiple haemorrhages and or exudates. Finally, images were classified as diabetic maculopathy if exudates were correctly identified within one disc diameter of the macula region.

Current guidelines recommend a sensitivity of >80% and specificity of >95% for a single modality screening process. Our method of combining pre-processing algorithms with neural networks fulfils this criterion by achieving a sensitivity of 85% and specificity of 100% for the identification of images displaying features associated with background diabetic retinopathy from normal images. When applied to the identification of sight-threatening maculopathy we achieved a sensitivity of 91% & specificity of 71% from non-maculopathy images. These results show that this method would successfully identify the greater majority of patients at risk of maculopathy but as a consequence it would also flag an additional number of patients who were not at risk.

## CHAPTER 8 – CONCLUSIONS AND FURTHER WORK

### 8.1. REVIEW

The images used for the training and testing of the NNW performance were selected from patients attending the diabetic review clinic at Gartnavel General Hospital. The selection of these images coincided with the commissioning of a new digital fundus camera that was purchased with funding from Diabetes UK. At the time of attendance to the review clinic the referring ophthalmologist graded each image. To minimise interobserver variability a consultant ophthalmologist subsequently graded the images.

The images were analysed for specific features using a combination of conventional image processing algorithms and neural networks. The Diabetic Retinopathy Image Classification Programme (DRICP) was a custom developed programme that was specifically written by the author to enable NNW training and learning data sets to be created. Additional components were written into the programme including image enhancement and automated feature detection algorithms. A detailed description of the programme and its functions were discussed in Chapter 4.

### 8.2. RECOGNITION OF NORMAL RETINAL FEATURES

The normal components of the retina were identified as being normal background retina, normal blood vessels, the optic disc (OD) and the macula.

Localisation of the optic disc and macular regions were achieved by identifying the areas of highest pixel and lowest pixel intensity values respectively. The accuracy for the identification of the optic disc and macula within a normal group and a diabetic retinopathy group of images was 100%, 98% and 91%, 89% respectively. These results are comparable with other researchers who applied a similar technique. *Sinthanayothin et al. 1999*, Selected 112 images from a diabetic review clinic and

successfully identified 91% of the OD's and 85% of the fovea's. The author does not indicate the classification of the images selected. Furthermore they have not stated the performance of their technique in identifying these features on normal fundus images.

Identification of normal retinal vasculature was performed using an optimally trained back-propagation neural network (NNW), yielding a sensitivity of 93% and specificity of 84%. The identification of normal retinal blood vessels is of particular importance when trying to detect abnormal vessel formation. While the NNW achieves a relatively high success rate in differentiating between background retina and larger blood vessels it is not as effective at identifying the fine new vessels. When applied to the detection of new vessels the NNW attained a sensitivity of 82% and specificity of 52%.

These results were comparable to the results obtained by researchers who also employed neural networks to classify vessels. *Gardner et al. 1996* reported a combined sensitivity and specificity of 92%. *Sinthanayothin et al. 1999* achieved a sensitivity of 83% and specificity of 91%. The slight differences within these results can be accounted by the discrepancies in the number of inputs and training examples. Neither of these studies provided information relating to the identification of new vessels.

Further investigation into the application of new algorithms for the detection of these sight-threatening features would be advantageous. One approach would be to utilise vessel tracking algorithms. However a certain amount of user input is required to define starting and end points and thus removes the automation of the technique. Nonetheless the benefit of this technique is that it allows the morphology and widths of vessels to be recorded. New vessels proliferate out into the vitreous cavity and are therefore a three dimensional feature. For this reason it will always be difficult to detect these features on two dimensional digital images.

### 8.3. RECOGNITION OF FEATURES ASSOCIATED WITH BACKGROUND DIABETIC RETINOPATHY

This thesis has concentrated on the automated identification of the common features associated with background diabetic retinopathy, namely hard exudates and haemorrhages. Exudates and haemorrhages can form as isolated lesions across the retina or as localised clusters. *Hipwell et al. 2000*, proposed that the number of micro-aneurysms was related to disease progression. They reported that their system could identify 76% of patients with no DR pathology at the expense of 15% of patient who actually have DR. Current screening guidelines require a sensitivity of 80% and specificity of 95%, therefore this technique would fail to meet this criteria

A fully automated technique was designed to segment digital colour fundus images into discreet 20 x 20 pixel examples. These were then used to successfully train a back-propagation neural network to identify exudates and haemorrhages from normal background retina achieving sensitivities and specificities of 80%, 81% and 98%, 85% respectively. The benefit of this approach is that it provides a fully automated method for identifying background diabetic retinopathy.

The results of this work can be compared with *Gardner* and *Sinthanayothin* who also employed neural networks. *Gardner* had a combined sensitivity and specificity of 93% for exudates and 74% for haemorrhages. *Sinthanayothin* reported a sensitivity of 86% & 78% and specificity of 100% & 89% for respective features, *Gardner et al. 1996, Sinthanayothin et al. 1999*.

The results obtained in this work are marginally poorer than those achieved by *Sinthanayothin*, this may simply be attributed to the difference in NNW design. *Sinthanayothin* presented the information to the NNW in a smaller matrix effectively reducing the contribution of other conflicting features. Other factors such as the number of training and testing examples can also contribute these differences.

At this stage these differences do not require the currently trained network to be redesigned. This will only come into effect when the system is tested against images taken from a true screening population.

The next stage would be to address methods for identifying pre-proliferative features such as cotton wool spots and vessel abnormalities. As with the more common features Neural Networks could be applied to the task. The shortfall of a neural network approach is that it requires a large quantity of good quality training examples. The features associated with pre-proliferative DR are less common and therefore it may prove more difficult to collect enough samples. As a result the trained NNW would yield poor specificity results similar to those obtained for new vessels.

#### **8.4. DETECTING DIABETIC MACULOPATHY**

As macular oedema is a major cause of treatable visual loss in diabetic patients early detection of its development is essential. The clinical definitions for classifying the varying degrees of diabetic related maculopathies are:

- **Exudative:** Characterised by exudates within the macular region, in particular causing visual damage if they accumulate at the centre of the fovea. This type of maculopathy is categorized as more threatening to sight if the exudates form groups or appear in complete or near-complete circular rings.
- **Diffuse:** This form of maculopathy is characterised by thickening or oedema of the retina; this may include little or no exudation but certainly microaneurysms will be present. Again at its most advanced stage there will be clusters of microaneurysms within the fovea region.
- **Ischaemic:** Presently, diagnosis of this form of maculopathy can only accurately be made through fundus fluorescein angiography

The accurate assessment of the macula for the detection of clinically significant macular oedema (i.e. diffuse and ischaemic strains) as defined by the Early Treatment Diabetic Eye Study group, *ETDRS 1991*, requires ophthalmoscopic screening utilising stereoscopic biomicroscopy and fluorescein angiography. The first technique provides the ophthalmologist with a 3-D view of the retina, enabling them to more accurately assess the extent of thickening within the patient's macula. Fluorescein angiography is an invasive technique which requires injecting a small amount of dye (sodium fluorescein) into the arm.

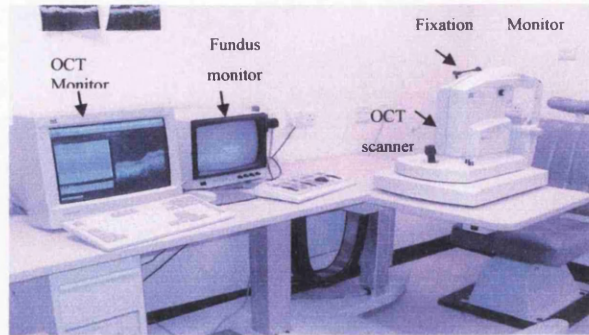
Images were classified as being at risk of developing maculopathy if exudates were identified within the macular boundaries. By extrapolating the co-ordinates of the exudates in relation to the co-ordinates of the macula and fovea boundaries images were graded according to the number of exudates identified within these boundaries. For the identification of diabetic maculopathy from non-maculopathy images our network achieved a sensitivity of 91% & specificity of 71%. There have been no similar attempts to identify maculopathy for comparison with these results.

There are a number of possible solutions to automatically detect diffuse and ischaemic diabetic maculopathy. The first would be to obtain a method of capturing 3-D fundus images. This would require the purchase of a new stereoscopic digital fundus camera. Once in place the actual process of analysing these images would follow a similar approach to those methods practised under the current study. It would involve training more neural networks to identify the differences under these new conditions. Hence, a new dataset of stereo images would have to be collected. However the accuracy of this technique being able to identify a significant increase in the thickness of the macula would have to be assessed.

Another more practical option for the department to pursue would be the inclusion of assessing macular thickening using optical coherence tomography (OCT). The department currently has a Humphrey-Zeiss Medical Systems (San Leandro, CA) system already in place, (*Fig 8.1.*). In addition to performing a full statistical analysis on the application of the technique including quantifying the repeatability and

reproducibility of the system, the EDIU department also has considerable experience of the clinical use of OCT, *Muscat et al. 2002, 2001a,b*.

*Fig 8.1. Humphrey OCT system, as currently set-up within the ElectroDiagnostic Imaging Unit at Gartnavel General Hospital.*



#### 8.4.1 OCT AND DIAGNOSING DIABETIC MACULAR OEDEMA

OCT provides a non-contact and non-invasive means for measuring cross-sectional or tomographical retinal thickness. Many groups have reported the assessment of macular oedema through OCT and have shown a correlation between visual acuity and relative central foveal thickness, *Yang et al. 2001, Yamamoto et al. 2001, Hee et al. 1998, 1995*. Morphologically, the changes in macular oedema include a decreased intraretinal reflectivity, arising from cystic changes and fluid accumulation. Chronic forms of cystoid macular oedema can lead to the development of macular holes, (*Fig 8.2.*). This is evident on OCT as a partial thickness loss of retinal tissue and an abnormal retinal contour.

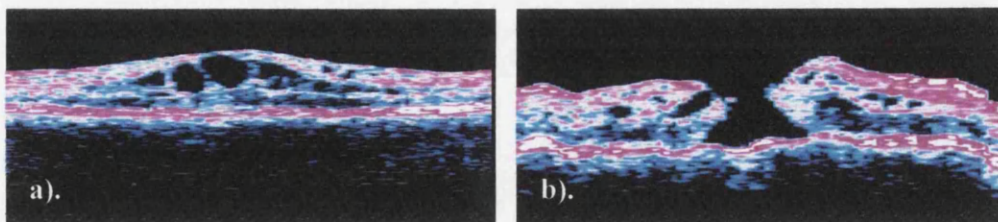


*Fig 8.2. a) Macular Oedema b) Macular hole  
Images obtained from the ElectroDiagnostic Imaging Unit, Gartnavel General Hospital, Glasgow*

Optical coherence tomography provides an objective assessment of diabetic macular oedema through cross-sectional images of the retina. It is a technique that can measure retinal thickness as well as the intraretinal structures of the eye. Combined with an automated diabetic retinopathy feature detection system it could provide the extra dimension required to successfully identify macular oedema.

### **8.5. DETECTING NEW VESSELS AT THE OPTIC DISC**

The identification of new vessels is particularly complex as they appear as very fine strands with highly irregular shapes and are difficult to distinguish from the background retinal hue. Their detection is marginally easier at the optic disc due to its brighter hue. Identification of new vessels at the optic disc was achieved by analysing the differences in pixel colour values. Normal profiles were compared against optic discs with new vessels.

When plotted in profile vessel edges appear as a trough, the adjacent peak making the other edge of the vessel and a return to the higher intensity background. Plateau between major vessel edges remain fairly uniform on normal OD profiles. However on OD's with new vessel growth the plateaus between major vessels exhibit an increase in the number of peaks suggesting the presence of further vessel activity. To quantify the difference between the circular intensity profiles (CIP) of OD's displaying normal retinal vasculature and OD's with new vessels, we employed a method of counting the relative number of turning points. We found that there was a significant difference  $p < 0.001$  between the average number of turning points on a normal optic disc (59.8, SD 2.41) with radius 40 pixels when compared to images with new vessels at the optic disc (66.6, SD 2.58). There has been no reports on similar work to compare these results to.

Circular intensity profiling is a promising automated technique for identifying new vessels within the optic disc. More examples have to be collected and further work has to be performed in this area. Some techniques that could be applied would involve the removal of the normal vessels and assessing the remaining intensity

profiles or quantifying the number of pixels between turning points as an assessment of vessel width.

## **8.6. DISCUSSION**

The aim of this work was to develop an automated computerised system to aid in the screening of diabetic retinopathy. To achieve this custom written software was developed to enable the integration of image acquisition, image processing, neural network (NNW) training and testing algorithms to be performed in a structured manner.

Images were collected from the Diabetic Review Clinic at Glasgow's GGH. The images were pre-selected by the author to represent an array of normal retinal examples and those containing specific features attributed to diabetic retinopathy. Images were initially graded by junior ophthalmologists at the time of photographic referral and subsequently graded by a consultant ophthalmologist. As the images were pre-selected from a review clinic they do not give a true representation of the screening population. This may account for the high sensitivities and specificities achieved. Therefore to provide an unbiased representation of the trained NNWs performance a future requirement would be to test the system on random images classified by trained screeners and taken from the screening population. The added benefit of this validation is that it would also test whether the current system is robust enough to identify retinal features from other digital fundus cameras with a similar success rate to that described in this thesis.

Further investigation into identifying other retinal pathologies will also have to be introduced into the screening algorithm. Diabetic retinopathy is a life long progressive disease, there are many other sight threatening conditions that also develop with age. Therefore the system must be developed so that patients are not misclassified.

The structure for this development is in place. This work has shown that NNWs are an efficient tool for feature classification therefore the same principles can be adapted for feature recognition associated with age related macular degeneration (ARMD) and glaucoma. Both these conditions can develop features similar to diabetic retinopathy. In glaucoma high intraocular pressure (IOP) can result in flame shaped haemorrhages while patients with ARMD can develop microaneurysms and lesions which are similar to DR exudates. These examples would be taken from the screening population so that the trained NNWs would be properly validated.

So far features have been classified in isolation and therefore cannot be directly compared to the clinical situation. One possible solution is to develop a multiple output NNW. The problem with this approach is that training times will increase. Moreover the performance will be compromised due to the greater need for feature generalisation. Another possibility is to develop a tiered classification structure which will identify the most severe features first.

Some progress was achieved in identifying the growth of new vessels. A NNW was trained to identify these features in the peripheral retina. Unfortunately the results obtained were poor due to the limited number of features collected. It may be valuable to repeat this process if access to screening centres provides a greater collection of new vessel examples. Promising results were shown in our analysis of optic discs. The use of circular intensity profiles revealed a significant difference ( $p < 0.001$ ) between the number of turning points (associated with vessel edges) between normal optic discs and those that have new vessels. These results were obtained from a small data set of images and again would benefit from re-analysis with a larger dataset. Progress was also made in diagnosing sight-threatening exudative diabetic maculopathy.

In conclusion, the author has developed a custom written program which enables image acquisition, image processing, neural network training and testing to be performed in a structured manner. The results obtained by the author agree with those reported by *Gardner et al. 1996* and *Sinthanayothin et al. 1999*. Both used neural networks to automatically identify background diabetic retinopathy features.

Moreover, the author has successfully combined feature location information enabling the identification of people with sight threatening exudative maculopathy. Diffuse and ischaemic maculopathy cannot be identified from standard two-dimensional images. This problem may be addressed by integrating the current system with visual acuity and macular thickness measurements. Recent technological advancements have resulted in new commercial systems that are capable of providing fast and accurate retinal thickness measurements. Optical coherence tomography (OCT) is a non-invasive procedure that can be combined with the current system to provide a real practical solution to the automated screening problem. The author has also proposed a method of analysing the circular intensity profile of the optic disc to identify new vessels. There are no other studies to date that have reported any success in classifying these sight threatening features. The next stage is to test the current computer program on images collected from a diabetic screening service. However, before the system can operate as a stand-alone screening tool it must be capable of identifying other pathologies. This will require further careful investigation.

APPENDIX I

IMAGE CLASSIFICATION AND FEATURES IDENTIFIED BY A CONSULTANT

OPHTHALMOLOGIST

	NVE	NVD	M'PTHY	PRE-PRO	PROLIF	B'GND	OTHER FEATURES	R Eye	L Eye
1							E, H		
2							E, H, CWS		
3				?			E, H, CWS		
4							E		
5							OV, Lx		
6				?			E, H, CWS		
7							E, H		
8			Rx				E		
9			?-Rx				E, H, CWS, Lx		
10							E, H, TV		
11							H		
12									
13			Rx				E, H		
14			Rx				E, H, Lx		
15			Rx				E, H, Lx		
16							E, H, AV		
17							E, H, CWS, Lx		
18							H		
19							H, OV		
20					Rx		E, H, Lx		
21							E, H		
22							E, H		
23			?				E		
24							E, H		
25							E, H, TV		
26							E, H		
27							E, H		
28			?				E, H		
29							E, H, Lx		
30					Rx		E, H		
31							asteroids		
32							asteroids		
33			?				E, H		
34							nasal view		
35			?	?			E, H, CWS		
36			?				E, H		
37							H		
38							E, H		
39							E, H		
40				?			H		
41							H, CWS		
42							E, H		
43							E, H		
44							E, H		
45							E, H, nasal view		

	NVE	NVD	M'PTHY	PRE-PRO	PROLIF	B'GND	OTHER FEATURES	R Eye	L Eye
46							E, H		
47							E, CWS		
48							E, H		
49							E, H, Lx		
50							reflex artefact		
51			?				E, H		
52							E		
53							E, H		
54							regressed		
55							E, H, OL		
56							E, H		
57							E, H		
58							E, H		
59							normal		
60							H		
61					?		E, H		
62									
63							artefact at macula		
64					Rx		E, H		
65					Rx		H, Lx		
66					Rx		H, OV, Lx		
67					Rx		H, OV, Lx		
68							E, H		
69							E		
70							E, regressed		
71							E		
72							E, H, OV		
73							E, H, CWS		
74							H, CWS, OV		
75									
76							E, H, Lx		
77							E, H		
78							E, H		
79					Rx		E, H, CWS, Lx		
80			?				E		
81							H		
82			?				E, H		
83									
84							E, H		
85			?				E, H		
86							E		
87			Rx				E, H, Lx		
88			?				E, H		
89			?				E, H		
90				?			E, H, CWS		
91							regressed		
92							post surgery		
93									
94				?			E, H, CWS		
95							H, CWS, nasal view		
96	?						E, H		
97							vitreous haemorrhage		
98							vitreous haemorrhage		

	NVE	NVD	M'PTHY	PRE-PRO	PROLIF	B'GND	OTHER FEATURES	R Eye	L Eye
99									
100			?				E, H		
101							E, H		
102							H		
103							E, H		
104							lesion at fovea		
105							post vitreous surg		
106							post vitreous surg		
107							E, H, CWS		
							H		
							E, H		
108									
109							OL, scar tissue		
110					Rx		Lx		
111							H		
112							Lx		
113							H, OL		
114							Lx		
115							Lx		
116							H, Lx		
117							E, H, Lx		
118							E, H, OL, Lx		
119							E, H		
120							E, H, Lx		
121							young normal		
122							young normal		
123							E, H, CWS		
124							E, H		
125							E, H		
126							E, H		
127							E, H, CWS		
128							E, H		
129							H		
130							E, H		
131							H		
132				?			H, CWS		
133							H		
134							H		
135							H		
136							E		
137							E, H		
138							E, H		
139							E, H		
140							E, H		
141							E, H		
142							E, H		
143							E, H, Lx		
144							OL, poor quality		
145		?					E, H		
146							E, H		
147							E		
148							E, Lx, poor quality		
149							E, H		

	NVE	NVD	M'PTHY	PRE-PRO	PROLIF	B'GND	OTHER FEATURES	R Eye	L Eye
150							E, Lx		
151			?				E, H, CWS		
152							E, H		
153							E, H		
154							E, H		
155					?		E, H		
156							E, H		
157							poor quality		
158							E, H		
159							E, H, OL		
160			?				E, H		
161							E, H		
162							E		
163							E, H		
164							E, H, OL, scar tissue @disc		
165							E, Lx		
167							E, H		
168				?			E, H, CWS		
169							E, H		
170							E, H		
171							E, H		
172							E, H, TV		
173					?		E, H		
174							E, H		
175							E, H, CWS		
176							E		
177							Lx		
178							H, Lx		
179							H		
180							E, Lx		
181							E, H		
182							poor quality		
183							E, H		
184							poor quality		
185							poor quality		
186							E, H, CWS		
187							E, H		
188							E, H, Lx		
189							E, H, Lx		
190							E, H		
191							H, poor quality		
192							E, poor quality		
193							E, H		
194							E, H		
195									
196							E, H		
197							E, H, CWS		
198							not diabetic		
199							E, H		
200							E, H		
201							H		
202							E, H, Lx		
203				Rx			E, H, Lx		

	NVE	NVD	M'PTHY	PRE-PRO	PROLIF	B'GND	OTHER FEATURES	R Eye	L Eye
204					Rx		H, Lx		
205							H		
206							poor quality		
207							E, H		
208							E, H		
209							E, H		
210							H		
211		?					H		
212		?					H		
213							E		
214							H		
215							H		
216							E, H		
217							? Non diabetic		
218							E, H		
219					Rx		poor quality		
220							E, H, CWS, AV		
221							H, CWS		
222							E, H, CWS		
223							E, H, CWS, TV		
224				?			E, H, TV		
225							E, H		
226							poor quality		
227							H		
228							H		
229							H, AV		
230									
231							E, H		
232							poor quality		
233							H		
234							E, H		
235							normal		
236							normal		
237									
238							H		
239							E		
240							E, H		
241							H, advanced DED		
242							Lx		
243							Lx		
244							advanced DED		
245							Lx		
246							OL, Lx		
247							advanced DED		
248							poor quality		
249		?					E, H, TV		
250	?						H		
251	?						E, H		
252									
253									
254							E, TV		
255							normal		
256							E, H		

	NVE	NVD	M'PTHY	PRE-PRO	PROLIF	B'GND	OTHER FEATURES	R Eye	L Eye
257							E, H		
258							E, H		
269							E, H		
260			???				jo ? M'pathy		
261							nasal view		
262							OL		
263							mag disc		
264			???				E, H		
265							E, H		
266							H		
267							E, H		
268			Rx				Rx		
269							E, H		
270							nasal view		
271							E, H, CWS		
272							age changes? Drusen		
273							E, H		
274							E		
275							poor quality		
276									
277									
278									
279									
280		?			?		poor quality		
281									
282									
283									
284			?				E		
285							E, H, Lx		
286							E, H		
287							poor quality		
288							poor quality		
289							poor quality		
290									
291							E		
292							E, H		
293							E, H, Lx		
294			?				E, H		
295							H		
296									
297									
298							E, H		
299							E, H		
300									
301							E, H		
302			?				E, H		
303							posterior pole		
304							nasal view		
305			?				E, H		
306							E, H		
307			?				poor quality		
308							poor quality		
309							E, H		

	NVE	NVD	M'PTHY	PRE-PRO	PROLIF	B'GND	OTHER FEATURES	R Eye	L Eye
310							E, H		
311			?				E, OL		
312							E		
313							E		
314									
315							H		
316				?			E, H		
317			?				E, H		
318							E, H		
319			Rx				E, H		
320			?				E, H		
321							H		
322			?				E, H		
323							E, H		
324			?				E, H, AV		
325			?				E, H, AV		
326					Rx				

*NB. The '?' represent images which may be classed as maculopathy but the ophthalmologist could not be 100% certain without the patient clinical records.*

E – Exudate, H – Haemorrhage, Lx – Laser burns, OV – Occluded vessels, TV – Tortuous vessels, OL – Omega loop, Rx – treated, AV – AV nipping

Images were selected from this group to create training and test data sets.

## APPENDIX II

## NEURAL NETWORK ASCII FILE FOR A SINGLE FEATURE

```

131 132 134 134 134 133 132 132 133 134 136
133 131 131 132 134 136 134 133 129 133
133 134 135 136 133 130 132 135 133 132
133 134 134 135 136 137 137 138 133 133
132 132 134 136 134 133 132 132 131 131
130 130 134 139 139 139 139 139 136 132
133 134 136 139 137 135 133 132 135 139
137 136 137 139 140 141 142 143 139 138
136 134 135 136 138 140 139 139 139 139
139 139 140 141 141 141 139 138 136 133
133 134 136 139 139 140 140 141 138 135
136 138 141 144 142 140 139 139 137 132
134 136 137 138 136 134 134 134 136 139
139 140 141 143 140 137 136 135 135 139
138 137 136 136 134 132 135 139 142 146
143 140 140 140 138 136 133 130 123 138
137 136 136 136 137 139 143 147 145 144
141 138 137 136 132 129 123 118 115 134
133 132 133 134 138 143 143 144 143 142
140 138 132 127 119 112 115 118 117 133
133 133 134 136 138 140 140 140 139 138
133 128 122 116 119 123 121 119 116 133
134 136 136 137 136 135 134 134 129 125
120 115 120 125 121 118 116 115 121 133
135 137 136 136 133 131 128 126 121 116
117 119 119 119 117 115 122 130 135 134
133 133 132 132 125 119 118 117 119 121
116 112 112 113 121 130 135 140 141 135
130 126 121 117 117 117 120 123 123 124
121 118 124 131 135 139 142 145 145 131
123 116 114 113 117 121 119 118 122 126
131 136 138 140 140 140 144 148 148 122
115 109 113 117 116 115 119 123 130 137
141 146 143 140 142 144 145 146 146 114
113 112 113 114 115 117 125 133 137 142
145 148 145 142 145 148 146 145 144 119
115 112 116 121 126 131 135 139 142 146
147 149 146 144 145 147 147 147 147 115
118 121 127 134 137 140 141 142 145 149
148 148 147 146 145 145 146 148 148 &
! 20 D:\Test\Js0025z1.bmp 410 111 430 131

```

\* The first 400 numbers are the green bit colour information values, the '&' indicates to the NNW that the next piece of information is the output classification value and the '!' begins a comment which holds the image name from which the feature was taken and its location within the image in terms of its TopLeft, BottomRight co-ordinates. This later information is required for assessing the network's performance and determining if there is a particular reason why the network may have misclassified an area

## APPENDIX III

## APHELION SOURCE CODE FOR OPTIC DISC DETECTION

*(this code was not written by the author)*

```

Public source$,target$,objt$
Sub main
'=====
===== ' user changeable parameters
    const percent=75
    const keepfiles=0 ' =0 to store, =1 to skip storage of
processed files
    const roiLLX=80      ' region of interest which cuts out black
surround and writing
    const roiLLY=80
    const roiURX=639
    const roiURY=479
    const startrad=150   ' assume that disc border is within
this radius of max point
    source$= "c:\ale\normals\" ' source directory
    target$= "c:\ale\processed\" ' target directory
    objt$= "c:\ale\objects\" ' objects directory
'=====
=====
    Dim b$(4)
    Const crlf = Chr$(13) + Chr$(10)
    dim maxLLX as double
    dim maxLLY as double
    dim maxURX as double
    dim maxURY as double
    dim thresh as double
    dim i as integer
    ChDir (source$)
    v$ = Dir$("*.*bmp")
    s$ = source$ & v$
    t$ = target$ & v$
    o$ = objt$ & Left$(v$,Len(v$)-4) & ".dat"
    i = 0
,
' Loop on all the images
,
    While (v$ <> "")
        u$ = "origin " & i
        w$ = "hsi " & i
        x$ = "iband " & i
        y$ = "rct " & i
        z$ = "out " & i
        original = AphImgNew(u$)
        hsi = AphImgNew(w$)
        iband = AphImgNew(x$)
        rct=AphImgNew(y$)
        out=AphImgNew(z$)
,
' Read the image from the disk, and get the intensity image
,
        AphImgRead original, s$
        AphImgRGBToHSI original, hsi

```

```

    AphImgSplitBands hsi,iband,2
,
' cut out the writing and black border
,
    AphImgDisableRoi iband,0
    AphImgAddRoi iband,
AphHRectRegion(roiLLX,roiLLY,roiURX,roiURY)
    AphImgSubCopy iband, rct
    AphImgResetRoi iband
    AphImgEnableRoi iband,0
,
' get the range
,
    Dim range() as double
    AphImgRange rct,range
    minf = range(0)
    maxf = range(1)
    thresh=minf+(percent*(maxf-minf)/100)
,
' apply threshold and create objects
,
    outObj = AphObjNew("discs")
    AphImgThresholdObj rct,outObj,AphThreshold(maxf,maxf)
,
' get the maximum coordinates
,
    Dim moments() as double
    AphObjMoments outObj,"REGION.EXTENTS.LL.X", moments
    maxLLX=moments(2)
    AphObjMoments outObj,"REGION.EXTENTS.LL.Y", moments
    maxLLY=moments(2)
    AphObjMoments outObj,"REGION.EXTENTS.UR.X", moments
    maxURX=moments(2)
    AphObjMoments outObj,"REGION.EXTENTS.UR.Y", moments
    maxURY=moments(2)
,
' now get disc coordinates
,
    dim point(2) as long
    dim value as integer
' first discLLX
    if ((maxLLX-starttrad)<0) then
        point(0)=0
    else
        point(0)=maxLLX-starttrad
    end if
    point(1)=maxLLY
    value=AphImgGetPixel(rct,point)
    while (value<=thresh)
        point(0)=point(0)+1
        value=AphImgGetPixel(rct,point)
    wend
    discLLX=point(0)
' then discURX
    if ((maxLLX+starttrad)>(roiURX-roiLLX)) then
        point(0)=roiURX-roiLLX
    else
        point(0)=maxLLX+starttrad
    end if
    point(1)=maxLLY

```

```

        value=AphImgGetPixel(rct,point)
        while (value<=thresh)
            point(0)=point(0)-1
            value=AphImgGetPixel(rct,point)
        wend
        discURX=point(0)
' first discLLY
        if ((maxLLY-startrad)<0) then
            point(1)=0
        else
            point(1)=maxLLY-startrad
        end if
        point(0)=maxLLX
        value=AphImgGetPixel(rct,point)
        while (value<=thresh)
            point(1)=point(1)+1
            value=AphImgGetPixel(rct,point)
        wend
        discLLY=point(1)
' then find discURY
        if ((maxLLY+startrad)>(roiURY-roiLLY)) then
            point(1)=roiURY-roiLLY
        else
            point(1)=maxLLY+startrad
        end if
        point(0)=maxLLX
        value=AphImgGetPixel(rct,point)
        while (value<=thresh)
            point(1)=point(1)-1
            value=AphImgGetPixel(rct,point)
        wend
        discURY=point(1)
,
' create the out image
,
        AphImgCopy iband,out
        AphImgSubtractConstFloor out,out,1
        AphImgDisableRoi out,0
        AphImgAddRoi
out,AphHRectRegion(roiLLX+discLLX,roiLLY+discLLY,roiLLX+discURX,roiL
LY+discURY)
        AphImgFill out,255
        AphImgResetRoi out
        AphImgEnableRoi out,0
        AphImgThresholdObj out, outObj, AphThreshold(255,255)
        if keepfiles=0 then
            AphImgWrite out, t$      ,"AphBmpFile"
        end if
        AphObjExport outObj, o$
,
' free images and objects
,
        AphImgFree original
        AphImgFree hsi
        AphImgFree iband
        AphImgFree rct
        AphImgFree out
        AphObjFree outObj
' get the next image

```

```

    v$ = Dir$
    i = i + 1
    If (v$ <> "") Then
        s$ = source$ & v$
        t$ = target$ & v$
        o$ = objt$ & Left$(v$,Len(v$)-4) & ".dat"
    End If

Wend
AphImgFreeAll
i = percent
call createAll(i)
MsgBox "End of the discs program !"
'
' End
'

End Sub

Sub createAll(j as integer)
    Dim a$()
    ChDir (objt$)
    FileList a$,"*.dat"
    If ArrayDims(a$) > 0 Then
        Open "discs.dta" For Append As #1
        Print #1,"discs macro with percent selected as " &
CStr(j)
        for i=0 to 1+ArrayDims(a$)
            Open a$(i) For Input As #2
            Line Input #2,lin$
            Do While Not EOF(2)
                Line Input #2,lin$
                Print #1,a$(i) & Chr$(9);
                Print #1,lin$
            Loop
            Close #2
        next i
        close #1
    end if
End Sub

```

## APPENDIX IV

## APHELION SOURCE CODE FOR MACULA DETECTION

*(this code was not written by the author)*

```

Public source$,target$,objt$
Sub main
'=====
=====
' user changeable parameters
  const percent=75 ' threshold value for detecting minimum
point
  const keepfiles=0 ' =0 to store, =1 to skip storage of
processed files
  const roiLLX=220 ' region of interest which excludes borders
of image
  const roiLLY=148
  const roiURX=499
  const roiURY=427
  const startrad=100 ' assume edge of fovea is within this
value of min point
  source$= "c:\ale\normals\" ' source directory
  target$= "c:\ale\processed\" ' target directory
  objt$= "c:\ale\objects\" ' objects directory
'=====
=====
  Dim b$(4)
  Const crlf = Chr$(13) + Chr$(10)
  dim maxLLX as double
  dim maxLLY as double
  dim maxURX as double
  dim maxURY as double
  dim thresh as double
  dim i as integer
  ChDir (source$)
  v$ = Dir$("*.bmp")
  s$ = source$ & v$
  t$ = target$ & v$
  o$ = objt$ & Left$(v$,Len(v$)-4) & ".dat"
  i = 0
'
' Loop on all the images
'
  While (v$ <> "")
    u$ = "origin " & i
    w$ = "hsi " & i
    x$ = "iband " & i
    y$ = "rct " & i
    yl$ = "rctin " & i
    z$ = "out " & i
    original = AphImgNew(u$)
    hsi = AphImgNew(w$)
    iband = AphImgNew(x$)
    rct=AphImgNew(y$)
    rctin=AphImgNew(yl$)
    out=AphImgNew(z$)

```

```

'
' Read the image from the disk, and get the intensity image
'
      AphImgRead original, s$
      AphImgRGBToHSI original, hsi
      AphImgSplitBands hsi,iband,2
'
' cut out the writing and black border
'
      AphImgDisableRoi iband,0
      AphImgAddRoi iband,
AphHRectRegion (roiLLX, roiLLY, roiURX, roiURY)
      AphImgSubCopy iband, rct
      AphImgResetRoi iband
      AphImgEnableRoi iband,0
'
' invert and filter
'
      AphImgInvert rct,rctin
      AphImgGaussianFilter rctin,rct,11
'
' get the range
'
      Dim range() as double
      AphImgRange rct,range
      minf = range(0)
      maxf = range(1)
      thresh=minf+(percent*(maxf-minf)/100)
'
' apply threshold and create objects
'
      outObj = AphObjNew("foveas")
      AphImgThresholdObj rct,outObj,AphThreshold(maxf,maxf)
'
' get the maximum coordinates
'
      Dim moments() as double
      AphObjMoments outObj,"REGION.EXTENTS.LL.X", moments
      maxLLX=moments(2)
      AphObjMoments outObj,"REGION.EXTENTS.LL.Y", moments
      maxLLY=moments(2)
      AphObjMoments outObj,"REGION.EXTENTS.UR.X", moments
      maxURX=moments(2)
      AphObjMoments outObj,"REGION.EXTENTS.UR.Y", moments
      maxURY=moments(2)
'
' now get fovea coordinates
'
      dim point(2) as long
      dim value as integer
' first foveaLLX
      if ((maxLLX-startrad)<0) then
          point(0)=0
      else
          point(0)=maxLLX-startrad
      end if
      point(1)=maxLLY
      value=AphImgGetPixel(rct,point)
      while (value<=thresh)
          point(0)=point(0)+1

```

```

        value=AphImgGetPixel(rct,point)
    wend
    foveaLLX=point(0)
' then foveaURX
    if ((maxLLX+startrad)>(roiURX-roiLLX)) then
        point(0)=roiURX-roiLLX
    else
        point(0)=maxLLX+startrad
    end if
    point(1)=maxLLY
    value=AphImgGetPixel(rct,point)
    while (value<=thresh)
        point(0)=point(0)-1
        value=AphImgGetPixel(rct,point)
    wend
    foveaURX=point(0)
' first foveaLLY
    if ((maxLLY-startrad)<0) then
        point(1)=0
    else
        point(1)=maxLLY-startrad
    end if
    point(0)=maxLLX
    value=AphImgGetPixel(rct,point)
    while (value<=thresh)
        point(1)=point(1)+1
        value=AphImgGetPixel(rct,point)
    wend
    foveaLLY=point(1)
' then find foveaURY
    if ((maxLLY+startrad)>(roiURY-roiLLY)) then
        point(1)=roiURY-roiLLY
    else
        point(1)=maxLLY+startrad
    end if
    point(0)=maxLLX
    value=AphImgGetPixel(rct,point)
    while (value<=thresh)
        point(1)=point(1)-1
        value=AphImgGetPixel(rct,point)
    wend
    foveaURY=point(1)
,
' create the out image
,
    AphImgCopy iband,out
    AphImgSubtractConstFloor out,out,1
    AphImgDisableRoi out,0
    AphImgAddRoi
out,AphHRectRegion(roiLLX+foveaLLX,roiLLY+foveaLLY,roiLLX+foveaURX,r
oiLLY+foveaURY)
    AphImgFill out,255
    AphImgResetRoi out
    AphImgEnableRoi out,0
    AphImgThresholdObj out, outObj, AphThreshold(255,255)
    if keepfiles=0 then
        AphImgWrite out, t$ , "AphBmpFile"
    end if
    AphObjExport outObj, o$
,

```

```

' free images and objects
'
    AphImgFree original
    AphImgFree hsi
    AphImgFree iband
    AphImgFree rct
    AphImgFree rctin
    AphImgFree out
    AphObjFree outObj

' get the next image
    v$ = Dir$
    i = i + 1
    If (v$ <> "") Then
        s$ = source$ & v$
        t$ = target$ & v$
        o$ = objt$ & Left$(v$,Len(v$)-4) & ".dat"
    End If

    Wend
    AphImgFreeAll
    i = percent
    call createAll(i)
    MsgBox "End of the foveas program !"
'
' End
'

End Sub

Sub createAll(j as integer)
    Dim a$()
    ChDir (objt$)
    FileList a$,"*.dat"
    If ArrayDims(a$) > 0 Then
        Open "foveas.dta" For Append As #1
        Print #1,"foveas macro with percent selected as " &
CStr(j)
        for i=0 to 1+ArrayDims(a$)
            Open a$(i) For Input As #2
            Line Input #2,lin$
            Do While Not EOF(2)
                Line Input #2,lin$
                Print #1,a$(i) & Chr$(9);
                Print #1,lin$
            Loop
            Close #2
        next i
        close #1
    end if
End Sub

```

## LIST OF REFERENCES

Abdul-Wahab SA, Al-Alawi SM. Assessment and prediction of tropospheric ozone concentration levels using artificial neural networks. *Environmental Modelling and Software* 2002;17:219-228.

Adams G, Takahashi Y, Ban S et al.. Artificial neural network for predicting the toxicity of organic molecules. *Bulletin of the Chemical Society of Japan* 2001;74:2451-2461.

Aiello LP, Gardner TW, King GL, et al.. Diabetic retinopathy. *Diabetes Care* 1998;21:157-159.

Aiello LP, Gardner TW, King GL, et al.. Diabetic retinopathy. *Diabetes Care* 1999;22:S70-S73.

Alberti KGMM, Zimmet PZ for the WHO Consultation. Definition, diagnosis and classification of diabetes mellitus and its complications. Part 1: diagnosis and classification of diabetes mellitus. Provisional report of a WHO Consultation. *Diabetic Medicine* 1998;15:539-553.

Aldington SJ, Kohner EM, Meuer S, et al.. Methodology for retinal photography and assessment of diabetic retinopathy: the EURODIAB IDDM Complications Study. *Diabetologia* 1995;38:437-444.

*Anatomy of the eye* 1999. The discovery fund for eye research. Accessed 1999: <http://www.discoveryfund.com/anatomyoftheeye.html>

Barrett SF, Naess E, Molvik T. Employing the Hough Transform to locate the optic disk. *Biomedical Sciences Instrumentation* 2001;37:81-86.

Basheer I. Selection of methodology for modelling hysteresis behaviour of soils using neural networks. *J of Computer-aided Civil Infrastructure & Engineering* 2000;5:445-463.

Bishop CM: *Neural Networks for Pattern Recognition*. 1995; ISBN 019-85-3864-2.

Bland JM, Altman DG. Statistical methods for assessing agreement between two methods of clinical measurement. *Lancet* 1986;i;307-310.

*British Diabetic Association Report* 1997. Retinal photography screening for diabetic eye disease. Accessed 1997: <http://www.diabetes.org.uk/infocentre/r.htm>.

Carpenter GA & Grossberg S. The ART of adaptive pattern recognition by a self-organizing neural network. *Computer* 1988;3;77-88.

Carpenter GA & Grossberg S. ART2: self-organization of stable category recognition codes for analog input patterns. *Appl Opt* 1987;26:4914-4930.

Carr RE: *Electrodiagnostic Testing of the Visual System: A Clinical Guide*. F.A. Davis Company, Philadelphia 1990; ISBN 0-8036-1682-1.

Cree MJ, Olson JA, McHardy KC et al.. A fully automated comparative microaneurysm digital detection system. *Eye* 1997;11:622-628.

Cree MJ, Olson JA, McHardy KC et al.. Automated Microaneurysm Detection, *IEEE International Conference on Image Processing* 1996;3:699-702.

Dauffenback LM. Simulation of the primate motor cortex and free arm movements in three-dimensional space: A robot arm system controlled by an artificial neural network. *Biomedical Sciences Instrumentation* 1999;35:360-365.

Davalos S, Gritta RD, Chow G. The application of a neural network approach to predicting bankruptcy risks facing the major US air carriers: 1979-1996. *J of Air Transport Management* 1999;5:81-86.

Ege BM, Hejlesen OK, Larsen OV, et al.. Screening for diabetic retinopathy using computer based image analysis and statistical classification. *Computer Methods and Programs in Biomedicine* 2000;62:165-175.

El-Din AG, Smith DW. A neural network to predict the wastewater inflow incorporating rainfall events. *Water Research* 2002;36:1115-1126.

ETDRS Research Group. Grading Diabetic Retinopathy from Stereoscopic Color Fundus Photographs – An Extension of the Modified Airlie House Classification. *Ophthalmology* 1991(a);98:786-806.

ETDRS Research Group. Early photocoagulation for diabetic retinopathy. ETDRS Report no. 9 *Ophthalmology* 1991(b); 98:766-785.

Evans J. Causes of blindness and partial sight in England and Wales 1990-91. HMSO  
Diabetic Retinopathy Research Group. Indications for photocoagulation treatment of diabetic retinopathy:diabetic retinopathy study report no. 14. *International Ophthalmol Clin* 1987; 27:239-253.

Everitt B. *Cluster analysis*. Heinemann Educational Books Ltd. 1977 ISBN 0-435-82297-7.

*Eye Anatomy* 1996. StLukesEye.com. Accessed 1998: <http://www.stlukes-eye.com/Anatomy.asp>

*Fact Sheet 1* 2000, Diabetes UK. Accessed 2000:  
<http://www.diabetes.org.uk/infocentre/fact/fact.htm>.

*Fact Sheet 2* 2000, Diabetes UK. Accessed 2000:  
<http://www.diabetes.org.uk/infocentre/fact/fact2.htm>

Fact Sheet 3 2000, Diabetes UK. Accessed 2000:  
<http://www.diabetes.org.uk/infocentre/fact/fact3.htm>.

Fariselli P, Casadio R. A neural network based predictor of residue contacts in proteins. *Protein Engineering* 1999;12:15-21.

Foulds WS, McCuish, A, Barrie, T, et al.. Diabetic retinopathy in the West of Scotland: its detection and prevalence, and the cost-effectiveness of a proposed screening programme. *Health Bull (Edinb)* 1983;41:318-326.

Frame AJ, Undrill PE, Cree MJ, et al.. A comparison of computer based classification methods applied to the detection of microaneurysms in ophthalmic fluorescein angiograms, *Computers in Biology and Medicine* 1998;28:225-238.

Frame AJ, Cree MJ, Olson JA, et al.. Computer-Based Classification of Retinal Microaneurysms, *Proceedings of the 2nd International Conference on Neural Networks and Expert Systems in Medicine and Healthcare* 1996:50-56.

Gardner GG, Keating D, et al.. Detection of Diabetic Retinopathy using Neural Networks Analysis of Fundus Images. *Proc 2<sup>nd</sup> International conf. On Neural Network and Expert Systems in Medicine and Healthcare* 1996:p28-35.

Gardner GG, Keating D, et al.. Automatic Detection of Diabetic Retinopathy Using Neural Networks. *IOVS* 1996;36(3):4453.

Gardner GG, Keating D, et al.. Automatic Detection of Diabetic Retinopathy Using An Artificial Neural Network: A Screening Tool. *BJO* 1996;30:940-944.

Gogou G, Maglaveras N, Ambrosiadou BV, et al.. A neural network approach in diabetes management by insulin administration. *Journal of Medical Systems* 2001;25:119-131.

Goldbaum M, Katz N, Chaudhuri M, et al.. Image understanding for automated retinal diagnosis. *Proceedings of IEEE Symposium for Computer Applications in Clinical Medicine* 1989:756-760.

Gonzalez RC & Woods RE. *Digital Image Processing*. Addison Wesley, 1992

Gregson P, Shen z, Scott R, et al.. Automated grading of venous beading. *Comput Biomed Res*, 1995;28:291-304.

Hamilton A, Ulbig M & Polinghorne P. *Management of diabetic retinopathy*. BMJ 1996, ISBN 0-7279-0919-3.

Hanley JA, McNeil BJ. The meaning and use of the area under a receiver operating characteristic (ROC) curve. *Radiology*, 1982;143:29-36.

Hanley JA, McNeil BJ. A method of comparing the areas under receiver operating characteristic curves derived from the same cases. *Radiology* 1983;148:839-843.

Hee MR, Puliafito CA, Duker JS, et al.. Topography of diabetic macular edema with optical coherence tomography. *Ophthalmology* 1998;105:360-370.

Hee MR, Puliafito CA, Wong C et al.. Quantitative assessment of macular edema with optical coherence tomography. *Archives of Ophthalmology* 1995;113:1019-1029.

Hierlemann A, Weimar U, Kraus G et al.. Polymer-based sensor arrays and multicomponent analysis for the detection of hazardous organic vapours in the environment. *Sensors and Actuators B : Chemical* 1995;26:126-134.

Hipwell JH, Strachant F, Olson JA, et al.. Automated detection of microaneurysms in digital red-free photographs: a diabetic retinopathy screening tool. *Diabetic Medicine* 2000;17:588-594.

Hoover A, Goldbaum M. Locating the optic nerve in a retinal image using the fuzzy convergence of the blood vessels. *IEEE Transactions on Medical Imaging*. 2003;22:951-958.

Hopfield JJ. Neurons with graded response have collective computational properties like those of two-state neurons. *Proc Natl Acad Sci* 1984;81:3088-3092.

Hopfield JJ & Tank DW. Computing with neural circuits: a model. *Science* 1986;233:625-633.

Huang CL, Huang YH, Chang T et al.. The construction of production performance prediction system for semiconductor manufacturing with artificial neural networks. *International J of Production Research* 1999;37:1387-1402.

Hutchinson A, McIntosh A, Peters J, et al.. Effectiveness of screening and monitoring tests for diabetic retinopathy – a systematic review. *Diabetic Medicine* 2000;17:495-506.

*Images of the human brain* 1999. Encarta. Accessed 1999:

[http://au.encarta.msn.com/media\\_121628229\\_781566624\\_1\\_1/Images\\_of\\_the\\_Human\\_Brain.html](http://au.encarta.msn.com/media_121628229_781566624_1_1/Images_of_the_Human_Brain.html)

Kanski JJ: *Clinical Ophthalmology*. Butterworths 1984; ISBN 0-407-00295-2.

Kirkpatrick JNP, Spencer T, Manivannan A, et al.. Quantitative image analysis of macular drusen from fundus photographs and scanning laser ophthalmoscope images. *Eye* 1995;9:48-55.

Klein R, Meuer SM, Moss SE, et al.. The relationship of retinal microaneurysm counts to the four year progression of diabetic retinopathy. *Archives of Ophthalmology* 1989;107:1780.

Kochner B, Schulman D, Michaelis M, et al.. Course tracking and contour extraction of retinal vessels from colour fundus photographs: most efficient use of steerable filters for model based image analysis. *Proceedings of SPIE Conference on Medical Imaging* 1998;755-761.

Kohner EM. Diabetic retinopathy. *BMJ* 1993; 307:1195-9

Kohner EM, Sleightholm M, KROC collaborative study group. Does microaneurysm count reflect the severity of early diabetic retinopathy? *Ophthalmology* 1986;93:586.

Kohonen T. *Self-organization and associative memory, 3<sup>rd</sup> Edition*. Springer 1989.

Lee S, Wang Y. Automated retinal image quality assessment and enhancement. *SPIE Conference on Image Processing* 1999;3661:1581-1590.

Leese GP, Morris AD, Olson J. A national retinal screening programme for diabetes in Scotland. *Diabetic Medicine* 2003;20:962-964.

Liu Y, Liu W, Zhang Y. Inspection of defects in optical fibres based on back-propagation neural networks. *Optics Communications* 2001;198:369-378.

Lyman Ott, R. *An introduction to statistical methods and data analysis 4<sup>th</sup> Edition*. Duxbury Press 1992;ISBN 0-534-93150-2.

Martini FH: *Fundamentals of Anatomy and Physiology 5<sup>th</sup> Edition*. Prentice Hall 2001; ISBN 0-13-017292-8.

McCollum P 1998. An Introduction to Back-Propagation Neural Networks. Accessed 1998: <http://www.seattlerobotics.org/encoder/nov98/neural.html>

Metz CE. Basic principles of ROC analysis. *Seminars in Nuclear Medicine* 1978;8:283-298.

Meusinger R, Moros R. Determination of octane numbers of gasoline compounds from their chemical structure by  $^{13}\text{C}$  NMR spectroscopy and neural networks. *Fuel* 2001;80:613-621.

Moshiri S, Cameron NE, Scuze D. Static, dynamic and hybrid neural networks in forecasting inflation. *Computational Economics* 1999;14:219-235.

Muller: *Neural Networks – An Introduction*. Springer 1995; ISBN 3-540-60207-0.

Murvai J, Vlahovic K, Szepesva C, et al. Prediction of protein functional domains from sequences using artificial neural networks. *Genome Research* 2001;11:1410-1417.

Muscat S, Parks S, Kemp E, et al. Repeatability and reproducibility of macular thickness measurements with Humphrey OCT system. *IOVS* 2002;43:241-245.

Muscat S, Fahad B, Parks S, et al.. Optical coherence tomography and multifocal electroretinography of X-Linked juvenile retinoschisis. *Eye* 2001 (a);796-799.

Muscat S, Srinivasan S, Kemp E, et al.. Optical coherence tomography in diagnosis of sub-clinical serous detachment of the macula secondary to a choroidal neavus. *Ophthalmic Surg Lasers* 2001 (b);32:474-476.

*National Screening Committee Rev 2004*. Workbook Version 3 rev Nov 2004. Accessed 2001 <http://www.nscetinopathy.org.uk/pages/nsc.asp>

NeuralWare: *Neural Computing – A Technology Handbook for Professional II/Plus and NeuralWorks Explorer*. NeuralWare Inc. 1996.

NeuralWare: *Reference Guide – Software Reference for Professional II/Plus and NeuralWorks Explorer*. NeuralWare Inc. 1996.

NeuralWare: Frequently asked questions. Accessed 1998:  
[http://www.neuralware.com/support\\_faq.jsp](http://www.neuralware.com/support_faq.jsp)

Olson JA 2001. Diabetic Retinopathy Grading & Burden. Accessed 2001:  
<http://www.abdn.ac.uk/~opt065/CRAG%20March%202001%20for%20website/index.htm>

Osareh A, Mirmehdi M, Thomas B, et al.. Automated identification of diabetic retinal exudates in digital colour images. *Br J Ophthalmol* 2003;87:1220-1223.

Ozkan M, Inoue K, Negishi K et al.. Defining a neural network controller structure for a rubbertuator robot. *Neural Networks* 2000;13:533-544.

Peli E. Enhancement of retinal images: pros and problems. *Neuroscience & Biobehavioral Reviews* 1993;17:477-482.

Quan Y, Zhou M, Luo Z. On-line robust identification of tool-wear via multi-sensor neural network fusion. *Engineering Applications of Artificial Intelligence* 1998;11:717-722.

*ROC curve analysis* 1993. MedCalc. Accessed 1999:  
<http://www.medcalc.be/manual/mpage06-13a.php>

Rumelhart DE: *Parallel distributed processing: explorations in the microstructure of cognition*. MIT Press 1986.

Ryan SJ: *Retina 2<sup>nd</sup> Edition Volume 1 & Volume 2*. Mosby 1994; ISBN 0-8016-8032-8.

Sardari S, Sardari D. Applications of artificial neural networks in AIDS research and therapy. *Current Pharmaceutical Design* 2002;8:659-670.

Schalkoff RJ: *Artificial Neural Networks*. McGraw-Hill 1997.

*Scottish Diabetes Framework* 2000. Scottish Executive. Accessed 2000:  
<http://www.scotland.gov.uk/library5/health/sdf.pdf>.

Sinthanayothin C, Boyce JF, Williamson TH et al.. Automated detection of diabetic retinopathy on digital fundus images. *Diabetic Medicine* 2002;19:105-112.

Sinthanayothin C, Boyce JF, Cook HL et al. Automated localisation of the optic disc, fovea and retinal blood vessels from digital colour fundus images. *BJO* 1999;83:902-910.

*Sobel edge detector* 2003. Image processing learning resources Accessed 2003:  
<http://homepages.inf.ed.ac.uk/rbf/HIPR2/sobel.htm#1>

Spencer T, Phillips RP, Sharp PF & Forrester JV. Automated detection and quantification of microaneurysms in fluorescein angiograms. *Grafe's Arch. Clin. Exp. Ophthalmol* 1992;230:36-41.

*Stergiou C & Siganos D* 1996. Neural networks. Accessed 1998:  
[http://www.doc.ic.ac.uk/~nd/surprise\\_96/journal/vol4/cs11/report.html](http://www.doc.ic.ac.uk/~nd/surprise_96/journal/vol4/cs11/report.html)

Tolias YA & Panas SM. A fuzzy vessel tracking algorithm for retinal images based on fuzzy clustering. *IEEE Trans on Medical Imaging* 1998;17:263-273.

Usher D, Dumsky M, Himaga M, et al.. Automated detection of diabetic reinopathy in digital retinal images: a tool for diabetic retinopathy screening. . 2003;21:84-90.

Walter T, Klein JC, Massin P, et al.. A contribution of image processing to the diagnosis of diabetic retinopathy-detection of exudates in color fundus images of the human retina. *IEEE Transactions on Medical Imaging* 2002;21:1236-43.

*WHO* 2004. Magnitude and causes of visual impairment. Accessed 2004:  
<http://www.who.int/mediacentre/factsheets/fs282/en/index.html>

- WHO Office of Health Communications and Public Relations: The Costs of Diabetes. *WHO Geneva 2002 Fact Sheet No 236*.
- WHO Office of Health Communications and Public Relations: Blindness and Visual Disability: *WHO Geneva 1997 Fact Sheet No 142 - 148*.
- WHO office of Health Communications and Public Relations. Diabetes Care and Research in Europe: The St. Vincent Declaration. *Diabetic Medicine* 1990;7:360.
- Wienke D, Xie Y, Hopke DK. Classification of airborne particles by analytical scanning electron microscopy imaging and a modified Kohonen neural network (3MAP). *Analytica Chimica Acta* 1995;310:1-14.
- Williamson TH, D. Keating D et al.. Final Performance of Artificial Neural Networks for Screening for Diabetic Retinopathy. *IOVS* 1997;38:5271.
- Wittkemper HG, Steiner M. Using neural networks to forecast the systematic risk of stocks. *European J of Operational Research* 1996;90:577-588.
- Yamamoto S, Yamamoto T, Hayashi M, et al.. Morphological and functional analyses of diabetic macular edema by optical coherence tomography and multifocal electroretinograms. *Grafe's Arch. Clin. Exp. Ophthalmol* 2001;239:96-101.
- Yang CS, Cheng CY, Lee FL, et al.. Quantitative assessment of retinal thickness in diabetic patients with and without clinically significant macular edema using optical coherence tomography. *Acta Ophthalmologica Scandinavica* 2001;79:266-270.
- Yang CW, Ma DJ, Wang CM, et al.. Computer aided diagnostic detection system of venous beading in retinal images. *Opt Eng* 2000;39:1293-1303.
- Yulong M & Dingru X. Recognising the glaucoma from ocular fundus image by image processing. *Proceedings of 12<sup>th</sup> Annual International Conference of the IEEE Eng. in Med. & Biol. Soc.* 1990;12:178-179.

Zadeh LA, Fuzzy sets. *Information Control* 1965;8:338-353.

Zahlmann G, Kochner B, Ugi I, et al.. Hybrid fuzzy image processing for situation assessment – A knowledge-based system for early detection of diabetic retinopathy. *IEEE Eng. in Med. & Biology* 2000;19:76-83.

Zweig MH, Campbell G. Receiver-operating characteristic (ROC) plots: a fundamental evaluation tool in clinical medicine.1993;39:561-7.

